AD-A163 939 RECONFIGURABLE FLIGHT CONTROL SYSTEM FOR A STOL (SHORT 1/3
TAKE-OFF AND LANDI..(U) AIR FORCE INST OF TECH
WRIGHT-PATTERSON AFB OH SCHOOL OF ENGI.. B T CLOUGH
UNCLASSIFIED DEC 84 AFIT/GE/ENG/85D-8 F/G 1/3 NL

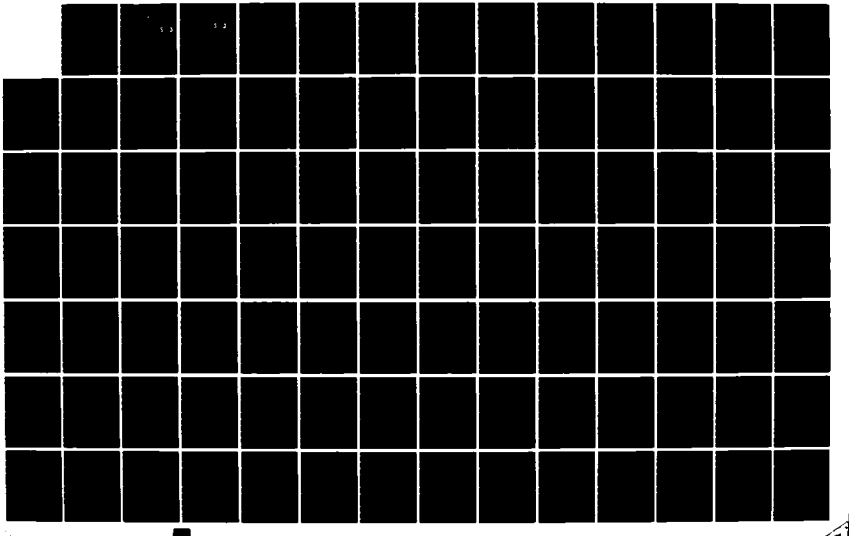

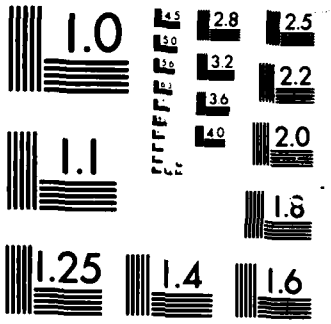

RECONFIGURABLE FLIGHT CONTROL SYSTEM FOR A STOL AIRCRAFT USING QUANTITATIVE FEEDBACK THEORY

THESIS

AFIT/GE/ENG/85D-8 Bruce T. Clough
1Lt USAF

DEPARTMENT OF THE AIR FORCE
AIR UNIVERSITY
AIR FORCE INSTITUTE OF TECHNOLOGY

Wright-Patterson Air Force Base, Ohio

AFIT/GE/ENG/85D-8

RECONFIGURABLE FLIGHT CONTROL SYSTEM FOR A STOL AIRCRAFT USING QUANTITATIVE FEEDBACK THEORY

THESIS

AFIT/GE/ENG/85D-8 Bruce T. Clough
1Lt USAF

AFIT/GE/ENG/85D-8

RECONFIGURABLE FLIGHT CONTROL SYSTEM FOR A STOL AIRCRAFT USING QUANTITATIVE FEEDBACK THEORY

THESIS

Presented to the Faculty of the School of Engineering
of the Air Force Institute of Technology
Air University
in Partial Fulfillment of the
Requirements for the Degree of
Master of Science

Bruce Thomas Clough, B.S.E.E.
First Lieutenant USAF
Graduate Electrical Engineering
December 1984

Approved for public release; distribution unlimited

Preface

I'd like to thank my thesis advisors, Dr. Isaac Horowitz and Dr. Constantine Houpis for their help, insight, and mostly patience. Without their help this thesis would've been in dire straights indeed. Thanks also goes out to my readers, Dr. John D'Azzo, Mr. Finley Barfield, Lt. Harry Gross, and Mr. Phillip Chandler for keeping me honest and providing improtant advice and feedback. A debt of gratitude must also go out to Captain Greg Mandt USAF, and Captain Harvey Russel of the Canadian Air Force for discussions on aircraft models and practical QFT design work respectively.

To my classmates, Captains Kevin Sheehan, Bruce Acker, Greg Gross, Steve Coucoules, and Lieutenants Bob Houston and Larry Jamerson , I give thanks for the insights, coffees, stale donuts, and laughs shared during this whole ordeal.

And to my wife Alice J., who had to put up with me all those long months I can only say thanks, I love you, I'm free now , and we can go shopping at night again.

Table of Contents

Preface ii

List of Figures v

List of Tables vii

Abstract 1

I. Introduction 3

I.1 Background 4
I.2 Problem Definition 6
I.3 Assumptions 6
I.4 Design Outline 7
I.5 Thesis Presentation. 9

II. Derivation of Plant Transfer Functions 10

II.1 Introduction 10
II.2 Aircraft 10
II.3 Aerodynamic Model 12

III. QFT Tneory 22

III.1 Introduction 22
III.2 QFT SISO Design Technique 23
III.3 MIMO System Reduction 39
III.4 Reconfigurability Theory 45
III.5 Summary 48

IV. Compensator Design 49

IV.1 Introduction 49
IV.2 Plant Equations 50
IV.3 Tracking Specifications 60
IV.4 Disturbance Rejection Specifications . . . 69
IV.5 Application of Reconfigurability Theory . 70
IV.6 Loop One Design 79
IV.7 Loop Two Design 94

V. Simulation Results 109

V.1 Introduction 109
V.2 Computer Model 109

V.3 Linear Simulation Results 112
V.4 Simulation Results Including Saturation .118
V.5 Summary 126

VI. Conclusions and Recommendations 127

VI.1 Discussion 127
VI.2 Conclusions 128
VI.3 Recommendations 131

Appendix A: Flight Parameters and Aerodynamic Derivatives A-1

Appendix B: State Space Models B-1

Appendix C: Control Surface Transfer Functions . . . C-1

Appendix D: Plant Matrices D-1

Appendix E: Frequency Response of Loop Tracking Bounds E-1

Appendix F: CAD Package STOLCAT F-1

Appendix G: Simulation Set-Up G-1

Appendix H: Reshaping of the Loop Transmissions . . . H-1

Appendix I: Derivation of Expanded Plant Determinant Equations I-1

Bibliography 135

Vita 138

List of Figures

Figure		Page
II.2-1	F-15 STOL Aircraft	11
II.3-1	Basic STOL Plant Signal Flow Graph . . .	15
II.3-2	General Plant Structure	18
II.3-3	Simplified Plant Structure	20
II.3-4	Entire Control Structure For STOL Aircraft	21
III.2-1	Two Degree of Freedom Structure	25
III.2-2	Time Domain Responses	27
III.2-3	Tracking and Disturbance Bounds in the Frequency Domain	27
III.2-4	Nichol's Chart	29
III.2-5	Typical Plant Templates	30
III.2-6	Loop Bounds	32
III.2-7	Typical Loop Transmission	37
III.2-8	Prefilter Frequency Response	39
III.3-1	MIMO Compensation Block Structure . . .	41
III.3-2	MIMO Compensation Signal Flow Graph . .	42
III.3-3	Equivalent SISO Plants of 2 X 2 MIMO Compensation Structure . . .	43
III.4-1	Reconfigurable Plant Structure	46
IV.3-1	Velocity Channel Time Response	66
IV.3-2	Velocity Channel Frequency Response Bounds	67
IV.3-3	Angle of Attack Step Response	69
IV.3-4	Angle of Attack Frequency Response Bounds	70

IV.6-1	Equivalent SISO Plants	30
IV.6-2	Q_{11} Plant Templates	84
IV.6-3	Loop One Bounds	85
IV.6-4	Polar Plot of Loop Transmission with an Unstable Pole that is Stable for Unity Feedback	86
IV.6-5	Root Locus of Unstable Plant	88
IV.6-6	Loop Transmission L_{1o}	91
IV.6-7	Log Magnitude of L_{1o} Verses Frequency . .	92
IV.6-8	Frequency Response of Compensation, g_1 .	93
IV.6-9	Prefilter f_{11} Frequency Response	93
IV.6-10	Comparison of Full and Reduced Order Loop One Compensators	94
IV.7-1	Q_{22eq} Templates	100
IV.7-2	Bounds on L_{2o}	102
IV.7-3	Loop Transmission L_{2o}	103
IV.7-4	Frequency Response of L_{2o}	104
IV.7-5	Loop Two Compensation	105
IV.7-6	Comparison of Full Order and Simplified Loop Two Compensators	105
IV.7-7	Frequency Response of Prefilter f_{22} . . .	106
V.2-1	Signal Flow Graph of Original Plant . .	110

V.2-2	Modified Signal Flow Graph of Actual Plant Simulation	111
V.3-1a	AOA Response to AOA Step Input	113
V.3-1b	Velocity Response to AOA Step Input . .	113
V.3-1c	Velocity Response to Velocity Step Input	113
V.3-1d	AOA Response to Velocity Step Input . .	113
V.4-1a	AOA Response to AOA Step Input	120
V.4-1b	Aerodynamic Surface Deflections for AOA Step Input	120
V.4-1c	Velocity Response to AOA Step Input . .	120
V.4-1d	Vane Deflection for AOA Step Input . . .	120
V.4-2	Unstable AOA Output for Step AOA Input with Plants Containing Double Surface Failures	121
V.4-3a	Velocity Response for Velocity Step Input	124
V.4-3b	Aerodynamic Surface Deflection for Velocity Step Input	124
V.4-3c	AOA Response to Velocity Step Input . .	124
V.4-3d	Vane Deflection for Velocity Step Input	124
VI.3-1	2 X 2 Signal Flow Graph for More General Control System of STOL F-15 . .	132
G-1	MATRIX X Simulation of STOL Aircraft . .	G-2
H-1	Loop One Bounds and the Reshaped Loop One Transmission . . .	H-2
H-2	Comparison of New and Old Compensators $\frac{g}{1}$	H-4
H-3	New $\frac{L}{20}$ and Respective Bounds	H-5
H-4	Comparison of Old and New Loop Two Compensation	H-6

List of Tables

Table		Page
II.2-1	STOL F-15 Aircraft Data	12
IV.2-1	Eigenvalues of the Open Loop System for the Three Flight Conditions	53
IV.2-2	DC Gains of Transfer Functions	56
IV.2-3	Weighting Factors for the Three Flight Conditions	57
IV.2-4	Modified Delta Vectors	59
IV.2-5	$\underline{P}$ Matrix Elements for Flight Condition One	61
IV.2-6	$\underline{P}$ Matrix Elements for Flight Condition Two	62
IV.2-7	$\underline{P}$ Matrix Elements for Flight Condition Three	63
IV.5-1	μ Terms Used to Give Basically Non-Interacting Systems Over the Three Flight Conditions	72
IV.5-2	Equivalent Plant Transfer Functions	74
IV.6-1	Original and Modified Difference Between b_{11} and a_{11} Tracking Bounds	89
IV.7-1	Equivalent Q_{22} for Flight Condition One . .	96
IV.7-2	Equivalent Q_{22} for Flight Condition Two . .	97
IV.7-3	Equivalent Q_{22} for Flight Condition Three .	98
IV.7-4	Modified Tracking Bounds for L_{2o} Design . .	101
V.3-1	Figures of Merit for AOA Command with Linear Simulation	114
V.3-2	Figures of Merit for Velocity Command Using Linear Simulation	116

IV.4-1 Figures of Merit for AOA Command Including Saturations 122

IV.4-2 Figures of Merit for Velocity Command with Saturations 125

A-1 Aerodynamic Data for Flight Condition One . . A-2

A-2 Aerodynamic Data for Flight Condition Two . . A-3

A-3 Aerodynamic Data for Flight Condition Three . A-4

B-1 State Space Model for Flight Condition One . B-2

B-2 State Space Model for Flight Condition Two . B-3

B-3 State Space Model for Flight Condition Three B-4

C-1 Control Surface Input to Velocity Output Transfer Functions C-2

C-2 Control Surface Input to Pitch Angle Output Transfer Functions C-4

C-3 Control Surface Input to Angle of Attack Output Transfer Functions . . C-6

D-1 Plant Matrix for FC1:No Failures D-2

D-2 Plant Matrix for FC1:Canards Failed D-2

D-3 Plant Matrix for FC1:Ailerons Failed D-2

D-4 Plant Matrix for FC1:Stabilators Failed . . . D-3

D-5 Plant Matrix for FC1:Stabilators, Ailerons Failed D-3

D-6 Plant Matrix for FC1:Stabilators, Canards Failed D-3

D-7 Plant Matrix for FC2:No Failures D-4

D-8 Plant Matrix for FC2:Canards Failed D-4

D-9 Plant Matrix for FC2:Ailerons Failed D-4

D-10 Plant Matrix for FC2:Stabilators Failed . . . D-5

D-11 Plant Matrix for FC2:Stabilators, Ailerons Failed D-5

D-12 Plant Matrix for FC2:Stabilators, Canards Failed D-5

D-13 Plant Matrix for FC2:Bottom Vanes Failed . . D-6

D-14 Plant Matrix for FC3:No Failures D-6

D-15 Plant Matrix for FC3:Canards Failed D-6

D-16 Plant Matrix for FC3:Stabilators Failed . . . D-7

D-17 Plant Matrix for FC3:Ailerons Failed D-7

D-18 Plant Matrix for FC3:Stabilators, Ailerons Failed D-7

D-19 Plant Matrix for FC3:Stabilators, Canards Failed D-8

D-20 $\underline{Q}$ Matrix for FC1:No Failures D-9

D-21 $\underline{Q}$ Matrix for FC1:Canards Failed D-9

D-22 $\underline{Q}$ Matrix for FC1:Stabilators Failed D-9

D-23 $\underline{Q}$ Matrix for FC1:Ailerons Failed D-10

D-25 $\underline{Q}$ Matrix for FC1:Stabilators, Ailerons Failed D-10

D-26 $\underline{Q}$ Matrix for FC1:Stabilators, Canards Failed D-12

D-27 $\underline{Q}$ Matrix for FC2:No Failures D-13

D-28 $\underline{Q}$ Matrix for FC2:Canards Failed D-13

D-29 $\underline{Q}$ Matrix for FC2:Stabilators Failed D-13

D-30 $\underline{Q}$ Matrix for FC2:Ailerons Failed D-14

D-31 $\underline{Q}$ Matrix for FC2:Stabilators, Ailerons Failed D-14

D-32 $\underline{Q}$ Matrix for FC2:Stabilators, Canards Failed D-14

D-33 $\underline{Q}$ Matrix for FC3:No Failures D-15

D-34 $\underline{Q}$ Matrix for FC3:Canards Failed D-15

D-35 $\underline{Q}$ Matrix for FC3:Stabilators Failed D-15

D-36 $\underline{Q}$ Matrix for FC3:Ailerons Failed D-16

D-37 $\underline{Q}$ Matrix for FC3:Stabilators, Ailerons Failed D-16

D-38 $\underline{Q}$ Matrix for FC3:Stabilators, Canards Failed D-16

E-1 Upper Frequency Bound for AOA Channel E-2

E-2 Lower Frequency Bound for AOA Channel E-3

E-3 Upper Frequency Bound for Velocity Channel . . E-4

E-4 Lower Frequency Bound for Velocity Channel . . E-5

AFIT/GE/ENG/85D-8

Abstract

Quantitative Feedback Theory developed by Dr. Isaac Horowitz of the University of Colorado is used to design the control laws for a Short Take Off and Landing(STOL) aircraft. Compensators are presented for two longitudinal variables, angle of attack and forward velocity, which are controlled via the use of five separate control surfaces: canard, stabilator, ailerons, upper and lower thrust reversing vanes. The final design must exhibit robust qualities over three flight conditions despite surface failures.

The state-space matrix representation of the aircraft is developed from pertubation equations using linearized aerodynamic data. Transfer functions relating servo input signals to aircraft outputs are obtained from the state-space equations. The original output set included the flight path angle and velocity; however, the non-minimum phase characteristics of the flight path angle precluded its use by the type of Quantitative Feedback Theory used in this thesis since unstable plants can arise. Instead, the minimum phase variables angle of attack and velocity are controlled. The ten separate transfer functions relating the two output variables to the five input commands form a 5 X 2 plant transfer function matrix. These separate transfer functions

are combined using a weighting vector into a 2 X 2 minimum phase plant matrix for each flight condition/failure combination. Quantitative Feedback Theory is applied to the resulting plants to yield robust control.

A single set of fixed compensators and prefilters are designed to handle the entire plant set, consisting of three single-surface failures and two dual-surface failures at each flight condition. For these failures neither Fault Detection/Identification, nor scheduled compensation, is required. Surfaces are assumed locked at zero degrees deflection after failure, generating no net moment after failure. Digital simulations have shown the control to be robust over the three flight conditions and surface failures. Loop bandwidths for the velocity and angle of attack loops are 35 and 12 rad/sec respectively. Control surface rates and deflections are shown to saturate only for the double failure cases.

Quantitative Feedback Theory effectively controls the aircraft despite large uncertainty due to flight condition changes and/or control surface failures without identification. Application of QFT eliminates the use of identification to acnieve robustness and the associated false alarm and missed detection problems. Efforts to expand upon the base of flight control design using this method are recommended, especially direct design in the discrete domain. Research should also continue on developing a computer-aided design program to expedite the synthesis of controllers using QFT.

ROBUST FLIGHT CONTROL SYSTEM FOR A STOL AIRCRAFT DESIGN USING QUANTITATIVE FEEDBACK THEORY

I. Introduction

Future aircraft may incorporate many control surfaces to meet stringent performance and aerodynamic efficiency requirements. These many surfaces increase the survivability of tne aircraft by providing redundant control in the event of surface failures. The design of a flight control system that automatically redistributes control authority among the remaining surfaces in the event of failure is a significant challenge. A control law sufficiently robust to encompass the dynamic uncertainty, as well as surface failures, is desired. Failure identification is useful but there is a trade off between the reliability of the failure identification and the time criticality of the failure. Thus a robust (non-identification) design provides control without the need of reliable identification.

Quantitative Feedback Tneory(QFT) developed by Dr. Isaac Horowitz promises to yield robustness witnout identification. Tnis tneory has been successfully applied to a number of difficult problems[1,2,3,4]. QFT inherently includes uncertainty and control system failures within the design procedure. One a priori designs for acceptable system responses with uncertainty and failures, making QFT well suited for designing aircraft flight control systems. Tnis

thesis uses QFT in the design of a flight control system for a future Air Force Short-Take-Off-and-Landing(STOL) experimental aircraft.The aircraft has additional control surfaces not found on current aircraft. Hence it provides an excellent platform for demonstrating reconfigureable flight control system design.

The remainder of chapter one provides additional background information, sets the scope of the problem, lists the assumptions made, and outlines the approach used.

I.1 Background

The Air Force Flight Dynamics Laboratory is currently investigating the development of reconfigurable flight control systems. The primary goals are better reliability, maintainability, survivability , simplicity, and reduced life cycle costs[5].

a. Reliability, maintainability, and economy will be enhanced by the use of simpler, smaller, and less redundant control system components. Identical components simplify maintainance problems by reducing the variety of parts required in inventory. Training and maintainance problems are reduced since personnel have to remember less about each system due to system simplicity. Larger numbers of each particular servo could reduce costs from economies of scale.

b. The existence of functionally redundant control surfaces on the airframe reduces the sensitivity of the control system to the loss of surfaces. The dependancy of aircraft flight control on any one surface is reduced. This

leads to increased survivability in the event of damage.

c. Many current aircraft have large control surfaces driven by redundant, expensive actuators. Less complex actuators promise to reduce procurement costs and maintenance of flight control systems. The current complex actuators driving critical control surfaces must withstand multiple failures and still function. Such actuators are expensive and difficult to maintain. It is estimated that simpler control actuators may decrease the life cycle cost(LCC) of the flight control system(FCS) by 30 percent[5]. Flight control surfaces utilized in this thesis include:

a. Canard
b. Stabilator
c. Ailerons
d. Thrust reversing vanes

As previously noted, QFT is inherently suited to design flight control systems for reconfigurable aircraft. In QFT the uncertainties and failures are considered beforehand, and the design achieves the desired response. QFT also allows the designer to see clearly the trade-offs between the extent of the resulting plant uncertainties, the narrowness of the performance tolerances, and the resulting bandwidth(the "cost of feedback"). For instance, certain flight conditions and failure sets may lead to compensation elements with unrealistically large bandwidths. QFT allows the designer to identify these problems at the beginning of the design cycle.

QFT employs well developed frequency domain design techniques that are simple to apply and give the designer a "feel" for the problem and its trade-offs.

I.2 Problem

The focus of this thesis is applying QFT to design a reconfigurable aircraft control system. Performance tolerences on two longitudnal outputs must be satisfied over a range of flight conditions including multiple control surface failures. Possible operating conditions are:

a. All surfaces operating normally.
b. Canard failed, fixed at trim position.
c. Ailerons failed, fixed at trim position.
d. Elevators failed, fixed at trim position.
e. Thrust vectoring failed, fixed at trim.
f. Combinations of the above.

I.3 Assumptions

The assumptions made in this thesis include:

a. The aircraft equations of motion can be linearized about an equilibrium(trim) position so that small perturbation models are valid.
b. Commands and aircraft responses do not invalidate the assumed linear model.
c. Mass remains constant during the command sequence.
d. The control surfaces failures are assumed symmetrical. This eliminates any cross coupling into

lateral modes. This thesis does not investigate cross coupling because there are already 7 control surfaces in the model(canard, ailerons, stabilator, top and bottom vane pair). Without this constraint the problem would be beyond the scope of a single thesis. Arnold[1] has applied QFT for the design of a reconfigurable FCS with cross coupling.

f. Actuator models given by McDonnell Douglas are assumed for the QFT design. They are third order for the canards, ailerons, and stabilators, and first order for the thrust reversing vanes.

These assumptions, as well as others introduced later, are explained in the body of the thesis. An additional assumption is that the reader is familiar with state-space representaion of dynamic systems, frequency response characteristics, transfer functions, matrix representations, and matrix algebra.

I.4 Design Outline

The folowing steps outline the control system design process used in this thesis:

a. The control structure and variables are defined.

b. Plant matrices are derived from aerodynamic data. These matrices are derived at each flight condition and failure case.

c. Transfer functions relating each of the five inputs to each of the two outputs are derived

from the plant matrices.

d. The ten individual transfer functions P_{ij} are combined into an equivalent two input and two output plant transfer function matrix, $\underline{P} = [p_{ij}]$, by combining the individual surfaces through the use of a weighting vector $\underline{\Delta}$. This vector is originally chosen to divide the control authority among the surfaces in a set percentage. The resulting non-minimum phase plants can lead to instability using QFT, so the $\underline{\Delta}$ vector is modified such that the resulting P are minimun phase.

e. Reconfigurable terms μ_{ij} are developed to make the plant matrix diagonally dominant. Diagonally dominant systems exhibit less cross coupling between channels which result in decreased loop transmissiom bandwidths. The μ_{ij} also increases robustness under failures by feeding command authority normally reserved for one control channel into the other in case of a failure.

f. The resulting plant matrices are inverted, $\underline{P}^{-1} = [p^*_{ij}]$, then each individual element inverted, to form the $\underline{Q}$ matrix, where

$$\underline{Q} = [q_{ij}] = [1/p^*_{ij}]. \qquad \text{(I.4-1)}$$

g. Aircraft time domain performance specifications

are converted into equivalent frequency domain specifications.

h. QFT converts the multiple input-multiple output(MIMO) synthesis problem into equivalent SISO synthesis problems. These are solved, resulting in loop compensation for the system.

g. The design is simulated and results analyzed over the design range of flight conditions and failures. Control surface deflections and rates are examined to ensure acceptable limits.

I.5 Thesis Presentation

This thesis is organized into six chapters. Chapter I is the introduction. Chapter II develops the control structure and develops the equivalent plant matrices from the aircraft equations of motion. In Chapter III, QFT for SISO systems is explained, as well as the development of the equivalent SISO systems from the original MIMO system and reconfiguration theory. Chapter IV applies QFT to the problem at hand, developing compensators and prefilters for the control system. The system is simulated in Chapter V to determine how well the design satisfies the desired performance specifications. Chapter VI contains the results, conclusions, and recommendations.

II. Derivation of Aircraft Transfer Functions and Control Structure from Aerodynamic Data

II.1 Introduction

This chapter develops the aircraft transfer functions needed in QFT design. The aerodynamic data is used to develop aircraft equations of motion around an equilibrium point. These equations of motion are then arranged in state equation format, and are then transformed to the complex frequency domain to form transfer functions relating each input to each output. The individual transfer functions are then grouped to form an equivalent two input-two output plant matrix. In the process weighting factors are introduced. These are chosen to maximize the ratios of the diagonal elements of the plant matrix to its off-diagonal elements(ensure diagonal dominance).

II.2 Aircraft

The aircraft that forms the basis for this thesis effort is the Short-Takeoff-and-Landing(STOL) F-15 currently under development by McDonnell Douglas[6]. Figure II.2-1 is a diagram of the proposed aircraft. This aircraft, derived from the F-15 Eagle air superiority fighter, incorporates two dimensional thrust vectoring vanes, thrust reversing vanes, and a forward canard. The original purpose for the extra control surfaces is to provide extra force and moment

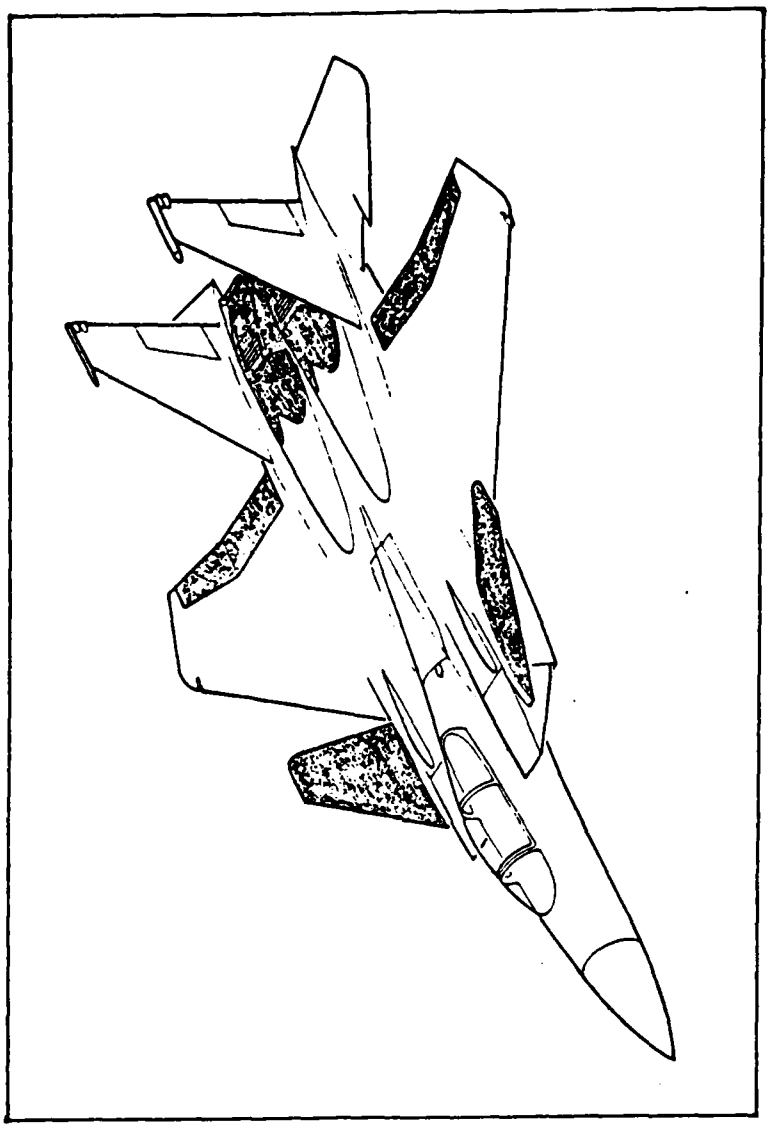

Fig.II.2-1: F-15 STOL Aircraft

production for STOL operation. However, these same extra control surfaces promise to provide redundant control under failure conditions. Basic specifications for the STOL F-15 aircraft are in Table II.2-1. Appendix A contains the aerodynamic data used to develope the state space models.

TABLE II.2-1

STOL F-15 Aircraft Data

Aircraft Parameters		
Wing Mean Aerodynamic Cord	c	15.8 ft
Wing Reference Area	S	608 sq-ft
Wing Span	b	42.7 ft
Weight	w	33576 lbs
Ixx		23634 slug-sq-ft
Iyy		181837 slug-sq-ft
Izz		199674 slug-sq-ft
Ixz		-3086 slug-sq-ft

II.3 Aerodynamic Model

The equation of motion for the aircraft are written in state matix format, with the individual elements derived from the aerodynamic data. This format is:

$$\underline{\dot{x}} = \underline{A}\underline{x} + \underline{B}\underline{u} \qquad (2.3\text{-}1a)$$

$$\underline{y} = \underline{C}\underline{x} + \underline{D}\underline{u} \qquad (2.3\text{-}1b)$$

where

$\underline{x}$ is the state vector

$\underline{A}$ is the plant matrix

$\underline{B}$ is the forcing function matrix

$\underline{y}$ is the output vector

$\underline{u}$ is the forcing function vector

$\underline{C}$ is the output matrix

$\underline{D}$ is the feedforward matrix

The elements of the $\underline{A}$ and $\underline{B}$ matrices are derived from the aerodynamic data in Appendix A. The $\underline{C}$ matrix is chosen to output the desired quantities while $\underline{D}$ is equal to $\underline{0}$, the null matrix. The data provided by McDonnell Douglas, which is defined in terms of the body axis, is converted to the stability axis. This conversion is done to facilitate analysis of the state space model by other thesis students using this aircaft both in the longitudnal and lateral directions. Since this thesis concerns only the longitudnal equations QFT will give a stable design in either axis system.

This thesis investigates only the longitudinal equations of motion for the aircraft. The model used consists of four states: the forward velocity, v, the pitch rate, q, the angle of attack, α , and the pitch angle, θ . Initially the outputs chosen were the forward velocity, and the flight path angle, γ. There are two longitudinal variables one would like to control, especially while landing. The state and output equations are then:

$$\begin{bmatrix} \dot{v} \\ \dot{q} \\ \dot{\alpha} \\ \dot{\theta} \end{bmatrix} = \begin{bmatrix} A_{ij} \end{bmatrix} \begin{bmatrix} v \\ q \\ \alpha \\ \theta \end{bmatrix} + \begin{bmatrix} B_{ij} \end{bmatrix} \underline{\delta}_i \qquad (2.3\text{-}2)$$

$$\begin{bmatrix} v \\ \gamma \end{bmatrix} = \begin{bmatrix} 1.0 & 0.0 & 0.0 & 0.0 \\ 0.0 & 0.0 & -1.0 & 1.0 \end{bmatrix} \begin{bmatrix} v \\ q \\ \alpha \\ \theta \end{bmatrix} \qquad (2.3\text{-}3)$$

The components of the A and B matrices are stability derivatives generated by linearizing the actual non-linear aircraft equations of motion about an equilibrium point. Entries in C are chosen to give the desired outputs.

Of the various control surfaces on the STOL F-15 the following are used in this thesis:

a. Canard

b. Stabilator

c. Ailerons

d. Top reversing vanes

e. Bottom reversing vanes

The flaps are not used since they only deflect downward. If they are used it is very likely that upward flap deflection would at times be demanded. Since this is impossible, a nonlinearity would result compounding the control problem. In this initial investigation it is desired to avoid such problems, so the flaps are excluded from the reconfigurable controller. However, in the actual aircraft design the flaps should be included as another possible useful surface in case of failure. The 2-D nozzles are not included since the stability derivatives required in the B matrix are not known at the time of this work. Appendix B details the state space model and the data involved.

Using the Computer-Aided-Design(CAD) package TOTAL[7], the transfer functions relating each input to each output are calculated. These are the original plant transfer functions that are combined to form the equivalent symmetrical plant

matrix(inputs = outputs) required for QFT. For the design in this thesis the plant matrix is 2 X 2. The signal flow graph relating the surface deflections to the aircraft responses is shown in Figure II.3-1. Assuming that the transfer functions do exist from each control surface to each output, the transfer function matrix representation of this relationship is:

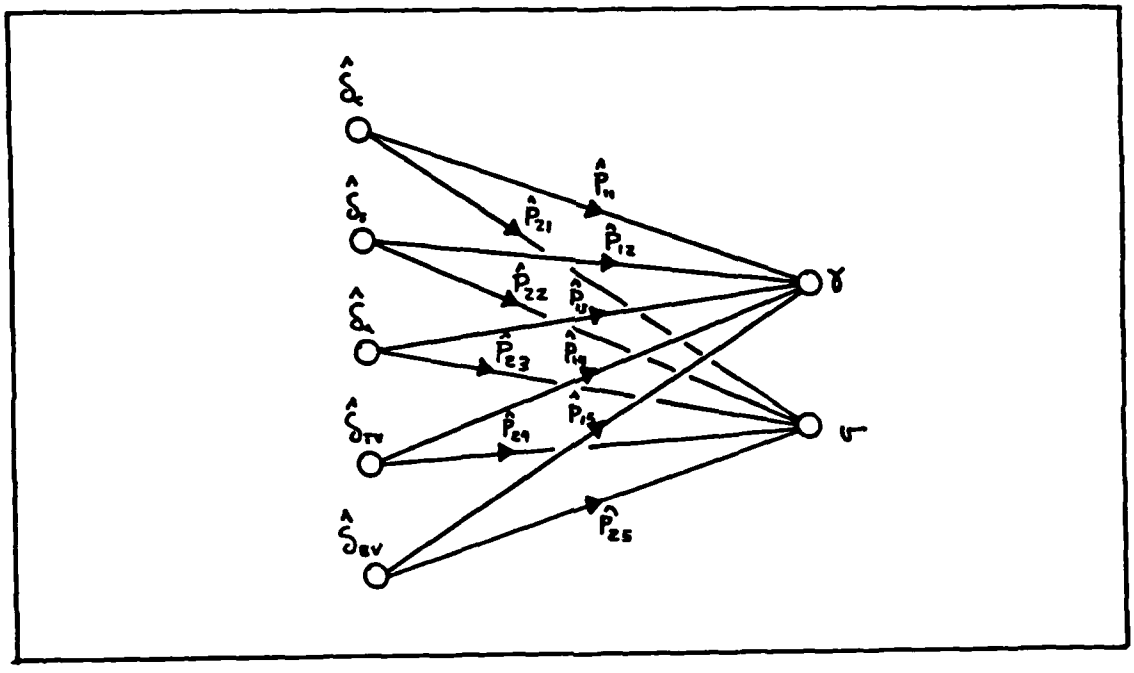

Fig.II.3-1: Basic STOL Plant Signal Flow Graph

$$\underline{O} = \begin{bmatrix} \gamma \\ v \end{bmatrix} = \begin{bmatrix} \hat{P}_{11} & \hat{P}_{12} & \hat{P}_{13} & \hat{P}_{14} & \hat{P}_{15} \\ \hat{P}_{21} & \hat{P}_{22} & \hat{P}_{23} & \hat{P}_{24} & \hat{P}_{25} \end{bmatrix} \begin{bmatrix} \hat{\delta}_c \\ \hat{\delta}_s \\ \hat{\delta}_a \\ \hat{\delta}_{tv} \\ \hat{\delta}_{bv} \end{bmatrix} \quad (2.3\text{-}4)$$

$$= \hat{\underline{P}}\,\hat{\underline{\delta}}$$

where

$\hat{\delta}_c$ is the canard deflection

$\hat{\delta}_s$ is the stabilator deflection

$\hat{\delta}_a$ is the aileron deflection

$\hat{\delta}_{tv}$ is the top vane deflection

$\hat{\delta}_{bv}$ is the bottom vane deflection

v is output 1, forward velocity

γ is output 2, flight path angle

As is seen later on the output vector had to be changed to forward velocity and angle of attack, but still with the same matrix structure.

The plant transfer function, P_{ij}, relates the ith output to the jth input. It is assumed that each control surface is driven by a servomechanism with a transfer function of M_i such that

$$O_j = P_{ij} \delta_i = M_i \hat{P}_{ij} \hat{\delta}_i \qquad (2.3\text{-}5)$$

where δ_i is the command input to the servo. The input-output relationship now becomes

$$\begin{bmatrix} \gamma \\ v \end{bmatrix} = \begin{bmatrix} P_{11} & P_{12} & P_{13} & P_{14} & P_{15} \\ P_{21} & P_{22} & P_{23} & P_{24} & P_{25} \end{bmatrix} \begin{bmatrix} \delta_c \\ \delta_s \\ \delta_a \\ \delta_{tv} \\ \delta_{bv} \end{bmatrix} \qquad (2.3\text{-}6)$$

Since two outputs are being controlled by two inputs through five separate control surfaces, there are many possible ways available for dividing the control effort between the surfaces. From preliminary discussions with personnel from the Air Force Flight Dynamics Laboratory[8] it was decided

that the control of the flight path angle would come primarily from the canard, stabilator, and ailerons while the reversing vanes(top and bottom) would provide the forward velocity control. A variable Δ_i is used to determine how much control authority is granted to the ith surface to control its respective output. This term does not have to be a constant, it could contain terms to compensate for the frequency response of the surface it weights. Next, the σ coefficients are another variable transfer function in the forward path that combine with the μ terms to provide the cross coupling required for robust control under surface failures and disturbance rejection for the aircraft under no-fail conditions. These terms can also be functions of frequency to correct for differences between control surfaces. Figure II.3-2 is the configuration of the plant and the control structure previously assumed. The equations relating the equivalent 2 X 2 plant to the individual control surface transfer functions are

$$P'_{11} = \sigma_1 (\Delta_{11} P_{11} + \Delta_{12} P_{12} + \Delta_{13} P_{13} + \Delta_{14} P_{14} + \Delta_{15} P_{15}) + \mu_{21} (\Delta_{21} P_{21} + \Delta_{11} P_{11} + \Delta_{22} P_{22} + \Delta_{23} P_{23} + \Delta_{24} P_{24} + \Delta_{25} P_{25}) \quad (2.3\text{-}7a)$$

$$P'_{12} = \sigma_2 (\Delta_{21} P_{21} + \Delta_{11} P_{11} + \Delta_{22} P_{22} + \Delta_{23} P_{23} + \Delta_{24} P_{24} + \Delta_{25} P_{25}) + \mu_{12} (\Delta_{11} P_{11} + \Delta_{12} P_{12} + \Delta_{13} P_{13} + \Delta_{14} P_{14} + \Delta_{15} P_{15}) \quad (2.3\text{-}7b)$$

$$P'_{21} = \sigma_1 (\Delta_{11} P_{11} + \Delta_{21} P_{21} + \Delta_{12} P_{12} + \Delta_{22} P_{22} + \Delta_{13} P_{13} + \Delta_{23} P_{23} + \Delta_{14} P_{14} + \Delta_{24} P_{24} + \Delta_{15} P_{15} + \Delta_{25} P_{25}) + \mu_{21} (\Delta_{21} P_{21} + \Delta_{21} P_{21} + \Delta_{22} P_{22} + \Delta_{22} P_{22} + \Delta_{23} P_{23} + \Delta_{23} P_{23} + \Delta_{24} P_{24} + \Delta_{24} P_{24} + \Delta_{25} P_{25} + \Delta_{25} P_{25}) \quad (2.3\text{-}7c)$$

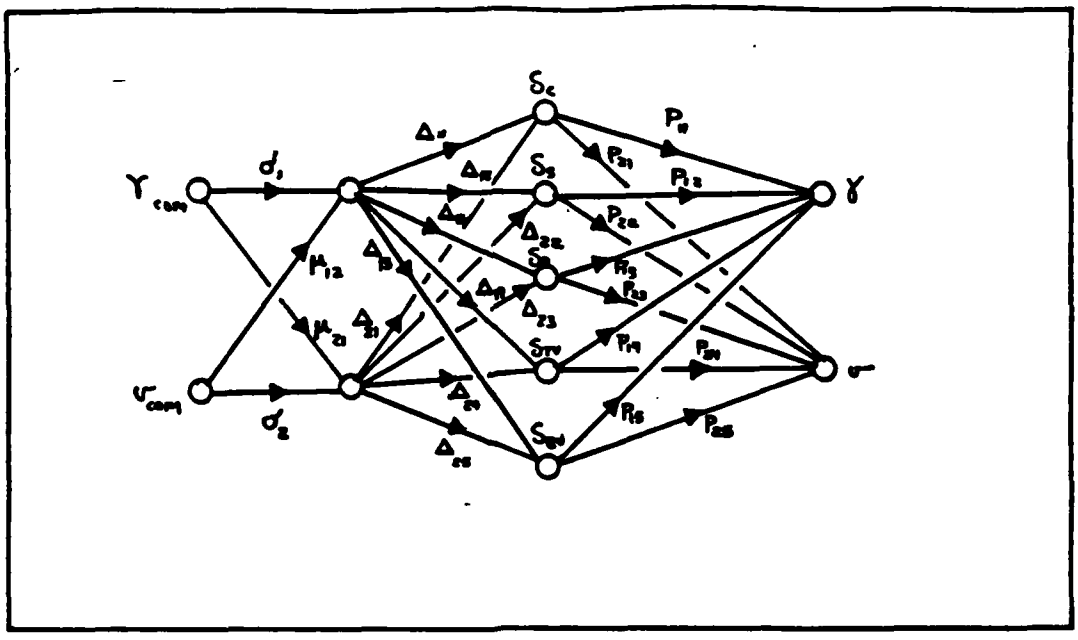

Fig.II.3-2: General Plant Structure

$$P'_{22} = \sigma_2 (\Delta_{21} P_{21} + \Delta_{22} P_{22} + \Delta_{23} P_{23} + \Delta_{24} P_{24} + \Delta_{25} P_{25}) + \mu_{12} (\Delta_{11} P_{21} + \Delta_{12} P_{22} + \Delta_{13} P_{23} + \Delta_{14} P_{24} + \Delta_{15} P_{25}) \quad (2.3\text{-}7d)$$

This is quite a complicated system, especially if Δ_{ij}, σ_i, and μ_{ij} are actually $\Delta_{ij}(jw)$, $\sigma_i(jw)$, and $\mu_{ij}(jw)$. The best choice for the Δ's, σ's, and μ's constitute an optimization problem beyond the scope of this masters thesis which is primarily dedicated to the reconfigurability synthesis problem. In order to simplify these relations to provide a better "feel" to the designer on how best to pick and choose the respective weighting terms, the σ terms are set equal to unity, the Δ's are reduced to five in all - set in the main forward path for the dominant variable each set of surfaces is primarily controlling. Δ_1, Δ_2,

and Δ_3 are in the forward path for the flight path angle channel while Δ_4, and Δ_5 are in the velocity channel. This simplified control scheme is shown in Figure II.3-3. Some freedom is of course lost by doing this, but the design process and assignment of the intermediate plant transfer functions(see below) are facilitated.

The equivalent plant transfer functions now become

$$P'_{11} = \Delta P_1 P_{11} + \Delta P_2 P_{12} + \Delta P_3 P_{13} + \mu_{21}(\Delta P_4 P_{14} + \Delta P_5 P_{15}) \quad (2.3\text{-}8a)$$

$$P'_{12} = \Delta P_4 P_{14} + \Delta P_5 P_{15} + \mu_{12}(\Delta P_1 P_{11} + \Delta P_2 P_{12} + \Delta P_3 P_{13}) \quad (2.3\text{-}8b)$$

$$P'_{21} = \Delta P_1 P_{21} + \Delta P_2 P_{22} + \Delta P_3 P_{23} + \mu_{21}(\Delta P_4 P_{24} + \Delta P_5 P_{25}) \quad (2.3\text{-}8c)$$

$$P'_{22} = \Delta P_4 P_{24} + \Delta P_5 P_{25} + \mu_{12}(\Delta P_1 P_{21} + \Delta P_2 P_{22} + \Delta P_3 P_{23}) \quad (2.3\text{-}8d)$$

Intermediate plant transfer functions in the parenthesis are defined as follows:

$$\tilde{P}_{11} = \Delta P_1 P_{11} + \Delta P_2 P_{12} + \Delta P_3 P_{13} \quad (2.3\text{-}9a)$$

$$\tilde{P}_{12} = \Delta P_4 P_{14} + \Delta P_5 P_{15} \quad (2.3\text{-}9b)$$

$$\tilde{P}_{21} = \Delta P_1 P_{21} + \Delta P_2 P_{22} + \Delta P_3 P_{23} \quad (2.3\text{-}9c)$$

$$\tilde{P}_{22} = \Delta P_4 P_{24} + \Delta P_5 P_{25} \quad (2.3\text{-}9d)$$

These equations are substituted into equations 2.3-8a-d to yield:

$$P'_{11} = \tilde{P}_{11} + \mu_{21} \tilde{P}_{12} \quad (2.3\text{-}10a)$$

$$P'_{12} = \tilde{P}_{12} + \mu_{12} \tilde{P}_{11} \quad (2.3\text{-}10b)$$

$$P'_{21} = \tilde{P}_{21} + \mu_{21} \tilde{P}_{22} \quad (2.3\text{-}10c)$$

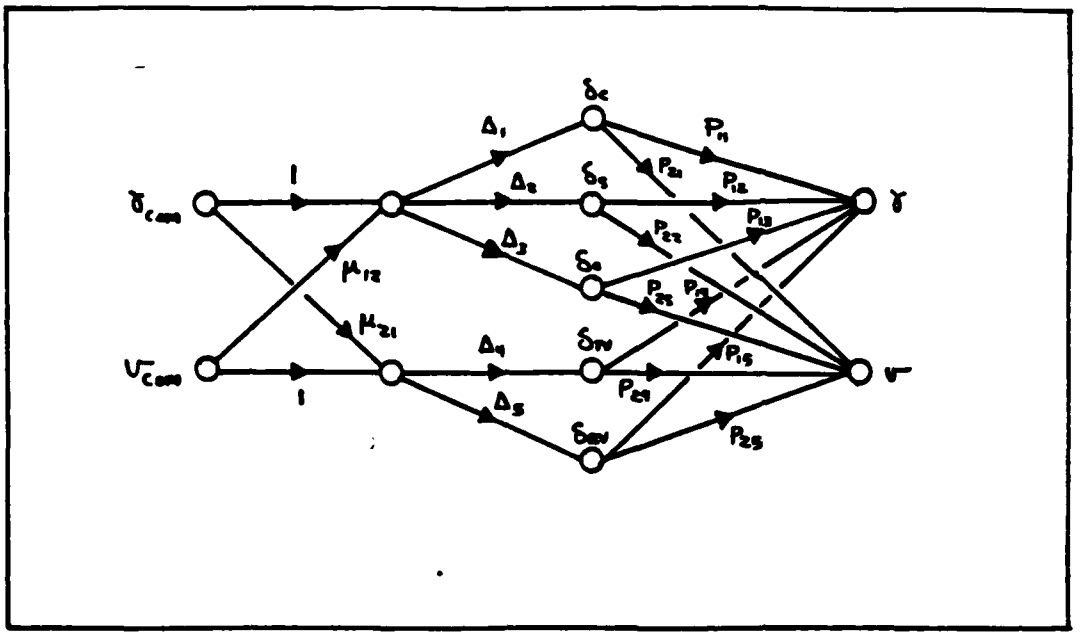

Fig.II.3-3: Simplified Plant Structure

$$P'_{22} = \tilde{P}_{22} + \mu_{12}\tilde{P}_{21} \qquad (2.3\text{-}10d)$$

The entire control structure with the feedback loops in place is in Figure II.3-4. The f_{ii} and g_i elements are prefilters and loop compensators respectively to be designed by QFT. The QFT design process is discussed in Chapter 3.

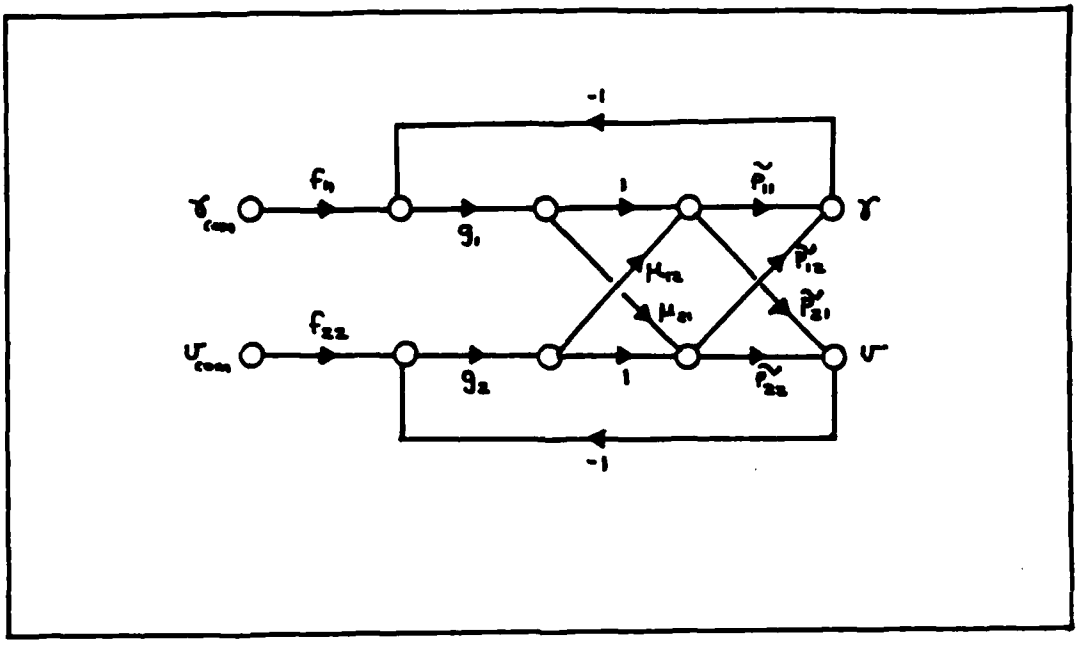

Fig.II.3-4: Entire Control Structure for STOL Aircraft

III. QFT Theory

III.1 Introduction

Most control system design techniques currently used design for a specific set of outputs given a particular system model. The designer hopes that in the process enough robustness has been built in to the design that it will tolerate some plant variations, failures, noise, and other types of uncertainty. If the first design is not satisfactory, the designer goes back and increases the gain, moves a pole, changes the weighting matrix, or possibly a combination of these things in order to arrive at a satisfactory design. Quantitative Feedback Theory(QFT), developed by Dr. Isaac Horowitz, allows the designer to put in the uncertainties a priori, and results in a design guaranteed to meet the system specifications. QFT has many advantages, including:

a. Uncertainties are included at the outset, resulting in a robust design.

b. Frequency domain design techniques, which are well developed and understood, are used.

c. Complicated multiple-input multiple-output systems(MIMO) are reduced to a set of single-input single-output systems(SISO) which simplifies the design process.

d. The design process is transparent, that is, it allows the designer to see exactly what "the cost of

feedback"(required loop transmission bandwidth) is for the range of uncertainties chosen. A problem which requires unrealistic compensation will be apparent from the outset of the design.

This chapter is broken into four separate parts. The introduction, QFT SISO system design technique, MIMO reduction into equivalent SISO systems, and the application of reconfigurablity. For a much more indeptn treatment the reader is urged to study the references[9, 10, 11, 12 ,13,14].

III.2 QFT SISO Design Technique

a. Overview

In order to develop QFT, a specific SISO structure used in this thesis is introduced. Next the system time domain specifications are translated into frequency domain specifications. The plant model and system specifications define the bounds of the system at every specific frequency value of interest. Uncertainties in the plant P at each frequency of interest are represented by an area on the Nichol's chart known as the plant template. Using the plant templates and system specifications, bounds on the nominal loop transmission L_o are derived. An L_o is then designed that satisfies the bounds. From the L_o a loop compensator G is determined, i.e.

$$G = L_o / P_o \qquad (3.2.a\text{-}1)$$

where P_o is the nominal plant transfer function chosen. A prefilter, F, is then designed to give the required tracking specifications over the range of plant uncertainties.

b. SISO System Definition

The system type that this thesis is concerned with is the two-degree of freedom structure in Figure III.2-1. In this thesis the disturbance is assumed to appear at the input of the plant rather than at the output. It is also assumed that the plant P has a known range of uncertainties, that the tracking input r(t), disturbance input d(t), and the output y(t) are given. Here y(t) is actually a member of the set of acceptable output responces Y(t). The signal x(t) is the plant input such that $y(t) = x(t) * p(t)$.

It is assumed that r(t) and y(t) are measureable, the output y(t) is fed back, and that Laplace transforms exist for every signal and system element present. For the two-degree-of-freedom structure the designer has to design two compensation elements, the prefilter F, and the loop compensator G. In terms of the loop transmission $L = P G$, four separate transfer functions can be defined to describe the behavior of the system. The responses due to the command input and disturbance input are:

$$y_c = \left[FGP/(1 + GP)\right] r = \left[FL/(1 + L)\right] r \qquad (3.2\text{-}1)$$

$$y_d = \left[P/(1 + GP)\right] d = \left[P/(1 + L)\right] d \qquad (3.2\text{-}2)$$

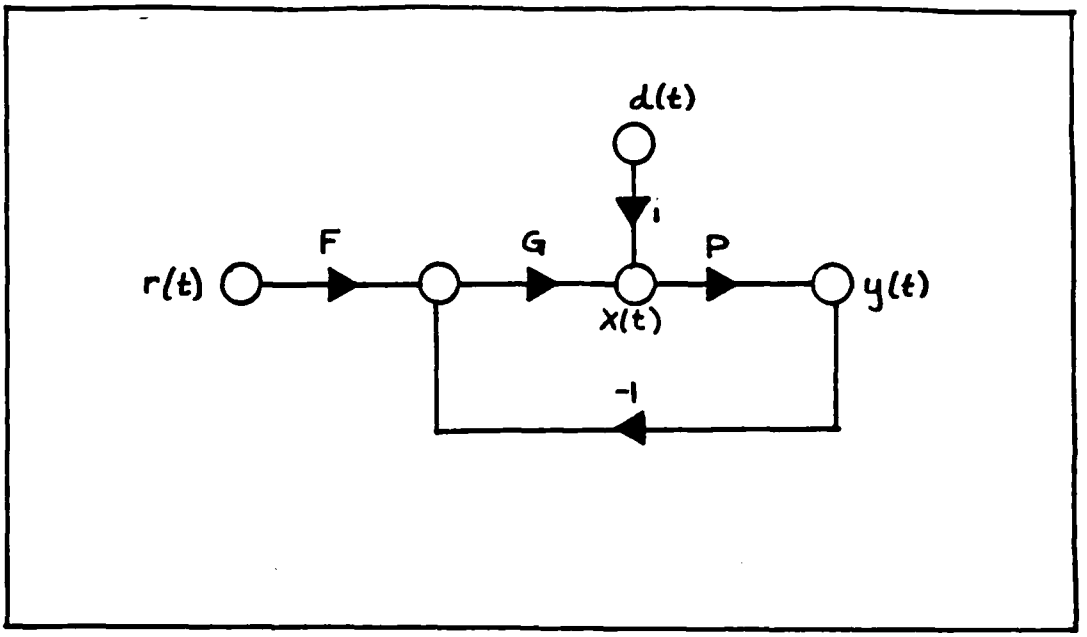

Fig.III.2-1: Two Degree of Freedom Structure

The transfer functions relating the plant input to command and disturbance inputs are respectively:

$$I_r = X(s)/R(s) = FG/(1 + L) \qquad (3.2\text{-}3)$$

$$I_d = X(s)/D(s) = 1/(1 + L) \qquad (3.2\text{-}4)$$

This thesis uses only the output equations to develop the loop compensations. The internal variables are ignored in this respect. This is not to say that the internal variables are not important. Some, such as control surface deflections or rates, can be critical. Quantitative methods exist to deal with the internal variables, but they are beyond the scope of tnis thesis[15]. Internal variables(such as the control surface deflections) are checked at the end of the design to

make sure that limits have not been exceeded. If they have, the designer must revaluate the problem, make appropriate changes, and begin again.

c. System Specifications

System specifications can be given in the time domain, such as rise time, settling time, overshoot, peak time, and final value, or they can be expressed in the frequency domain, such as bandwidth, DC gain, resonant frequency, phase margin, and gain margin. Which domain they are given in does not matter since they can always be transposed to the other. Typical time response curves are shown in Figure III.2-2. The faster rising, underdamped response has a higher bandwidth and is known as the upper bound T_U. The overdamped response has a lower bandwidth so it is known as the lower bound T_L. The disturbance, d , is shown at its maximum allowable value. These same specifications, now expressed in the frequency domain, are in Figure III.2-3 . The upper and lower bounds are evident as is the "typical" disturbance rejection shape of $d(j\omega)$. However the specifications are displayed, the range between the bounds reflects the uncertainty in the output which leads to an acceptable response.

The time response of a desired output variable of a control system is very rarely a single function, ratner a set of functions is specified tnat meet tne given response specifications.

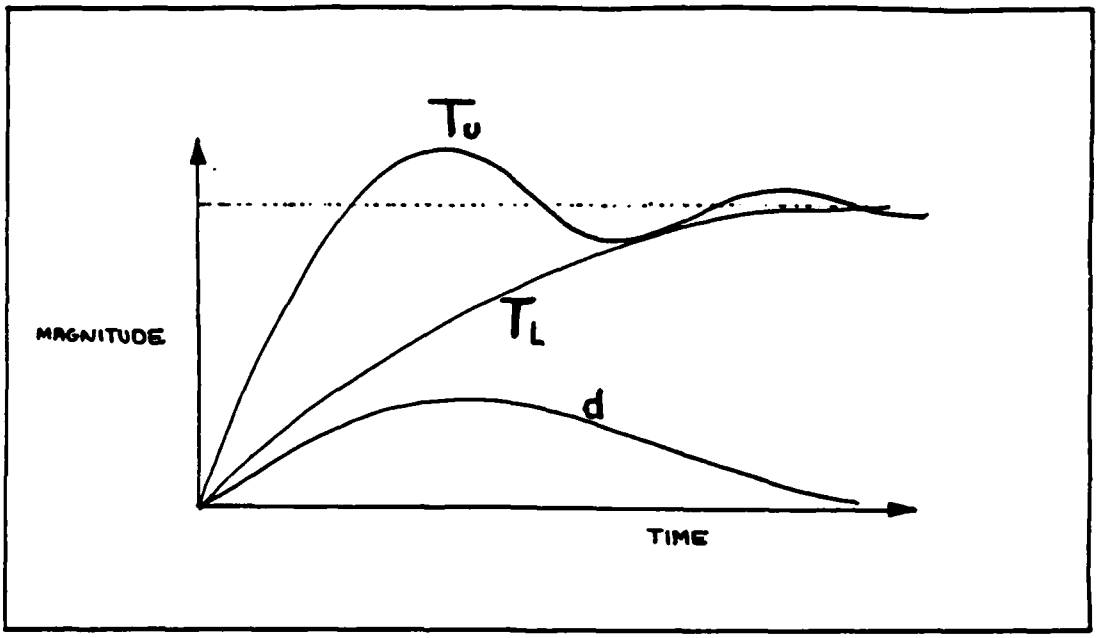

Fig.III.2-2: Time Domain Responses

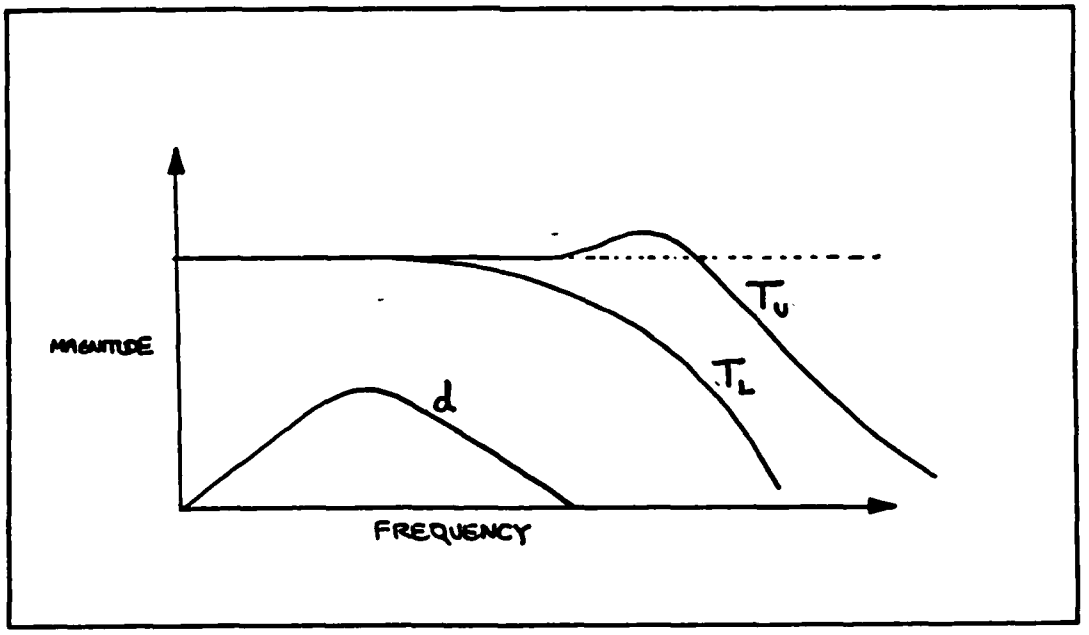

Fig.III.2-3: Tracking and Disturbance Bounds in the Frequency Domain

d. Derivation of Plant Templates

In QFT contraints on the free functions F, G are found so that the specifications are satisfied. The great advantage of frequency response is pointwise synthesis-the constraints are found pointwise at each ω value. The set of all possible plants P(jw) at a specified frequency ω_i form an area on the log-magnitude/ phase angle chart, the Nichol's Chart(N.C.), Figure III.2-4. In this respect it matters not whether the plant has one state or a thousand. This means that for the frequency in question all possible plant phasors lie within this area. The size and shape of the area, known as the plant template,is a function of frequency. It is assumed that the plant does not have any RHP zeros(non-minimum phase zeros). RHP zeros limit the maximum loop bandwidth which can be used in design, and the bandwidth is the factor which QFT manipulates to yield a design that meets system performance tolerances. Normally, the plant templates start out as a vertical line at DC, fatten out as the frequency increases, then converge to a vertical line as $\omega \rightarrow \infty$. The height(in decibels) of this line is given by the high frequency gain uncertainty.

Figure III.2-5 shows various plant templates as a function of frequency for some simple plant. The shape is not typical, it could have been an amorphous blob, or even several disjoint areas. However for design purposes any separate areas should be combined into a single area. In order to draw the plant template at any ω_i simply connect the periphery plant points to create an area on the Nichol's

chart. This area is the template.

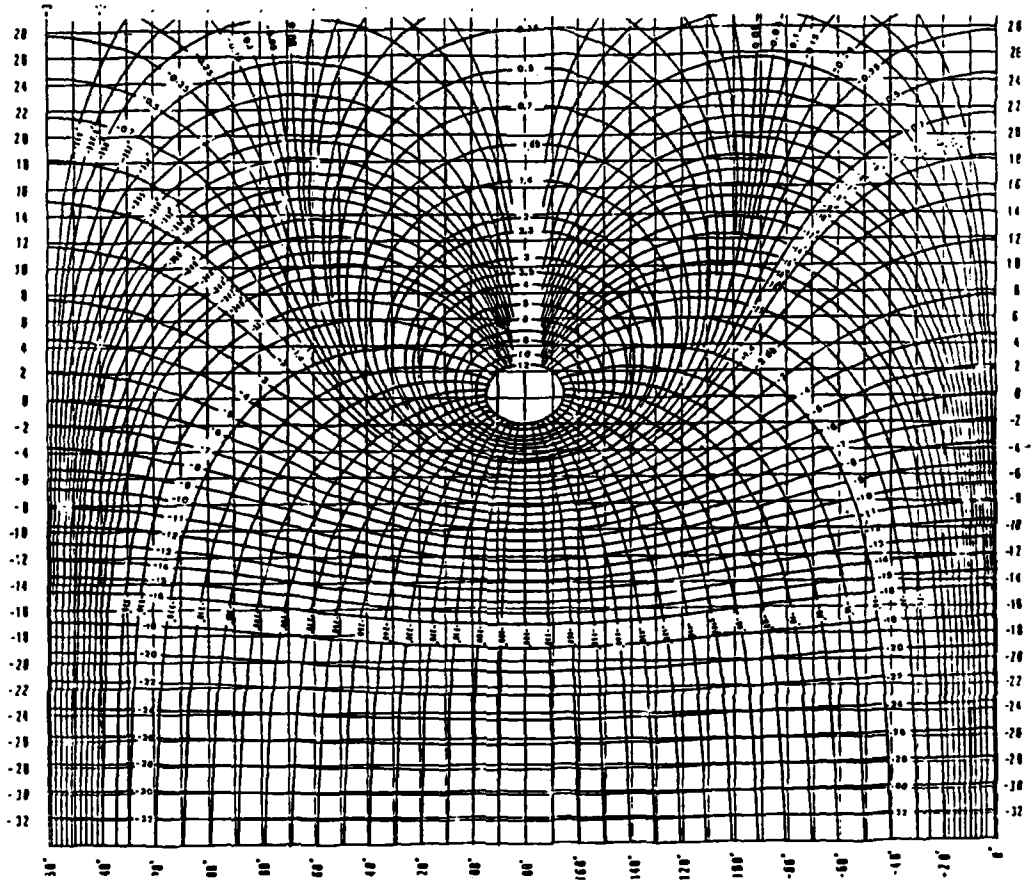

Fig. III.2-4: Nichol's Chart

Templates should be drawn approximately at every octave to give enough bounds for proper design. It is convenient that once all the templates are drawn on the N.C. they are transfered onto clear plastic sheets and cut out. Later on in the design process these templates are translated on the Nichol's chart to obtain frequency bounds for both disturbance rejection and tracking responses. From these bounds a nominal loop transfer function is derived.

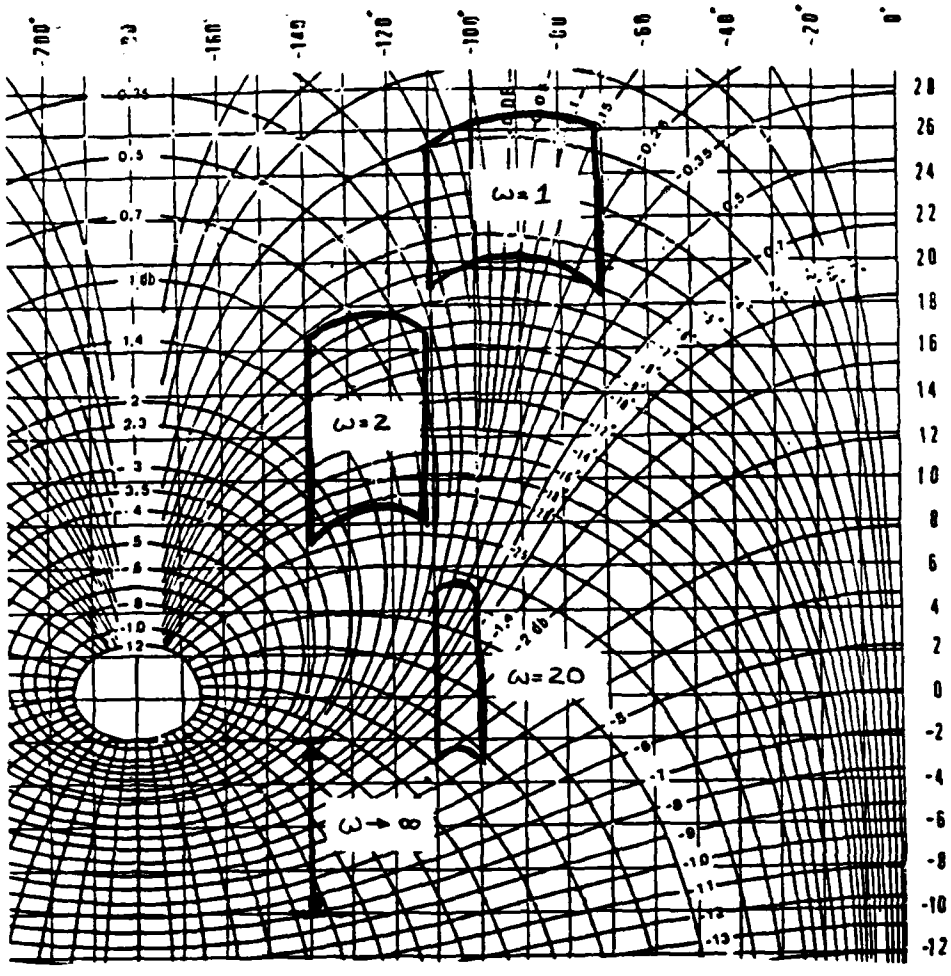

Fig. III.2-5: Typical Plant Templates

e. Use of the Nichol's Chart

Quantitative Feedback Theory relies on the Nichol's Chart to design the loop compensators and prefilters required to meet the specifications for a unity feedback system. By plotting the frequency response data for the open-loop transmission function L on the N.C. the closed-loop frequency response L/(1 + L) is known. That is, the frequency response data for the open loop is plotted using the rectangular grid

having magnitude and phase markings outside the chart. Thus from the intersection of $L(j\omega)$ with the M contours on the N.C. yield data points to plot the closed loop response as a function of frequency.

f. Nominal Plant

In order to arrive at compensation, a nominal plant P_o is chosen from all the possible plants. This plant is used to develop the loop compensation G from the shaped loop transfer function L_o, where $G = L_o / P_o$. This plant should be stable (if possible) and should lie on the lower left hand side of the plant template. This location results in loop bounds closer to the center of the Nichol's chart[16]. Other nominal plants result in loop compensators that work as well, but the actual compensator design process is more difficult because the bounds are located farther up on the Nichol's Chart. The nominal loop transmission function L_o is determined by $L_o = G P_o$, or the compensator using this P_o is $G = L_o / P_o$.

g. Derivation of Open Loop Bounds

For both the disturbance rejection and tracking parts of a control problem the loop transmission must satisfy certain bounds such that the specifications are met over the range of uncertainty. QFT represents these bounds as lines traversing, or closed contours, on the Nichol's Chart. The loop transmission must stay above the lines, or stay outside the closed contours, at each frequency. Two bounds exist for each frequency, tracking and disturbance rejection, with the loop

transmission greater in magnitude than the highest bound. Figure III.2-6 is an example of possible bounds. Notice that at ω = 1 rad/s the tracking bound, $B_r(j\omega)$, is greater than the disturbance rejection bound, $B_d(j\omega)$, while at ω = 8.0 rad/s this role is reversed.

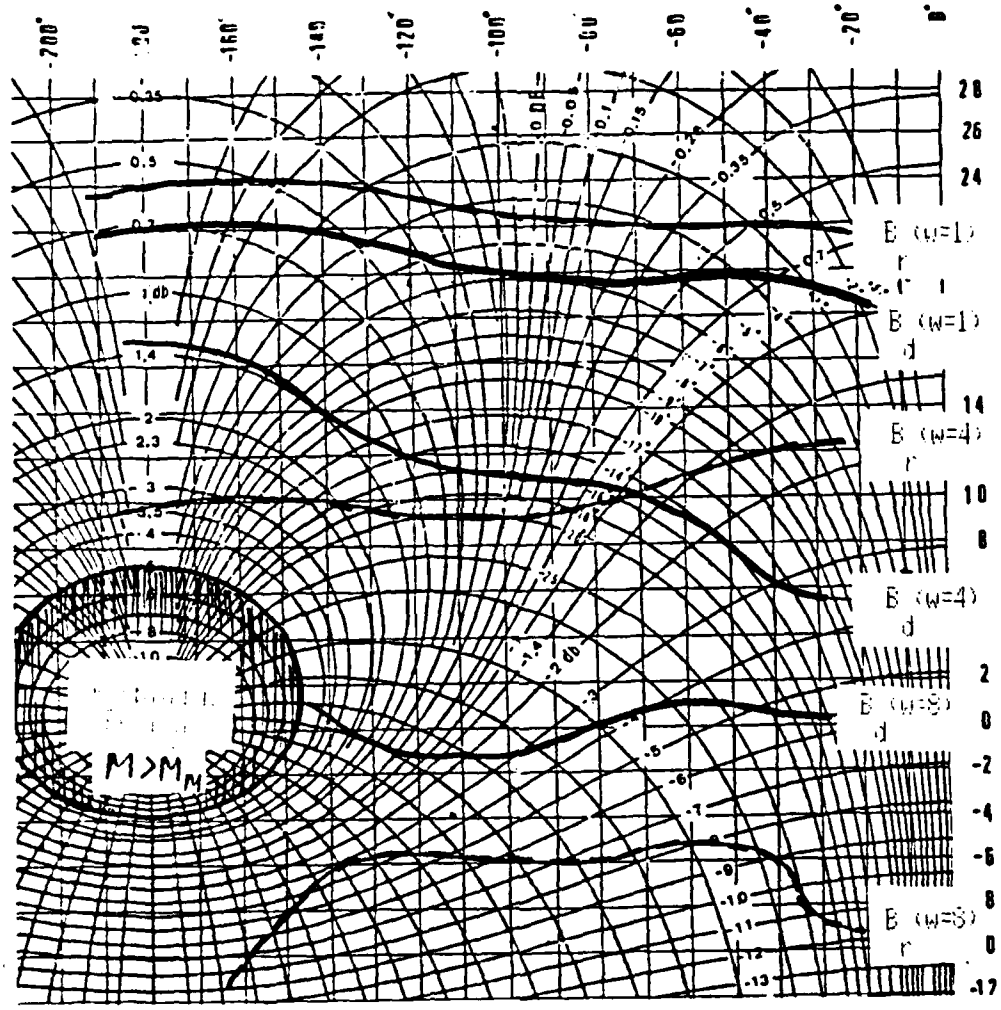

Fig. III.2-6: Loop Bounds

At ω = 4.0 rad/s the bounds cross. In this case a composite bound, $B_c(j\omega)$, is constructed out of the higher portions of the two individual bounds.

To find the bounds it is necessary to ensure that the output of the system y satisfies both the disturbance rejection and tracking specifications of Figure III.2-3 . First of all the maximum allowable value of the closed loop system frequency response M_m over its bandwidth is determined. This number corresponds to an M contour on the N.C. . The closed-loop transmission, $M_L = L/(1 + L) < M_m$, is required to stay outside the particular M contour corresponding to the chosen M_m . The area enclosed by the M contour is referred to as the "Forbidden Region". As an example, in Figure III.2-6 the $|M_m|$ is 5 dB, and the "Forbidden Region" is enclosed by the $|M_m| = 5$ dB contour.

The uncertainty in the closed loop response is entirely due to the plant since F and G are known. This implies that the uncertainty in L is the same as P . The uncertainty in the magnitude of the output is:

$$Lm[\Delta Y(j\omega)] = Lm[\Delta T(j\omega)] \qquad (3.2\text{-}5)$$

where

$$Lm[\Delta T(j\omega)] = Lm[T_U(j\omega)] - Lm[T_L(j\omega)]$$

$$= \Delta Lm[L/(1 + L)] \qquad (3.2\text{-}6)$$

L must be found such that $T(j\omega)$ remains within the acceptable range of Figure III.2-3. To ensure this the plant template at each frequency is first placed on the Nichol's Chart(remember that the plant template represents the range of uncertainty of the plants at any given frequency). Thus

since Lm[L] = Lm[P] + Lm[G], Ang[L] = Ang[G] + Ang[P], and G is LTI, then the template can be translated vertically and horizontally to determine the bounds that ensure that the performance specifications are met. The template cannot be rotated, only translated. With the template at an angle marking near the left hand side of the N.C., vertically translate the template up or down until the T_{max} and T_{min} values, the largest and smallest magnitude M contours respectively that the template is touching, satisfy the requirement:

$$\left| T_{max} \right| - \left| T_{min} \right| \leq \left| T_U \right| - \left| T_L \right| \qquad (3.2\text{-}7)$$

When this requirement is satisfied mark the nominal plant point on the N.C., then move over ten degrees and repeat the process. If in this process the template penetrates the M_m contour, the template must be translated on the N.C. until it is out of the contour even if the tracking bounds are not met. Since the gap between $T_U(j\omega)$ and $T_L(j\omega)$ becomes wider as $\omega \rightarrow \infty$ this translation is vertical. At lower frequencies the template can literally "ride" the upper portion of the M_m contour when this happens. At higher frequencies the difference in magnitude can result in the bound completely enclosing the M_m contour. From this step, the lines representing the tracking bounds $B_r(j\omega)$ on L are derived.

To derive the disturbance bounds the output under disturbance is considered. Assuming a disturbance input of d, the closed-loop output of the system is:

$$y_d = d\,P/(1 + L) \qquad (3.2\text{-}8)$$

This can be rearranged until it is of the form

$$\left|1 + L\right| \geq \left|d\,P/b_d\right| \qquad (3.2\text{-}9)$$

where b_d is the upper bound of the disturbance response. At this point the modified Nichol's Chart(MNC) is used to finish the bound determination. Flip the normal Nichol's Chart upside down, change the magnitude signs of the open-loop grids(-24 dB becomes 24 dB) and reverse the open-loop angle markings(-60° becomes -300°, -170° becomes -190°, etc.). Now it is possible to design L directly on the MNC with the superimposed lines now representing the magnitude and phase of 1/[1+ L]. For disturbance rejection the phase of the signal does not matter, just the magnitude. This assumes that the disturbance has the maximum effect at every frequency, i.e., worst case scenario. Take the plant template and place it on the MNC. Now translate the template until its lowest point rests on the contour of constant Lm[1 + L] equal to -Lm[D(jw)] at that frequency. Shift the nominal point along the chart as before, recording the bound for the nomial plant. Repeat this for each template in the plant set. Invert the chart and translate the $B_d(jw)$ bounds to the normal Nichol's Chart.

g. Derivation of Loop Transmission

With the bounds in place on the Nichol's chart, the design of L itself is started. The initial choice of where to start depends on a number of factors. If the open-loop plant

contains an unstable pole this must be included in L_o. For steady-state error reduction a Type 1, 2, 3, or more system could be desired. If so, the proper number of poles at the origin must be included in L at the onset of design. The resulting L should barely meet the bound at each frequency to give minimum bandwidth compensation. If such an L is achieved, then the system is optimally compensated(with respect to the performance specifications) A typical L satisfying a set of typical bounds is shown in Figure III.2-7. The actual "shaping" of L is a cut-and-try process where poles and zeros are added and shifted to conform to the bounds at each frequency ω_i. Sometimes a complicated bound structure can result in very complicated(high order) compensation. In this case it may be better to use a smaller order compensator, trading simplicity for a wider bandwidth.

h. Loop Compensation

The compensator G_o for the nominal plant is determined as follows:

$$G_o = L_o / P_o \qquad (3.2\text{-}10)$$

i. Prefilter Design

Once the loop compensation has been found the tracking response must be shifted to give the specified output to a command input. The prefilter, F, shifts the frequency

response of the closed-loop system(L/(1 + L)) until it lies within the tracking response bounds.

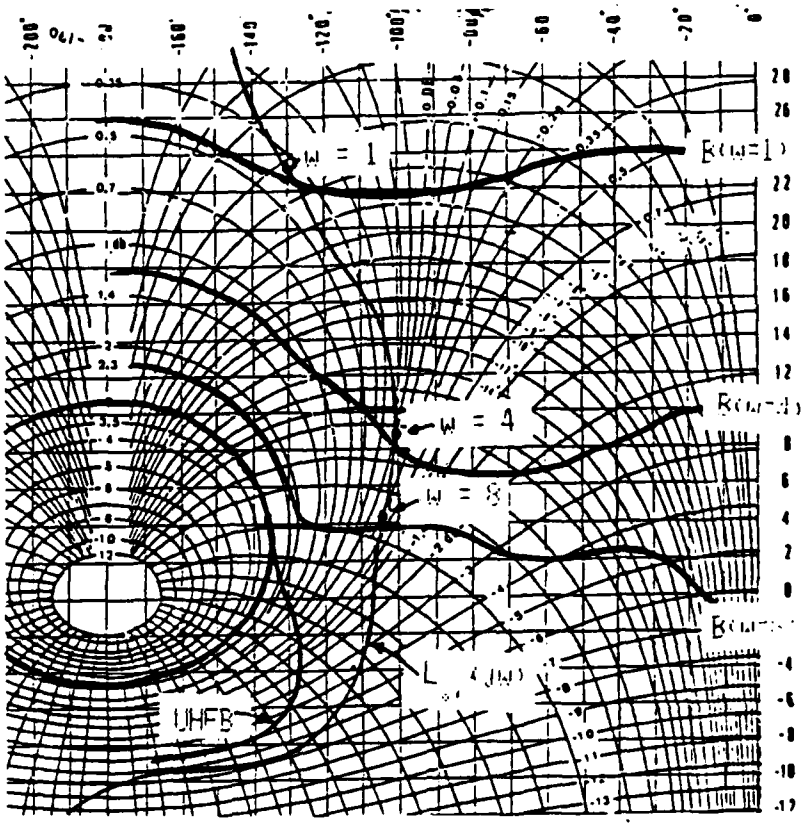

Fig.III.2-7: Typical Loop Transmission

Place the plant template for a given frequency ω_i on L_o with the nominal point resting directly over the top of the corresponding frequency point on L_o. Record the maximum and minimum closed-loop magnitudes that the template touches, $Lm[T_{max}(j\omega)]$ and $Lm[T_{min}(j\omega)]$. Next obtain the upper and lower tracking bounds for the same frequency, $Lm[T_U(j\omega)]$ and $Lm[T_L(j\omega)]$ as in Figure III.2-3. Now defining two quantities:

$$A = Lm[T_U(j\omega)] - Lm[T_{max}(j\omega)] \qquad (3.2\text{-}11)$$

and

$$B = Lm\left[T_U(j\omega)\right] - Lm\left[T_{min}(j\omega)\right] \qquad (3.2\text{-}12)$$

The response of the prefilter must be such that

$$\left|A(j\omega)\right| \leq \left|F(j\omega)\right| \leq \left|B(j\omega)\right| \qquad (3.2\text{-}13)$$

A good way to do this is to make an $Lm(\bullet)$ verses ω plot for botn A and B, and then chose an $Lm\left[\dot{F}\right]$ bounded by A and B ($Lm\left[F\right]$ plot lies between A and B). Figure III.2-8 shows one possible design of F given the indicated bounds. This F is not unique, since any function that does not violate those bounds satisfies them.

j. Summary

This completes the description of the QFT design method for compensating SISO plants utilizing output feedback with wide plant uncertainty. Using the design technique is straightforward without any guesswork. If the design is followed to the letter, a design guaranteed to meet the specifications over the range of uncertainty results. Also, QFT is transparent, allowing the designer to see the trade-offs required for meeting the specifications as the design process procedes, which can eliminate time wasted on tries at tne compensation of "uncompensatable" plants.

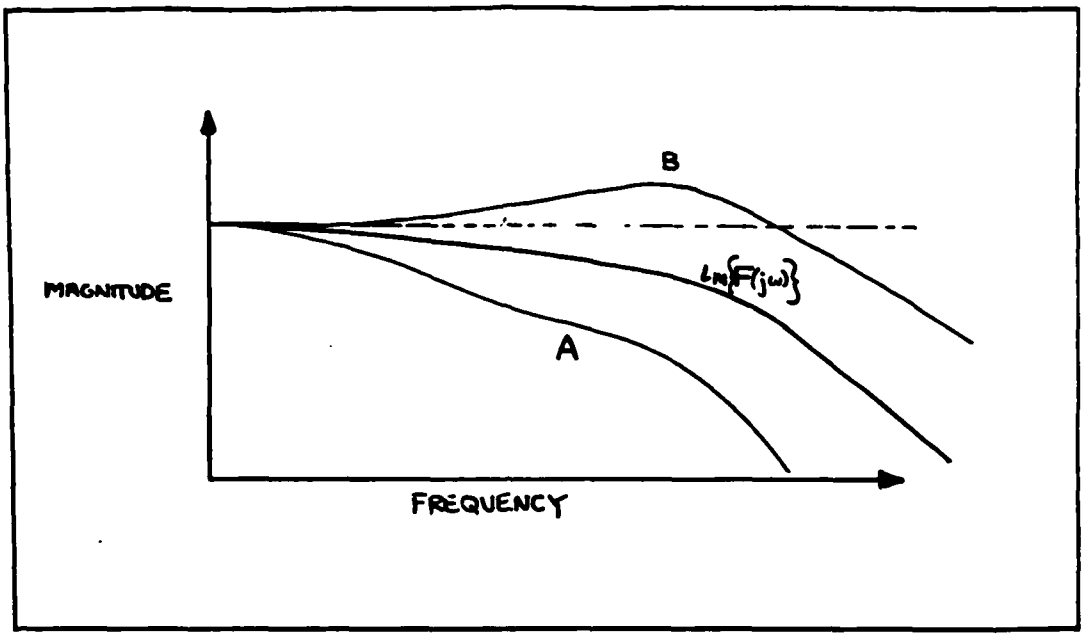

Fig.III.2-8: Prefilter Frequency Response

III.3 Reduction of MIMO systems into Equivalent SISO Systems

In order to use the QFT design technique for MIMO systems they must first be decomposed into a matrix of SISO systems. Dr. Horowitz has developed a method to do this using fixed point theory. This section describes the steps taken, but not the functional analysis behind it, leaving that to the reader from references[17, 18, 19, 20]. As a further simplification only a 2 X 2 system is examined, since that is the type of system used in this thesis.

a. Description of MIMO Plant

The general description of the MIMO input-output relationship is:

$$\underline{y} = \underline{P}\,\underline{u} \tag{3.3-1}$$

where

$\underline{Y}$ = vector of plant outputs

$\underline{P}$ = matrix of plant transfer functions

$\underline{u}$ = vector of plant inputs

$\underline{P}$ is derived from either the state-space matrices or the system linear differential equations. The plant has m inputs and m outputs, i.e., $\underline{y}$ and $\underline{u}$ are m X 1 vectors. The plant uncertainty is bounded with $\underline{P}$ being a member of all possible plants$\{\underline{P}\}$. Notice that the input and output dimensions are the same. With m inputs at most m outputs are independently controllable. If more than m inputs exist, the system is modified until it is m X m.

For this 2 X 2 system the MIMO compensation structure is shown in Figure III.3-1 . It consists of the plant matrix $\underline{P}$, a diagonal loop compensation matrix $\underline{G}$, and a prefilter matrix $\underline{F}$. The matrices are of the form:

$$\underline{P} = \begin{bmatrix} p_{11} & p_{12} \\ p_{21} & p_{22} \end{bmatrix} \tag{3.3-2}$$

$$\underline{G} = \begin{bmatrix} g_1 & 0 \\ 0 & g_2 \end{bmatrix} \tag{3.3-3}$$

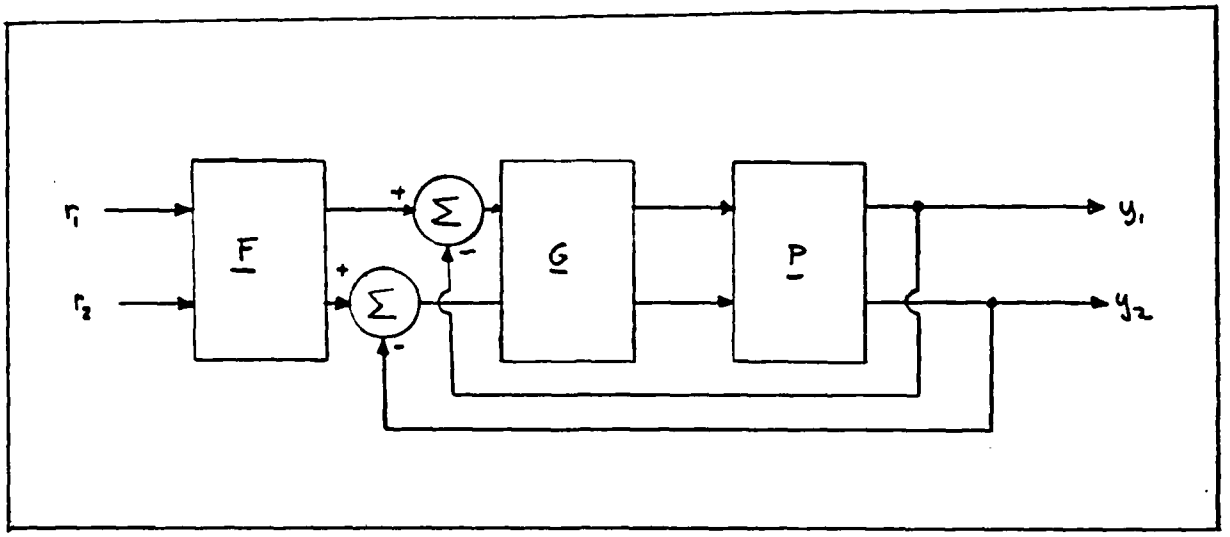

Fig.III.3-1: MIMO Compensation Block Structure

$$\underline{F} = \begin{bmatrix} f_{11} & f_{12} \\ f_{21} & f_{22} \end{bmatrix} \qquad (3.3\text{-}4)$$

Figure III.3-2 is a more detailed look at the 2 X 2 MIMO compensated system. In general $\underline{F}$ can be fully populated; however, in this thesis the cross coupling terms f_{12} and f_{21} are set equal to zero. This is done since in this design the velocity input commands only the velocity output, with the same thing true of the flight path angle. No cross coupling is desired.

The plant matrix must satisfy a few constraints:

a. $\underline{P}$ must be invertible. In other words $\underline{P}$ must not be singular.

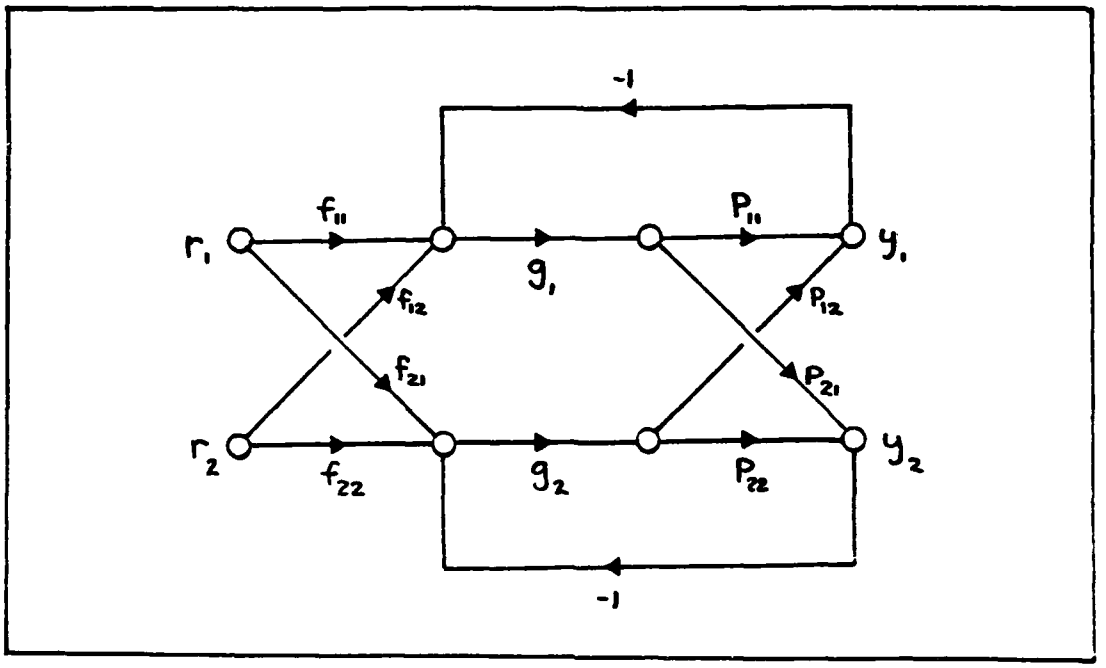

Fig.III.3-2: MIMO Compensation Signal Flow Graph

b. The main diagonal terms must dominate as $s \to \infty$ for all $\underline{P} \in \{P\}$, i.e.,

$$\lim_{s \to \infty} \left[\left| p_{11} p_{22} \right| - \left| p_{12} p_{21} \right| \right] > 0$$

This is referred to as the diagonal dominance condition.

c. Generation of Equivalent SISO Loops

With $\underline{P}$ defined and meeting the conditions above, the inverse of $\underline{P}$, $\underline{P}^{-1}$, exists, where

$$\underline{P}^{-1} = \begin{bmatrix} p^*_{11} & p^*_{12} \\ p^*_{21} & p^*_{22} \end{bmatrix} \qquad (3.3\text{-}6)$$

A new matrix, $\underline{Q}$, is now introduced with the individual elements being the inverse of the individual elements of $\underline{P}^{-1}$,

$q_{ij} = p^{*-1}_{ij}$. These q's are the effective SISO transfer functions, thus the m X m MIMO problem is transformed into m SISO systems. Figure III.3-3 shows these equivalent plants. The plants have two inputs, one due to tracking and the other due to a "disturbance" caused by the other SISO loops in the system(this accounts for the MIMO interactions).

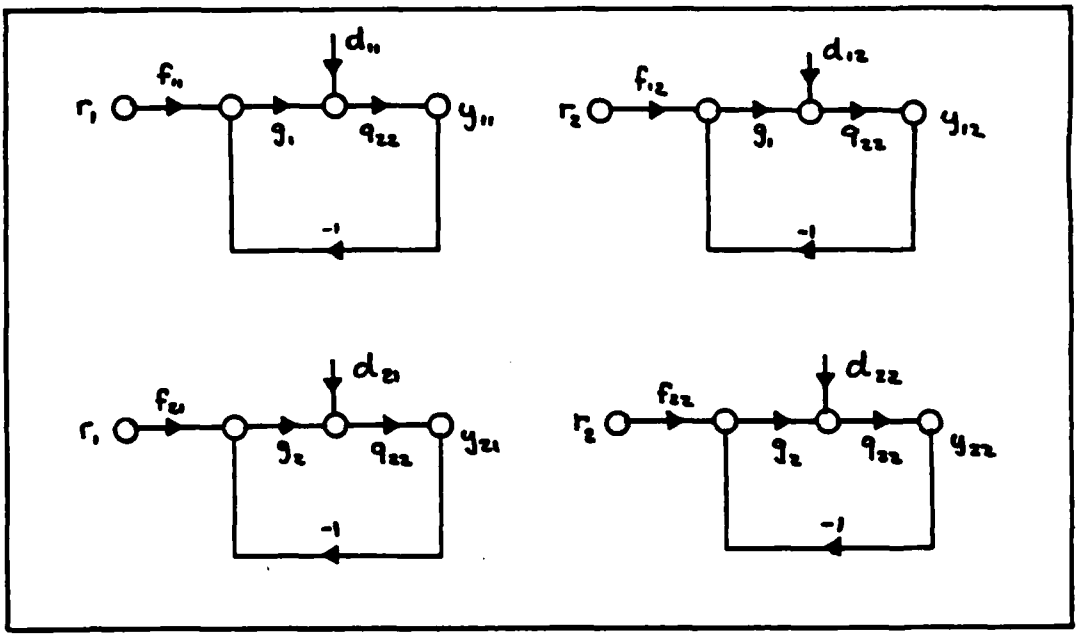

Fig.III.3-3: Equivalent SISO Plants of a 2 X 2 MIMO Compensation Structure

d. Equivalent SISO Inputs

As was stated above, the output of each equivalent SISO system is due to two factors, the command input and the disturbance, with the disturbance due to loop interaction. The equivalent disturbances d_{kl} are given by the equation:

$$d_{kl} = -\sum_{i \neq k} \left[t_{il} / q_{ki} \right]^{kl} \qquad (3.3\text{-}7)$$

e. Loop Design

The MIMO problem begins loop shaping by designing first the loop that has the strictest tolerances. These can be due to tracking, disturbance rejection, or plant uncertainty. Doing so results in the smallest loop transmission bandwidths. Once the decision is made as to which loop to shape first, each output of each transfer function of that row is examined to find out which one places the highest bounds on L. From these bounds L is shaped. This L is then used to define a modified q_{ii} for the remaining loop. This last loop design is an exact solution, minimizing the bandwidth.

f. Summary

Designing compensation for a MIMO sytem using QFT requires that the MIMO system be broken down into a set of equivalent SISO plants, with the interaction in the MIMO system represented as disturbance inputs in equivalent SISO systems. Once the decomposition is performed, QFT is used as described earlier.

III.4 Introduction to Reconfigurability Theory

a. Introduction

As is seen in Chapter IV, QFT can be used to design fixed compensators to meet tolerances in the face of wide plant parameter uncertainties. In this thesis the plant uncertainties are due to the range of flight conditions and of control surface failures. The advantage of fixed compensators over ones that are scheduled with the failure is that they don't require failure identification with its associated time delay. If acceptable performance is possible, then there is time for reliable identification after which an "optimum" compensator can be switched in. This chapter develops the QFT method for dealing with the reconfigurable aspects of the control problem. The available free μ terms of Chapter II are chosen so that the healthy aircraft is basically non-interacting(BNIA), i.e., the off diagonal terms are much less in magnitude than the diagonal terms. From the theory an equivalent MIMO plant matrix is developed that is used in Chapter IV.

b. Reconfigurable System Model

The feedback control structure is shown in Figure III.4-1 . The plants $\tilde{P}_{ij}$ are the constituent surface

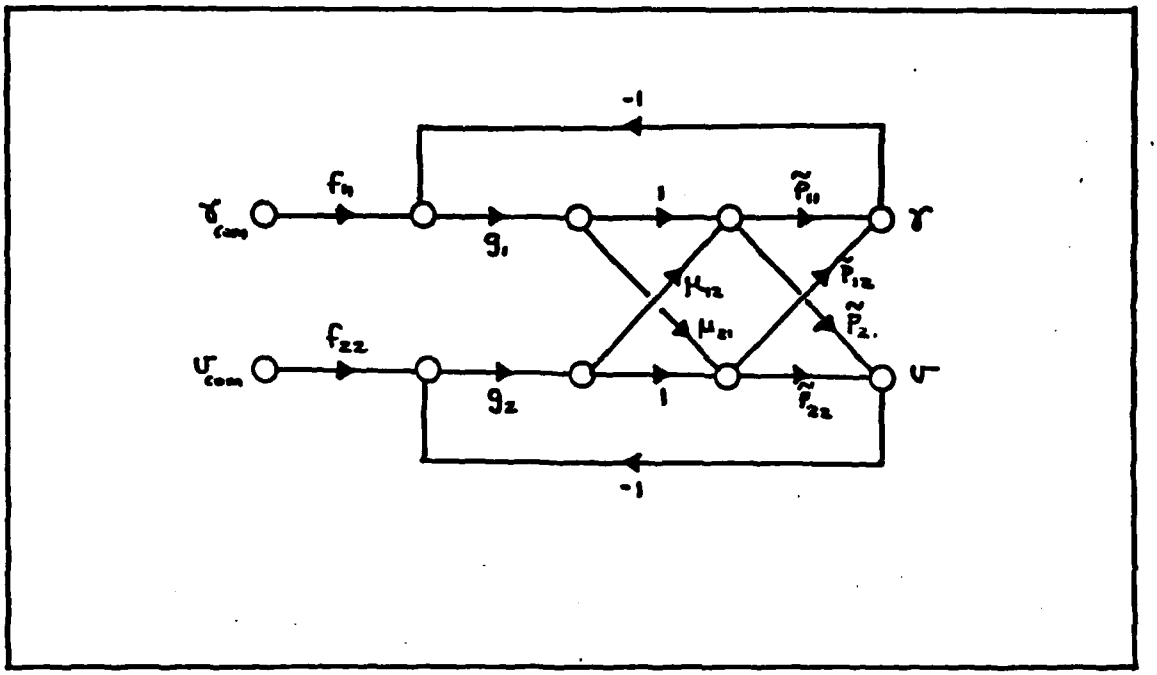

Fig.III.4-1: Reconfigurable Plant Structure

deflection vs. output transfer functions from Chapter II. The objective is to design the system such that there is as little interaction as possible between the loops for the healthy(no failure) aircraft, but also allowing cross coupling during failures which results in a redistribution of the remaining control authority. The $\mu_{i,j}$ are chosen to give this type of interaction. From Figure III.4-1, the equivalent plant matrix is:

$$\underline{P}' = \begin{bmatrix} P'_{11} & P'_{12} \\ P'_{21} & P'_{22} \end{bmatrix} \qquad (3.4\text{-}1)$$

where

$$P'_{11} = \tilde{P}_{11} + \mu_{21} \tilde{P}_{12} \quad (3.4\text{-}2a)$$

$$P'_{12} = \tilde{P}_{12} + \mu_{12} \tilde{P}_{11} \quad (3.4\text{-}2b)$$

$$P'_{21} = \tilde{P}_{21} + \mu_{21} \tilde{P}_{22} \quad (3.4\text{-}2c)$$

$$P'_{22} = \tilde{P}_{22} + \mu_{12} \tilde{P}_{21} \quad (3.4\text{-}2d)$$

c. Choice of Weighting Factors

For an ideal non-interacting system, it is desired that

$$P'_{21} = P'_{12} = 0 \quad (3.4\text{-}3)$$

requiring

$$\mu_{12} = - P'_{12} / P'_{11} \quad (3.4\text{-}4a)$$

$$\mu_{21} = - P'_{21} / P'_{22} \quad (3.4\text{-}4b)$$

These μ's in general are functions of frequency since in the majority of systems each P'_{ij} has its own set of poles, or at least, zeros. An exact μ_{ij} may not always be the best solution, especially when the denominator terms in equations (3.4-4a,b) contain non-minimum phase(right half plane) zeros. In this case the appropriate μ contains an unstable pole, and requires an exact cancellation to keep the system response stable. Since exact cancellation is impossible in reality, this choice of μ can cause problems. In this case

a minimum phase μ that will diminish the cross terms as much as possible is required - not perfect, but practical. Note that under failure conditions equations 3.4-4a,b are no longer valid, i.e., since the μ terms are derived for a particular no-failure plant, failures will change those plants, eliminating the cancellation. This causes the plant matrix to contain non-zero off diagonal terms. These off diagonal terms lead to loop interaction which allows control surfaces in the "healthy" loop to assist in control of the loop containing the failed surface(s).

III.5 Summary

Chapter III presents an overview of QFT as used in this thesis. Rigorous mathematics are not used, rather a more informal approach, explaination with words, is used to give the reader some idea of the power and the procedures of QFT. In Chapter IV more of the exact equations are introduced when used. If the reader wishes to delve deeper into the background behind QFT he is encouraged to read the references listed in the bibliography.

IV. Compensator Design

IV.1 Introduction

This chapter uses QFT to design the necessary compensation, g_1, g_2, f_{11}, and f_{22}, such that the design specifications are satisfied at the three flight conditions for a set of possible failures. The equivalent plant matricies are developed first. From these matrices the $\underline{G}$ matrices are found. Next the AOA control channel is developed using SISO design techniques. Then using information found during the design of the AOA channel, the second channel design is completed. To give the proper tracking response, the prefilters are then developed using frequency response data of each loop transmission function. During the design process it is noted that problems occur due to the aircraft's configuration. The problems stem from the non-minimum phase characteristics of the flight path angle responses. These problems lead to a re-evaluation of the control system, and a suggestion to ease the application of QFT to MIMO systems with non-minimum phase terms and/or unstable open-loop poles. From the steps taken a plant emerges that is amenable to QFT design techniques. It is shown that certain failures can be tolerated while others lead to plant matricies for which the QFT technique cannot be applied. For such plants a modification of the QFT technique has been developed to acnieve an acceptable system design for such plants, but doing this is beyond the scope of this thesis[11].

IV.2 Plant Equations

The first step to design compensators for the control problem at hand is to construct the equivalent plant matricies, $\underline{P}'$, from which the $\underline{Q}$ matricies are obtained. These plant matrices are developed from the state equation models in Appendix B. Initially the transfer functions relating surface deflections to outputs are used to construct plant matrices as is done in Chapter II. From these transfer functions, proper μ_{ij} to satisfy BNIA system requirements are found. Using the μ_{ij} and the plant matrices, another set of equivalent matrices with reconfigurability "built in" are designed. Next various surfaces are failed and new plant matrices are developed at each failure condition. Each matrix requires examination to determine whether it can be used in the QFT design process, or whether it contains non-minimum phase terms which cause that particular flight condition/failure not to be included in the plant set. The equivalent plant matrices are inverted and the equivalent SISO systems are developed. For these equivalent SISO systems, frequency response bounds at each frequency are used to describe the uncertainty in the plant. This uncertainty results in areas on the Nichols chart within which the plant lies at each frequency. Using these areas and bounds constructed with either tracking or disturbance rejection criteria (whichever places stricter requirements on the loop transmission, i.e., greater bandwidth , which is a "cost of feedback". A loop

[illegible] that satisfies these bounds and at the same time

minimizes loop bandwidth is then designed. From this loop transmission, the required compensation g_i is constructed. Prefilters f_{ii} are built such that the tracking response meets the performance specifications in the frequency domain, and thus the time domain specifications are also satisfied.

Two condidtions must be satisfied such that the design specifications are guaranteed to be met.

a. The inverse of the equivalent plant $\underline{P}'$ must exist. This is a controllability condition and must be satisfied for each flight condition and failure case. Thus the determinant of the plant cannot be allowed to become zero.

b. The second condition, the diagonal dominance condition, requires that

$$\lim_{s\to\infty} \left[\left| Q_{11} \; Q_{22} \right| / \left| Q_{12} \; Q_{21} \right| \right] > 1 \qquad (4.2\text{-}1)$$

This must be satisfied for each $\underline{P} \in \{\underline{P}\}$ and all frequencies ω_i greater than some frequency ω_b, wherever the quantity $|1 + L| > 1$, where L is the loop transmission function.

From the state space models in Appendix B transfer functions relating each control surface input to each output are generated using the Computer Aided Design(CAD) package TOTAL[7]. The resulting transfer functions are in Appendix C. The relationship between the flight path angle, pitch angle, and angle of attack to the jth control surface input is

$$\gamma(s)/\delta(s) = \theta(s)/\delta(s) - \alpha(s)/\delta(s) \qquad (4.2\text{-}2)$$

The actual flight path equations are developed directly from the state space representation by modification of the C matrix. The aircraft has three stable and one unstable root for the three flight conditions. A listing of these roots is given in Table IV.2-1. Note that the airplane becomes more unstable as forward velocity increases, with one short period root moving out along the real axis and the phugoid roots approaching the imaginary axis. Open-loop instability is not a problem for QFT since a stable closed-loop system is developed inherently by the design technique.

Almost immediately a problem arose in the design process. The surface to flight path angle transfer functions are all non-minimum phase, having at least two zeros in the RHP. These transfer functions always resulted in a non-minimum phase(nmp) equivalent plant matrix. The sensitivity reduction properties of a nmp plant is inherently limited, so it may be impossible to achieve the desired performance. One could proceed using the "Singular G" technique for nmp plants[11], but the result may be that a fixed LTI(linear, time invariant) compensator cannot handle the uncertainty range. Another way of looking at this is that the gain cannot be increased too much since an open-loop pole will migrate to the nmp zero causing instability. From discussions with Dr. Horowitz, the decision was made to continue the analysis using a different output variable other than flight path angle to control, which would hopefully provide a nmp plant determinant. It is determined that the angle of attack always

has minimum phase transfer functions. Thus the output variables chosen are the velocity and the angle of attack rather than the velocity and flight path angle. This is not ideal for aircraft landing control; however, it does have the advantage of guaranteeing beforehand that a design does exist which satisfied the specifications over the range of uncertainty. No such guarantees can be made apriori for nmp plants.

TABLE IV.2-1

Eigenvalues of the Open Loop System

for the Three Flight Conditions

Flight Condition 1:(Sea Level 100 kts)

s = 0.2846
s = -0.01897 + j0.2508
s = -1.546

Flight Condition 2:(Sea Level 120 kts)

s = 0.3851
s = -0.01104 + j0.2031
s = -1.979

Flight Condition 3:(Sea Level 180 kts)

s = 0.1603
s = -.003206 + j0.1090
s = -2.386

The next step is to chose which control surfaces are to execute the primary control over which variable. This is done by examining the magnitude of the frequency response for each transfer function, and choosing the dominant control surface of each output as that control which has the most

effect upon that variable. The stabilators and canards influence angle of attack about equaly, much greater than any of the other surfaces. Likewise, the top and bottom vanes have the greatest effect on velocity. The ailerons influence velocity slightly more than they influence the angle of attack; however, they are added to the angle of attack control to give that channel greater robustness under failure. This thesis assigns canards, stabilators, and ailerons as the primary angle of attack control, while the reversing vanes provide primary velocity control. This means that the "crosstalk terms" are the velocity change due to canard, stabilator, or aileron deflection, and the change in angle of attack due to reversing vane deflection.

Once the primary surfaces for each variable are defined the amount of control authority each surface has in controlling the assigned variables must be calculated. The method used in this thesis first assigns a percentage of control effort to each control surface involved in the primary control of a variable. The percentages for the angle of attack(AOA) are:

Canards	40%
Stabilators	50%
Ailerons	10%

These percentages were suggested by Capt. Greg Mandt[8]and assume the STOL aircraft has the ability to symmetrically deflect the ailerons. As mentioned earlier, the stabilators and canards influence angle of attack about equally, with the stabilator being slightly stronger. The small percentage

chosen for the aileron reflects the fact that this surface must also be used to control lateral variables as well. Choosing a large percentage could cause saturation, especially if large lateral manuevers are called for. For velocity control the percentages picked are:

Top vanes	50%
Bottom vanes	50%

In order to achive these percentages the amount of control exerted by a particular surface over a variable is assumed to be represented by the DC gain of its transfer function. The weighting terms Δ_i from Chapter II are chosen such that the new DC gains reflect the percentage values picked. These DC gain terms are in Table IV.2-2 for the three flight conditions. The signs of these Δ terms are chosen such that all the control surfaces work together. This is done by referencing the Bode plot for each transfer function and choosing the sign that results in similar frequency response. It turns out that simple sign changes on the Δ terms ensure that this occurs. As an example, for flight condition one the DC gains for the angle of attack are:

Canards	1.349
Stabilators	2.835
Ailerons	0.3961

As a first try Δ_1 is set to unity. This implies that 40% of tne control authority is equal to 1.349. The negative sign is dropped(but is dealt with later). This implies that the total effort has a magnitude of 3.373. In order to achieve the

proper percentages of control authority, the required values are:

$$\Delta_2 = 0.5948$$

$$\Delta_3 = 0.8514$$

Finally the signs on Δ_2 and Δ_3 are changed so that all the surfaces are working together.

TABLE IV.2-2

DC Gains of Transfer Functions

Response	Flight Condition		
	1	2	3
v/δ_C	314.2	466.8	3299
v/δ_S	-700.9	-987.3	-5934
v/δ_A	-107.4	-236.4	-1902
v/δ_{TV}	477.2	533.9	1536
v/δ_{BV}	-287.1	-260.0	-595.6
α/δ_C	-1.349	-1.124	-2.622
α/δ_S	2.835	2.210	4.558
α/δ_A	0.3961	0.4946	1.423
α/δ_{TV}	-0.9608	-0.5595	-1.150
α/δ_{BV}	0.5917	0.5686	0.4466

Likewise the vane Δ's are found. For flight condition one

the terms are:

	Top vanes	1.000
	Bottom vanes	1.662

Now, to make sure all the surfaces are working together, i.e., are in phase, signs on Δ's 2, 3, and 4 must be changed. For the first flight condidtion the $\underline{\Delta}$ vector is:

$$\underline{\Delta}^T = [\ 1.000\ -0.5948\ -0.8514\ -1.000\ 1.662]$$

The $\underline{\Delta}$ vectors for all flight conditions are in Table IV.2-3 At this point the reader might ask if choosing a $\underline{\Delta}$ vector at each flight condition is not actually scheduling $\underline{\Delta}$, implying that the design is not really robust. The intent is to examine the plants resulting from each of the vectors, and select the $\underline{\Delta}$ vector which results in the greatest number of minimum phase P' under failures for all three flight conditions.

TABLE IV.2-3

Weighting Factors for the Three Flight Conditions

Flight condition		1	2	3
Deltas	Δ_1	1.000	1.000	1.000
	Δ_2	-0.5948	-0.6357	-0.7191
	Δ_3	-0.8514	-0.5681	-0.2303
	Δ_4	-1.000	-1.000	-1.000
	Δ_5	1.662	2.053	2.579

Using these $\underline{\Delta}$ values, equivalent plant matricies $\underline{P}$ are developed for each flight condition. Here a problem occurs because of the structure of the velocity to top and bottom vanes transfer functions. For instance, at flight condition one the velocity to top vane transfer function is:

$$\frac{v(s)}{\delta(s)} = \frac{-9.496(s+0.2328+j0.4762)(s+4.979)}{(s+0.01897+j0.2508)(s+1.546)(s+0.2846)} \qquad (4.2\text{-}3)$$

while the velocity to bottom vane transfer function is:

$$\frac{v(s)}{\delta(s)} = \frac{-9.496(s+0.5715+j0.1485)(s-2.415)}{(s+0.01897+j0.2508)(s+1.546)(s-0.2846)} \qquad (4.2\text{-}4)$$

Using the proper $\underline{\Delta}$ vector from Table IV.2-3, the two transfer functions are added together to form P_{22}, i.e.,

$$P_{22} = \frac{v(s)}{\delta(s)} = \frac{-3.143(s-12.29)(s+0.4202+j0.4092)}{(s+0.01897+j0.2508)(s+1.546)(s-0.2846)} \qquad (4.2\text{-}5)$$

which is non-minimum phase. Using this P_{22} transfer function results in μ- values with RHP poles. For this transfer function to be minimum phase the condition

$$\Delta_5 < \Delta_4 \qquad (4.2\text{-}6)$$

must be satisfied. However Δ_5 must not be too small. This places much more control emphasis on the top vanes, possibly leading to their saturation during a maneuver or after a failure. This, in turn, can lead to the loss of aircraft control from effects of nonlinear elements(such as limit cycles). As a compromise, Δ_5 is chosen as 0.926. This delta value results in a minimum phase system and also leads

to a zero at s = -88.7 which cancels out the pole of the reversing vane servos, simplifying the final transfer function. The resulting $\tilde{P}_{22}$ before multiplying by the servo transfer function is:

$$\tilde{P}_{22} = \frac{0.2027(s+88.7)(s+0.3661+j0.4445)}{(s+0.01897+j0.2508)(s+1.546)(s-0.2846)} \qquad (4.2\text{-}7)$$

This modification of the $\underline{\Delta}$ vectors is required for each flight condition in order to guarantee minimum phase plants. The modified $\underline{\Delta}$ vectors are in Table IV.2-4. Using the modified $\underline{\Delta}$ vectors, the $\tilde{P}$ transfer functions are calculated and are then multiplied by their respective servo transfer functions. The canard, ailerons, and stabilator servo transfer function is:

$$\frac{\delta(s)}{\delta_{com}(s)} = \frac{2.28(10^6)}{(s+30.62)(s+138.6+j235.1)} \qquad (4.2\text{-}8)$$

TABLE IV.2-4

Modified Delta Vectors

Flight Condition	1	2	3
Δ_1	1.000	1.000	1.000
Δ_2	-0.5948	-0.6357	-0.7191
Δ_3	-0.8514	-0.5681	-0.2303
Δ_4	-1.000	-1.000	-1.000
Δ_5	0.926	0.95	0.98

The servo transfer function for the top and bottom vanes is:

$$\frac{\delta(s)}{\delta_{COM}(s)} = \frac{89}{s + 89} \qquad (4.2\text{-}9)$$

With the servo transfer functions, the $\tilde{P}$ matrices for the three flight conditions are calculated using the modified vectors and are in Tables IV.2-5 through IV.2-7. Now that a satisfactory plant model is designed, QFT reconfigurability theory can be applied as discussed in Chapter III.

IV.3 Tracking Specifications

In a control problem one is seldom confronted with the situation where a specific response to an input is required. Usually a range of acceptable responses is specified. QFT provides the minimum bandwidth compensators which guarantee that the closed-loop response remains within the assigned tolerances over the given range of the plant parameter uncertainty. The acceptable responses are often defined in either the time domain or the frequency domain. If they are in the former they can be converted to the latter. This step is essential since QFT design is performed in the frequency domain.

From data provided by McDonnell Douglas[6], ranges of frequency response for both velocity and flight path angle are defined. For the velocity, the desired response is a single order system

$$T(s) = \frac{5a}{s + a} \qquad (4.3\text{-}1)$$

where 'a' can range between 0.6 and 1.0 . The lower bound

TABLE IV.2-5

$\tilde{P}$ Matrix Elements for Flight Condition One

$$\tilde{P}_{11} = 94692(s+34.51)(s+0.01850\pm j0.2568)/\Delta_1$$

$$\tilde{P}_{12} = -6.668(s+16.87)(s+0.01834\pm j0.2576)/\Delta_2$$

$$\tilde{P}_{21} = -6438000(s+26.41)(s+0.3369\pm j0.4395)/\Delta_1$$

$$\tilde{P}_{22} = 62.54(s+88.7)(s+0.3661\pm j0.4445)/\Delta_2$$

$$\Delta_1 = (s+30.62)(s+138.6\pm j235.1)(s-0.2846)(s+1.546)(s+0.01897\pm j0.2508)$$

$$\Delta_2 = (s+1.546)(s-0.2846)(s+0.01897\pm j0.2508)(s+89)$$

TABLE IV.2-6

$\tilde{P}$ Matrix Elements for Flight Condition Two

$$\tilde{P}_{11} = 95025(s+46.83)(s+0.01510\pm j0.2178)/\Delta_3$$

$$\tilde{P}_{12} = -5.269(s+19.39)(s+0.01480\pm j0.2182)/\Delta_4$$

$$\tilde{P}_{21} = -7008144(s+26.33)(s+0.6516\pm j0.2793)/\Delta_3$$

$$\tilde{P}_{22} = 44.64(s+91.19(s+0.6973.j0\pm 2348)/\Delta_4$$

$$\Delta_3 = (s+30.62)(s+138\pm j235.1)(s+1.979)(s-0.3851)(s+0.01104\pm j0.2081)$$

$$\Delta_4 = (s+1.979)(s-0.3851)(s+0.01104\pm j0.2081)(s+89)$$

TABLE IV.2-7

$\tilde{P}$ Matrix Elements for Flight Condition Three

$$\tilde{P}_{11} = 122711(s+79.60)(s+0.01050\pm j0.1459)/\ \Delta_5$$

$$\tilde{P}_{12} = -3.505(s+27.24)(s+0.01060\pm j0.1472)/\ \Delta_6$$

$$\tilde{P}_{21} = -6146000(s+32.98)(s+0.3911\pm j1.084)/\ \Delta_5$$

$$\tilde{P}_{22} = 20.06(s+92.29)(s+0.4517\pm j1.150)/\ \Delta_6$$

$$\Delta_5 = (s+30.62)(s+138\pm j235.1)(s-0.4608)(s+2.686)$$
$$*(s+0.003206\pm j0.1090)$$

$$\Delta_6 = (s+89)(s-0.4608)(s+2.686)(s+0.003206\pm j0.1090)$$

transfer function is

$$T_{v_L}(s) = \frac{3.0}{s + 0.6} \qquad (4.3\text{-}2)$$

while the upper tracking bound is

$$T_{v_U}(s) = \frac{5.0}{s + 1.0} \qquad (4.3\text{-}3)$$

In the time domain $T_{v_L}(s)$ has the step response specifications:

Rise time(t_r)	=	3.662 s
Settling time(t_s)	=	6.520 s
Peak value(M_p)	=	5.000 ft/sec
Final value(F_v)	=	5.000 ft/sec

Likewise, the upper bound specifications are:

Rise time	=	2.197 s
Settling time	=	3.912 s
Peak value	=	5.000 ft/sec
Final value	=	5.000 ft/sec

Figure IV.3-1 shows the time responses for both the upper and lower velocity response bounds.

It is essential in any practical design that at large ω, the permissable range of $|T(jw)|$ exceed the range of $|P(jw)|$. This is always guaranteed if an infinite difference between the upper and lower bound is specified as $\omega \to \infty$. Stated more succinctly:

$$\lim_{s \to \infty} \left[Lm \left[T_U(s) - T_L(s) \right] \right] = \infty \qquad (4.3\text{-}4)$$

One way to do this that works well is to add a zero to T_{v_U}

and a pole to T_{v_L} . This gives an order of two difference between the bounds and ensures an infinite spread as $\omega \rightarrow \infty$. The required poles and zeros for this purpose are added as close as possible, subject to the time response being negligibly affected - this is easily done on the computer. The first choice can be very far off. If no great deviation in time response is noticed, the pole and/or zero can be brought in toward the origin. This is continued until an excessive deviation in time response results, after which it is backed out a bit. This thesis uses a 5 percent deviation in tne settling time and/or rise time as the limit of pole/zero movement. For the velocity reponse upper bound a zero cannot be added realistically since it is a first order transfer function, instead two poles are added to T_{v_L} to give the same effect. These modified upper and lower bound velocity transfer functions are:

$$T_{v_U}(s) = \frac{5.0}{(s + 1)} \qquad (4.3\text{-}5)$$

and

$$T_{v_L}(s) = \frac{2100}{(s + 0.6)(s + 20)(s + 35)} \qquad (4.3\text{-}6)$$

Tne resulting frequency response bounds for velocity are in Figure IV.3-2 . The range between T_{v_U} and T_{v_L} gives the set of allowable frequency responses that result in the desired time responses.

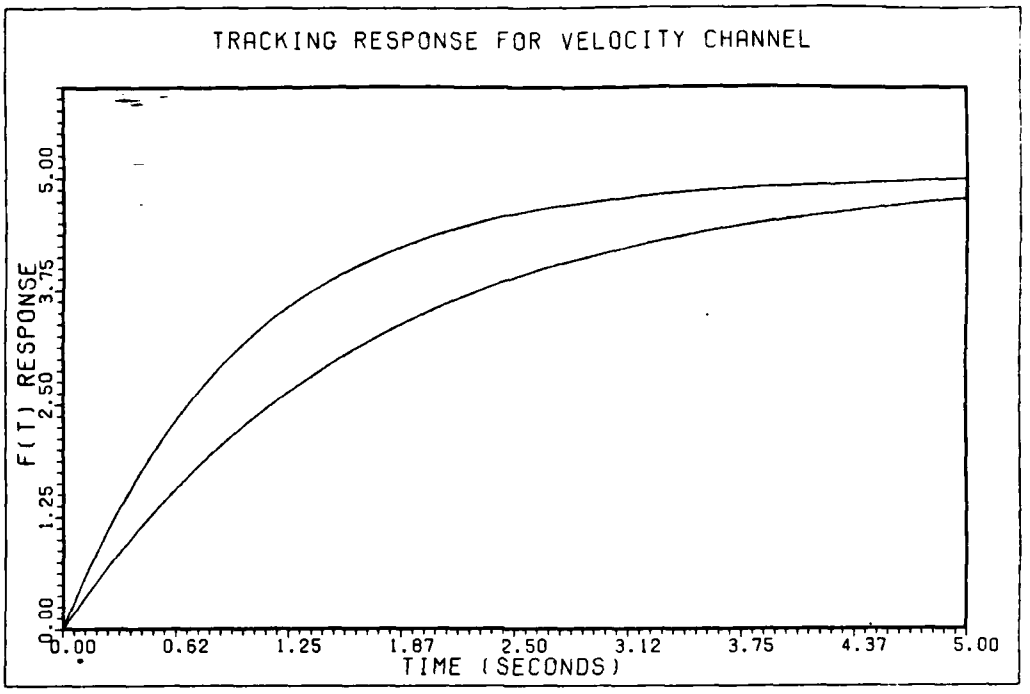

Fig.IV.3-1: Velocity Channel Time Response Bounds

The tolerances of the flight path angle are assumed to be the same as that of the angle of attack(AOA) since the flight path angle is a linear function of both the angle of attack and the pitch angle. The desired response is a second order transfer function

$$T(s) = \frac{G\omega_N^2}{s^2 + 2\zeta\omega_n s + \omega_n^2} \qquad (4.3\text{-}7)$$

where

G is 0.06109 rad/in = 3.5 deg/in

ζ can range from 0.35 to 1.2

minimum bandwidth $\omega > 3$ rad/sec

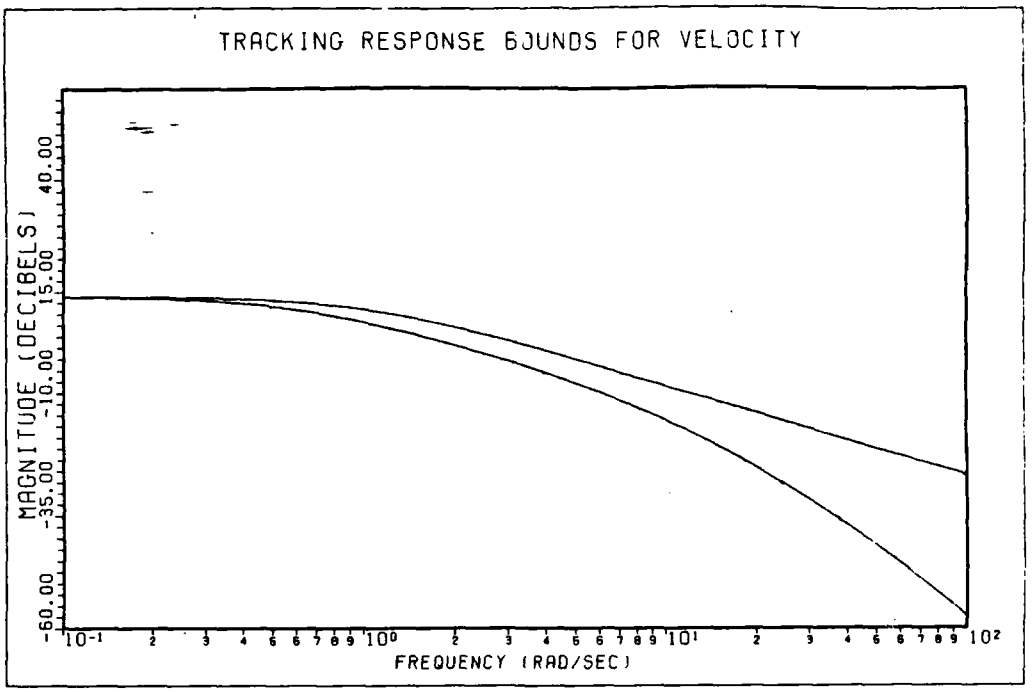

Fig.IV.3-2: Velocity Channel Frequency Response Bounds

For the overdamped case, a transfer function that meets the specifications is

$$T_{\alpha_L}(s) = \frac{196}{(s+4)(s+14)} \qquad (4.3\text{-}8)$$

The bandwidth of T_{α_L} is slightly more than 3 rad/sec. Since this is an overdamped case without a resonant frequency peak, it is natural to think of T_{α_U} as the lower bound. For the upper bound, with a ζ of 0.35, a maximum crossover frequency of 10 rad/sec is used. This is a reasonable value selected on the basis of conversations with personnel from the Air Force Flight Dynamics Laboratory[22]. The upper bound transfer function is:

$$T_{\alpha_u}(s) = \frac{350}{s^2 + 7s + 100} \qquad (4.3\text{-}9)$$

The respective figures of merit for the time responses of the

AOA bounds are, for the lower bound:

Rise time = 0.5859 s

Settling time = 1.062 s

Peak value = 3.500°

Final value = 3.500°

and for the upper bound

Rise time = 0.1389 s

Peak time = 0.3354 s

Settling time = 1.098 s

Peak value = 4.582°

Final value = 3.500°

The plots of the time response bounds for AOA are in Figure IV.3-3 .

As is done earlier with the velocity response the transfer functions are modified to provide an infinite separation of T_{α_L} and T_{α_U} as $\omega \rightarrow \infty$. A zero is added to T_{α_U} and a pole to T_{α_L}. The resulting bounds are:

$$T_{\alpha_U}(s) = \frac{7(s+50)}{s^2 + 7s + 100} \qquad (4.3\text{-}10)$$

$$T_{\alpha_L}(s) = \frac{3920}{(s+4)(s+14)(s+20)} \qquad (4.3\text{-}11)$$

Figure IV.3-4 shows the resulting frequency bounds.Again the bounded area represents the range of frequency responses which satisfy the given specifications. The next step is to determine the bounds on disturbance rejection.

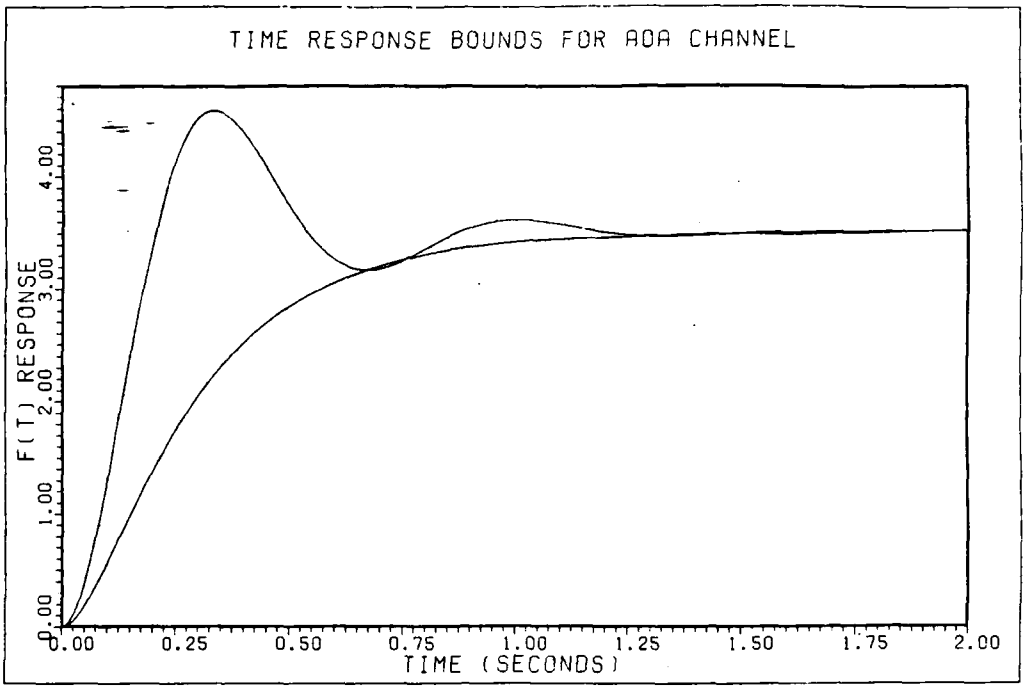

Fig.IV.3-3: AOA Step Response

IV.4 Disturbance Rejection Specifications

Since the type of aircraft this thesis uses as a basis for reconfigurable controller design is just in the preliminary design stages itself, the basic control laws are still in development. The desired disturbance rejection has not been established at the time of this writing, but from discussions with FDL personnel[**22**] the level has been set at $|t_{12}| = |t_{21}| < -10dB$ for all flight conditions for the healthy aircraft. Under failure the ideal situation is to meet the same bounds; however, the remaining surface deflections, and the required compensator bandwidth, may become too large for a realistic design. In this case the disturbance rejection bounds are sacrificed for stability in

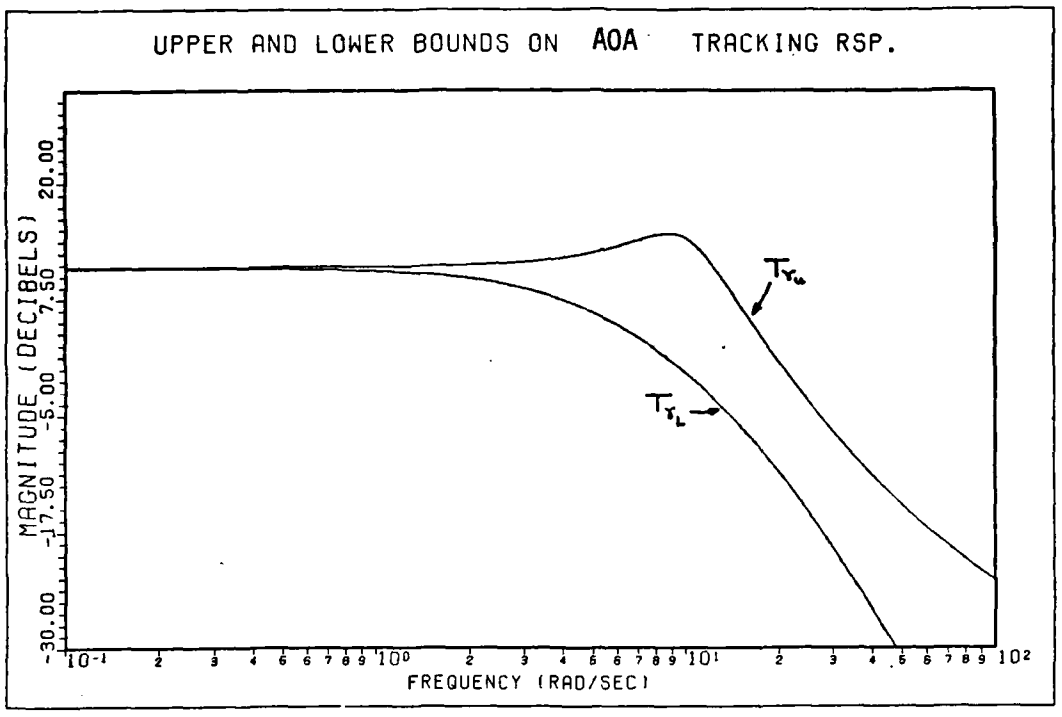

Fig.IV.3-4: AOA Frequency Response Bounds

the event of control surface failures. QFT is very transparent and allows the designer to see the "cost of feedback" for the various failures. It gives a direct indication of whether or not the failure in question leads to an unrealistic loop bandwidth. If it does the designer knows it before the compensator is designed.

IV.5 Application of Reconfiguration Theory

With the equivalent plant equations defined the calculation of the ideal μ_{ij} terms is required to develop the Q matrices (that decompose the 2X2 MIMO system into 4 SISO systems) for the reconfigurable system. For no-failure conditions the P matrix should be basically noninteracting (BINA) which means that the main diagonal terms dominate, giving good decoupling even without feedback.

Configuring the plant in this manner leads to smaller loop transmission bandwidths. A method using ideal crossfeed terms μ_{21} and μ_{12} is developed in Chapter III. These ideal μ_{ij} terms are defined in equations 3.4-1 through 3.4-7 . Using the equivalent plant matrices in Tables IV.2-3 through IV.2-7 the individual μ_{ij} terms are calculated. As a sample calculation, at flight condition one the μ_{12} term is

$$\mu_{12} = \frac{7.042(10^{-5})(s+16.87)(s+30.62)(s+138.6+j235.1)}{(s+34.51)(s+89)} \quad (4.5\text{-}1)$$

Likewise the μ_{21} term is:

$$\mu_{21} = \frac{102942(s+26.41)}{(s+30.62)(s+138.5+j235.1)} \quad (4.5\text{-}2)$$

The rest of the μ's are developed in the same manner and are in Table IV.5-1. With the μ values the plant matrix becomes:

$$\underline{P}' = \begin{bmatrix} \tilde{P}_{11} + \mu_{21}\tilde{P}_{12} & \tilde{P}_{12} + \mu_{12}\tilde{P}_{11} \\ \tilde{P}_{21} + \mu_{21}\tilde{P}_{22} & \tilde{P}_{22} + \mu_{12}\tilde{P}_{21} \end{bmatrix} \quad (4.5\text{-}3)$$

Using Eq(4.5-3) the equivalent reconfigurable plant matrices composing $\underline{P}'$ for the first flight condiditon are:

$$P'_{11} = \frac{1.639(s-0.4618)(s+5.772)(s+134.2+j221.3)}{(s+30.62)(s+138.6+j235.1)(s+89)} \cdot \frac{(s+23.45)(s+7.257)}{(s+1.546)(s-0.2846)(s+0.01897+j0.2508)} \quad (4.5\text{-}4)$$

$$P'_{12} = P'_{21} = 0.0 \quad (4.5\text{-}5)$$

TABLE IV.5-1

μ Terms Used to Give BNIA Systems Over the Three Flight Conditions

Flight Condition One:

$$\mu_{12} = \frac{7.042(10^{-5})(s+16.87)(s+30.62)(s+138.6\pm j235.1)}{(s+34.51)(s+89)}$$

$$\mu_{21} = \frac{102942(s+26.41)}{(s+30.62)(s+138.6\pm j235.1)}$$

Flight Condition Two:

$$\mu_{12} = \frac{5.545(10^{-5})(s+19.39)(s+30.62)(s+138.6\pm j235.1)}{(s+46.83)(s+89)}$$

$$\mu_{21} = \frac{156992(s+26.33)}{(s+30.62)(s+138.6\pm j235.1)}$$

Flight Condition Three:

$$\mu_{12} = \frac{2.856(10^{-5})(s+27.24)(s+30.62)(s+138.6\pm j235.1)}{(s+79.60)(s+89)}$$

$$\mu_{21} = \frac{306381(s+0.3911.j1.084)}{(s+0.4517\pm j1.150)(s+138.6\pm j235.1)}$$

$$P'_{22} = \frac{405.9(s+0.2524+j0.4044)(s+4.912)}{(s+30.62)(s+138.6+j235.1)(s+89)(s+1.546)} \cdot \frac{(s+140.3+j240.2)(s+1.642)}{(s-0.2846)(s+0.01897+j0.2508)} \qquad (4.5\text{-}6)$$

Note that these μ terms, even though they are minimum phase, have resulted in a non-minimum phase plant transfer functions. It turns out that the plant determinant is also non-minimum phase, but this stems from the choice of Δ rather than μ terms(since these can be factored out of the determinant expression). This also occurs using the other vectors as shown in Table IV.5-2. Non-minimum phase determinants limit the loop transmission bandwidth and can cause instability using the MIMO QFT design process. For either problem re-examination is required, or an extension of QFT for non-minimum phase plants, the "Singular G" method should be used[23]. Singular G is beyond the scope of this thesis, thus the $\underline{\Delta}$ vector is examined to see if it can be used to drive the system minimum phase.

Upon a close examination of the aircraft and the related equations of motion and resulting matrices, the main cause of problems seem to be the close coupling of v and α within the plant and their respective signs. With the current scheme of choosing the $\underline{\Delta}$ vector, as explained above, the equivalent plant before the reconfigurable μ terms are added is:

TABLE IV.5-2

Equivalent Plant Transfer Functions

Flight Condition One:

$$P'_{11} = 1.64(s-0.462)(s+5.77)(s+134\pm j221)(s+23.5)(s+7.26)/\Delta_1$$

$$P'_{12} = P'_{21} = 0$$

$$P'_{22} = 405(s+0.252\pm j0.404)(s+4.91)(s+140\pm j240)(s+1.64)/\Delta_1$$

Flight Condition Two:

$$P'_{11} = 2.42(s+0.892)(s+0.049\pm j0.407)(s+32.5)(s+133\pm j247)/\Delta_2$$

$$P'_{12} = P'_{21} = 0$$

$$P'_{22} = 128(s-0.484)(s+2.33)(s+0.385)(s+135\pm j245)(s+35.4)/\Delta_2$$

Flight Condition Three:

$$P'_{11} = 3.15(s+0.0052\pm j0.183)(s+42.9)(s-0.688)(s+134\pm j222)/\Delta_3$$

$$P'_{12} = P'_{21} = 0$$

$$P'_{22} = 164(s-0.476)(s+0.89)(s+2.53)(s+42.5)(s+134\pm j237)/\Delta_3$$

$$\Delta_1 = (s+30.6)(s+138\pm j235)(s+89)(s+1.55) * (s-0.285)(s+0.0189\pm j0.251)$$

$$\Delta_2 = (s+30.6)(s+138\pm j235)(s+89)(s1.98) * (s-0.385)(s+0.011\pm j0.208)$$

$$\Delta_3 = (s+30.6)(s+138\pm j235)(s+89)(s+2.69) * (s-0.461)(s+0.00321\pm j0.109)$$

$$\underline{\tilde{P}} = \begin{bmatrix} |\tilde{P}_{11}| & -|\tilde{P}_{12}| \\ -|\tilde{P}_{21}| & |\tilde{P}_{22}| \end{bmatrix} \qquad (4.5\text{-}7)$$

where the $|P_{ij}|$ operation causes the leading gain value in the transfer function to be greater than zero(an 'absolute value' type function). As stated earlier , the μ values are:

$$\mu_{12} = - - |\tilde{P}_{12}| / |\tilde{P}_{11}| = |\tilde{P}_{12}| / |\tilde{P}_{11}| \qquad (4.5\text{-}8a)$$

$$\mu_{21} = - - |\tilde{P}_{21}| / |\tilde{P}_{22}| = |\tilde{P}_{21}| / |\tilde{P}_{22}| \qquad (4.5\text{-}8b)$$

Using these, the reconfigurable equivalent plant is:

$$\underline{P'} = \begin{bmatrix} |\tilde{P}_{11}| - \left(|\tilde{P}_{21}| / |\tilde{P}_{22}|\right)|\tilde{P}_{12}| & -|\tilde{P}_{12}| + \left(|\tilde{P}_{12}| / |\tilde{P}_{11}|\right)|\tilde{P}_{11}| \\ -|\tilde{P}_{21}| + \left(|\tilde{P}_{21}| / |\tilde{P}_{22}|\right)|\tilde{P}_{22}| & |\tilde{P}_{22}| - \left(|\tilde{P}_{21}| / |\tilde{P}_{22}|\right)|\tilde{P}_{21}| \end{bmatrix} \qquad (4.5\text{-}9)$$

Note that to zero out the off diagonal terms of $\underline{P'}$ a subtraction of positive, minimum phase transfer functions, occurs to develop each P'_{ii} . The different dynamics of the velocity control channel compared with the AOA channel seem to result in the non-minimum phase plants when the addition using μ's is accomplished. In order to circumvent this problem various combinations of different $\underline{\Delta}$ vectors that, see from the surface, might give minimum phase plants are chosen. The det[$\underline{P'}$] is calculated for various failure conditions and $\underline{\Delta}$ vectors, again without finding a minimum phase $\underline{P'}$. In each case at least one zero is in the RHP.

At this point it becomes evident that some

problem modification is required to provide a solution to this problem using QFT without using the "Singular G" method. As a simplification measure, the second order servo poles are deleted. The assumption is that the final loop transmissions will have a small enough bandwidth not to excite the neglected servo poles, or have the additional phase lag drive the system unstable. To guarantee that combinations of control surfaces will result in minimum phase plants, the plant determinant must not have RHP zeros. The determinant of $\underline{P}'$ is given by

$$P'_{11} P'_{22} - P'_{12} P'_{21} \qquad (4.5\text{-}10)$$

Factoring out the reconfigurable terms, the servo transfer functions, and the square of plant poles, results in the determinant being

$$\det[P'] = \frac{K(s+30.62)(s+89)}{(\text{plant poles})^2}(1-\mu_{12}\mu_{21}) \left[N(P_{11})N(P_{22}) - N(P_{12})N(P_{21}) \right] \qquad (4.5\text{-}11)$$

Where N(.) stands for the numerator of the transfer function in question. Only the term $[N(P_{11})N(P_{22}) - N(P_{12})N(P_{21})]$ can contain non-minimum phase terms(assuming $1-\mu_{12}\mu_{21}$ is minimum phase). This quantity expanded out with the $\underline{\Delta}$ vector terms and separate surface transfer functions (Appendix I) is:

$$\begin{aligned} &(P_{11} P_{24} - P_{14} P_{21}) + \psi(P_{11} P_{25} - P_{15} P_{21}) \\ &+ \Delta_2/\Delta_1 [P_{12} P_{24} - P_{14} P_{22} + \psi(P_{12} P_{25} - P_{15} P_{22})] \\ &+ \Delta_3/\Delta_1 [P_{13} P_{24} - P_{14} P_{23} + \psi(P_{13} P_{25} - P_{15} P_{23})] \end{aligned} \qquad (4.5\text{-}12)$$

where $\psi = \Delta_5 / \Delta_4$.

The separate difference terms can be combined to simplify the equation:

$$A_1 + \psi B_1 + \Delta_2/\Delta_1 (A_2 + \psi B_2) + \Delta_3/\Delta_1 (A_3 + \psi B_3) \qquad (4.5\text{-}13)$$

There are three unknowns in this expression: ψ, Δ_2/Δ_1, and Δ_3/Δ_1. The nominal plant used to develop $\underline{\Delta}$ is FC2:No Failures. The ψ value is chosen to make as many of the individual A_k, B_k pairs minimum phase as possible. Then the remaining Δ_2/Δ_1 and Δ_3/Δ_1 terms are picked to de-emphasise any remaining non-minimum phase tendencies. The vector chosen is:

$$\underline{\Delta}^T = [\ -1 \quad 1 \quad 1 \quad 1 \quad -0.6\ ]$$

This vector also results in minimum phase plants at the other two flight conditions(no failures). Variations of individual Δ_i terms ±20% still resulted in minimum phase plants. In addition the plants remained minimum phase for the following failures at each flight condition:

a. Canards

b. Ailerons

c. Stabilators

d. Stabilators and Ailerons

e. Stabilators and Canards

Also at FC2 failure of the bottom vanes results in minimum phase $\underline{P}'$. Top reversing vane failure never results in a minimum phase plant. Other $\underline{\Delta}$ vectors have been tried,

however the above $\underline{\Delta}$ vector gave the most minimum phase plants with failures out of all $\underline{\Delta}$ tried. In other word, that particular $\underline{\Delta}$ results in the 'robustest' behavior. Even with the plant being minimum phase the diagonal elements were not dominant, signified by the determinant being negative. For diagonal dominance the columns are swithched, and the signs of the individual Δ_i terms changed to flip the sign of the determinant. Physically this means that the role of primary control of the variables has changed. The aerodynamic surfaces are now controlling velocity while the reversing vanes are controlling AOA. This result is interesting since it is opposite of what one would think is logical. The switch seems to stem from forcing P' into minimum phase behavior to use QFT(but not caused by QFT directly). Why this happens is not clear; however, for small signals the approximation should still be valid.

The $\underline{\Delta}$ vector is now:

$$\underline{\Delta}^T = [\ 1.0 \quad -1.0 \quad -1.0 \quad -1.0 \quad 0.6]$$

The $\underline{P}'$ matrices used in loop design are in Appendix D along with the equivalent $\underline{Q}$ matrices derived from them.

A moral to this story is that when dealing with a MIMO QFT design problem the very first step taken should be to find the range of weighting functions(Δ in this thesis) that results in minimum phase plant matrices before even thinking about division of control authority(or anything else). Without this characteristic the problem becomes much more difficult. If this had been done in this chapter several

weeks of work, as well as ten pages of writing, could have been spared. Had this fact been brought out at the beginning of this effort, possibly a $\underline{\Delta}$ vector could have been found to enable control of the flight path angle.

IV.6 Loop Bound Design L

Since it is desired that only AOA commands should command AOA, and likewise with velocity, the equivalent closed-loop SISO structure is in Figure IV.6-1 . Notice that f_{12} and f_{21} have been set to zero to reflect this. To begin the design of the loop transmissions, the designer must first decide which loop to design first. Loop 1, the AOA channel, has less uncertainty and smaller associated disturbance rejection bounds(as determined by looking at both the size of the plant templates and the area between tracking response frequency bounds), thus it is designed first. This is an empirical decision since the same steps are used to design both loops; however, beginning with the loop having the stricter tolerances leads to a design with smaller loop bandwidth. Plant templates for both Q_{11} and Q_{22} are drawn, and from this it is seen that Q_{11} has less area enclosed by the contour for every frequency, thus this loop is designed first.

The loop transmission L_1 must satisfy all its frequency bounds(derived from the plant uncertainty and performance tolerances). Examining each FC:Failure case it is

found that the transfer functions have the form:

$$\frac{K\ (\text{LHP Zeros})}{(\text{RHP Pole})(\text{LHP Poles})} \qquad (4.6\text{-}1)$$

where K is a positive constant. The plant template for Eq(4.6-1) is a line at low frequencies, becoming wider at middle frequencies, and narrows to a line as ω tends toward infinity.

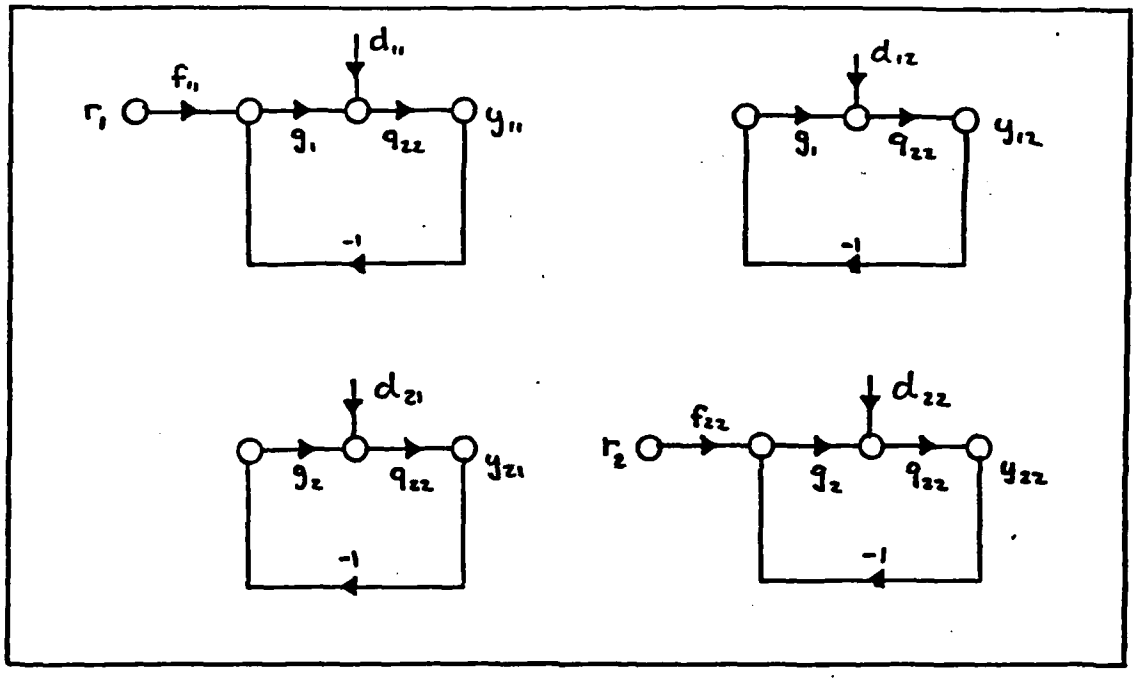

Fig.IV.6-1: Equivalent SISO Plants

In order to derive the frequency bounds for the disturbance rejection, $B_d(j\omega)$, it is noted that the output y_{21} is due to disturbance only since f_{12} is set to zero(a change in AOA for a velocity input is not desired). The output in this case is:

$$y = d_{12}\, Q_{11}/(1 + L_1) \qquad (4.6\text{-}2a)$$

$$= t_{22}\, Q_{11}/[Q_{12}\,(1 + L_1)] \qquad (4.6\text{-}2b)$$

Assuming the worst case, i.e.,set $t_{22} = b_{22}$,and also assume that the response is less than or equal to b_{12} , the disturbance rejection bound. Then

$$\left|y_{12}\right| = \left|b_{22} Q_{11} / [Q_{12} (1 + L_1)]\right| \leq b_{12} \qquad (4.6\text{-}3a)$$

rearranging

$$\left|1/(1 + L_1)\right| \leq \left|b_{12} Q_{12} / [b_{22} Q_{11}]\right| \qquad (4.6\text{-}3b)$$

This must be investigated for each flight condition and failure case. Q_{11} and Q_{12} at each FC:Failure case are used to find the most demanding bounds. The FC2:Stabilator Failed case is chosen as the nominal plant. At low frequencies it is normally located on the left side of the template, close to, if not at, the bottom point of the template. Such a choice makes it easier, from the author's experience, for design of L_1 by moving the loop bounds lower on the Nichol's chart. Using this equation and the inverted Nichol's chart, bounds for L_1 can be found. However, if the frequency response data shows that $|L_1| \gg 1$, then the above equation is simplified to:

$$\left|L_1\right| > \left|b_{22} Q_{11} / [b_{12} Q_{12}]\right| \qquad (4.6\text{-}4)$$

or

$$\left|L_1\right| > \left|b_{22} Q_{11o} / [b_{12} Q_{12o}]\right| \qquad (4.6\text{-}5)$$

where Q_{11o} and Q_{12o} correspond to the FC:Failure that causes the worst bound. As long as $|L_1| \gg 1$, the bounds for L_1 are

plotted directly on the Nichol's chart. When $|L_1| = 1$ the inverted Nichol's chart is required . With the log-magnitude measure(Lm(x) = 20*log(x)), L_1 must satisfy

$$Lm(L_1) = Lm(b_{22}) + Lm(Q_{11}) - Lm(b_{12}) - Lm(Q_{12}) \quad (4.6\text{-}6)$$

From the specifications, $b_{12} = -10$ dB, while b_{22} is found in Figure IV.3-2 . The calculations show that $|1 + L_1|$ is very small for even low frequencies. This implies that L_1 is very close to the -1 + j0 point at those frequencies, well within the +4 dB contour on the Nichols chart chosen as the forbidden region. The reason that $|1 + L_1|$ is so small is that $|Q_{12}| \gg |Q_{11}|$, which makes sense since $|P'_{22}| \gg |P'_{12}|$. Thus the bounds on the first loop are determined by the output y_{11}. This output is composed of two parts: tracking, y_{11t}, and disturbance, y_{11d} where

$$y_{11t} = f_{11} Q_{11} g_1 /(1 + L_1) = f_{11} L_1 /(1 + L_1) \quad (4.6\text{-}7)$$

$$y_{11d} = d_{11} Q_{11} /(1 + L_1) = b_{21} Q_{11} /[Q_{12} (1 + L_1)] \quad (4.6\text{-}8a)$$

$$y_{11} = y_{11t} + y_{11d} \quad (4.6\text{-}8b)$$

The maximum value for the disturbance is

$$|y_{11d}| = |b_{21} Q_{11} /(Q_{12} L_1)| = |b_{21} /(Q_{12} g_1)| \quad (4.6\text{-}9)$$

for cases where $|L_1| \gg 1$. With $|Q_{12}| \gg |Q_{11}|$, $b_{21} > 1$, and $|L_1|$ larger than $|Q_{11}|$ at every frequency(which should be so since $L_1 = g_1 Q_{11}$, and realistic loops that provide sensitivity reduction tend to be larger than the plants they

contain), the disturbance output is very small when compared to the command output within the passband of f_{11} and can be ignored. At higher frequencies the disturbance may be larger than the tracking since y_{11t} may be smaller than y_{11d}. To meet specifications in this case L_1 must stay out of the forbidden region. This is done by translating the templates around the forbidden region and noting the trace of the nominal plant. This defines a zone that L_1 cannot be within at that frequency. In the tracking case with the disturbance small, the bound for L_1 satisfies the following equation:

$$\left| T_{max} - T_{min} \right| \leq \left| h_{11} - a_{11} \right| \qquad (4.6\text{-}10)$$

where T_{max} and T_{min} are the maximum and minimum closed loop magnitude line touched by the template respectively. Table IV.6-1 contains the tracking bounds for loop one. The lower bound is dropped in magnitude to ease the bounds on the first loop; however, any simplifications here are made up by wider bandwidths of f_{11} and the second loop's compensation. The plant templates for Q_{11} are in Figure IV.6-2 . The nominal plant is FC2:Canard Failed. From the Nichol's chart they are transferred to a clear sheet of plastic and using the previously defined tracking bounds, the bounds on L_1 are drawn and lie in Figure IV.6-3 . At low frequencies the bound for ω = 1 dominates since it is well above the bound for ω = 2 and ω = 4. For high frequencies the bounds wrap around the forbidden region, satisfying both the tracking and

AD-A163 939 RECONFIGURABLE FLIGHT CONTROL SYSTEM FOR A STOL (SHORT 2/3
TAKE-OFF AND LANDI..(U) AIR FORCE INST OF TECH
WRIGHT-PATTERSON AFB OH SCHOOL OF ENGI.. B T CLOUGH
UNCLASSIFIED DEC 84 AFIT/GE/ENG/85D-8 F/G 1/3 NL

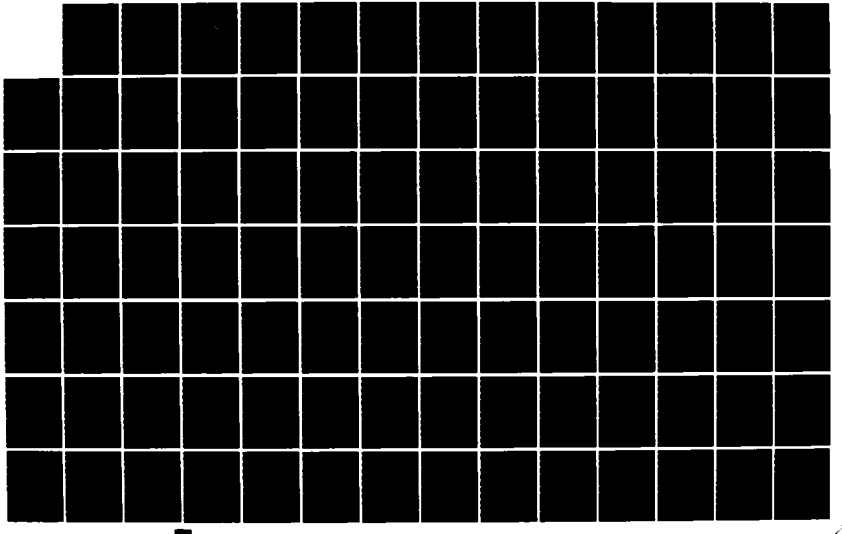

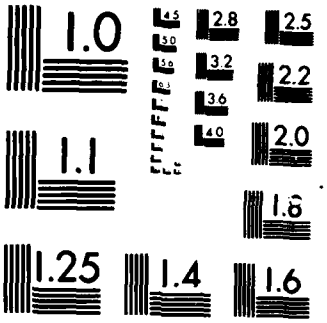

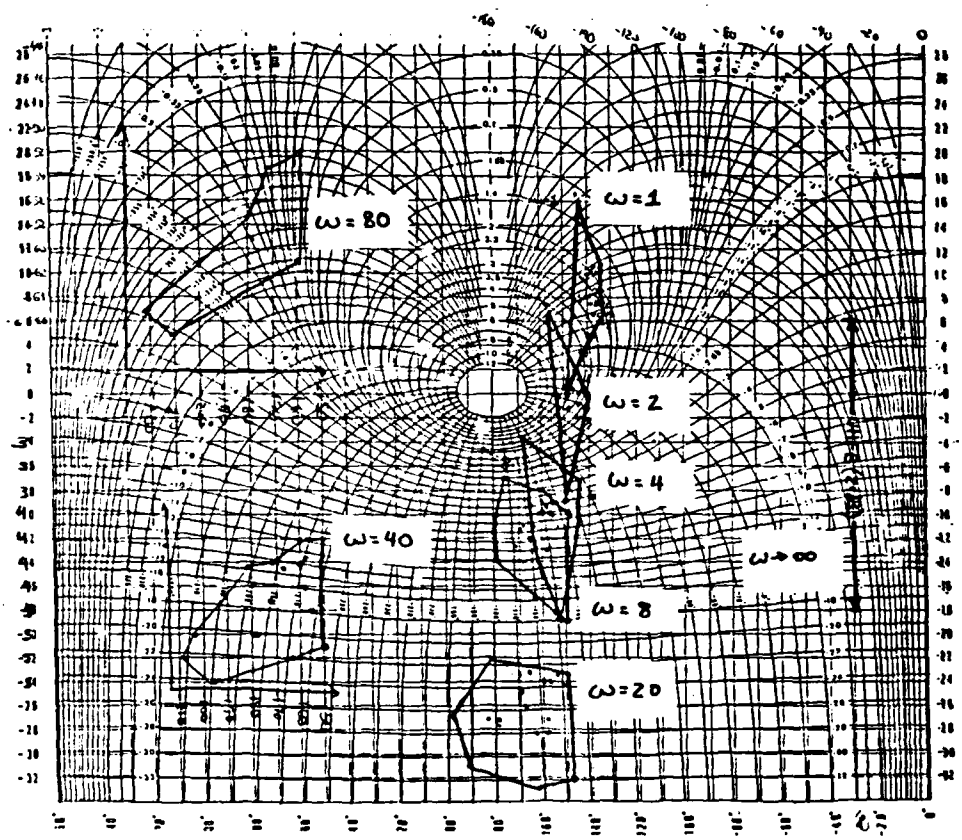

Fig.IV.6-2: Q_{11} Plant Templates

disturbance rejection cases, finally resulting in an UHFB 24 dB high. In designing the actual L_1 a choice has to be made as to the shape and magnitude of L_1. Since the open loop transfer function contains an unstable pole the Nyquist Stability Criterion should be used to establish what frequency characteristics the loop transmission should have for stability under feedback. A polar plot of an open- loop transmission containing an unstable pole which is stable for unity feedback is shown in Figure IV.6-4 .

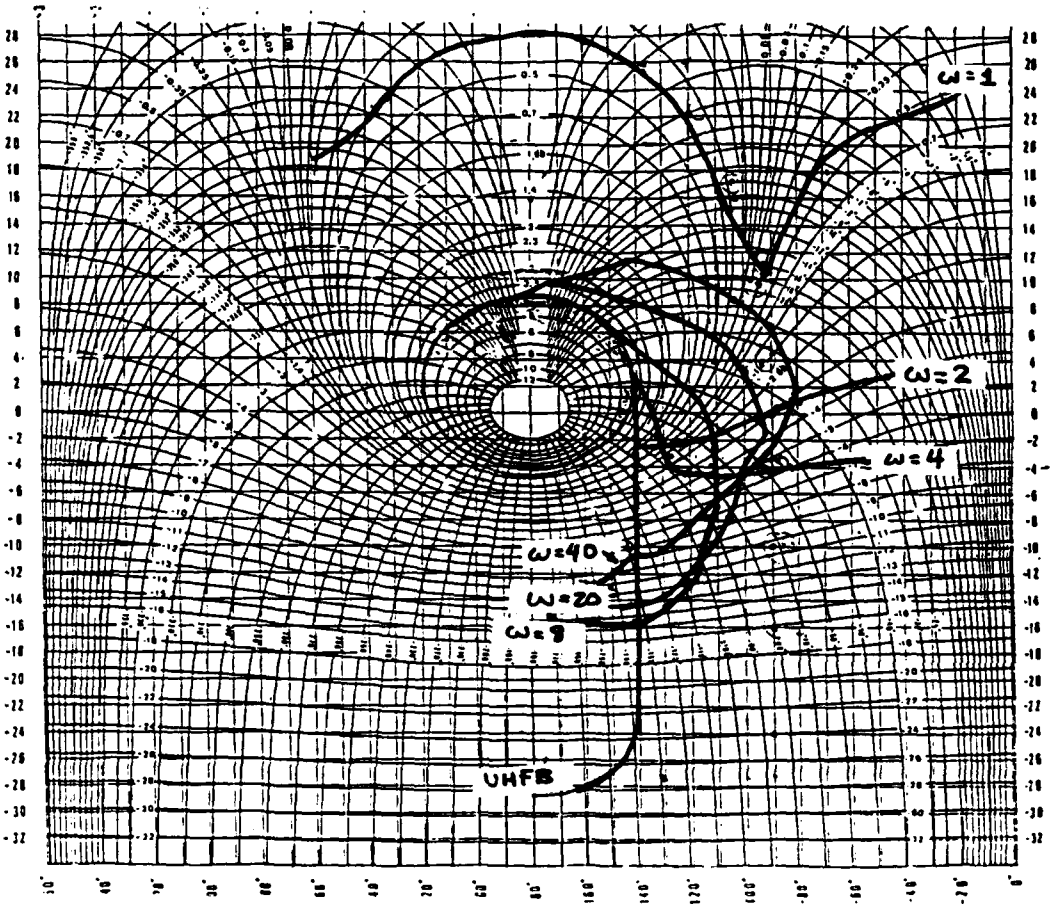

Fig.IV.6-3: Loop One Bounds

For a stable system Nyquist states that the number of RHP zeros must be equal to zero[13:144] . The equation which relates the number of these zeros to the number of open loop RHP poles and the number of encirclements of the -1 point is:

$$Z = N + P \qquad (4.6\text{-}11)$$

where

Z = Number of close-loop RHP zeros

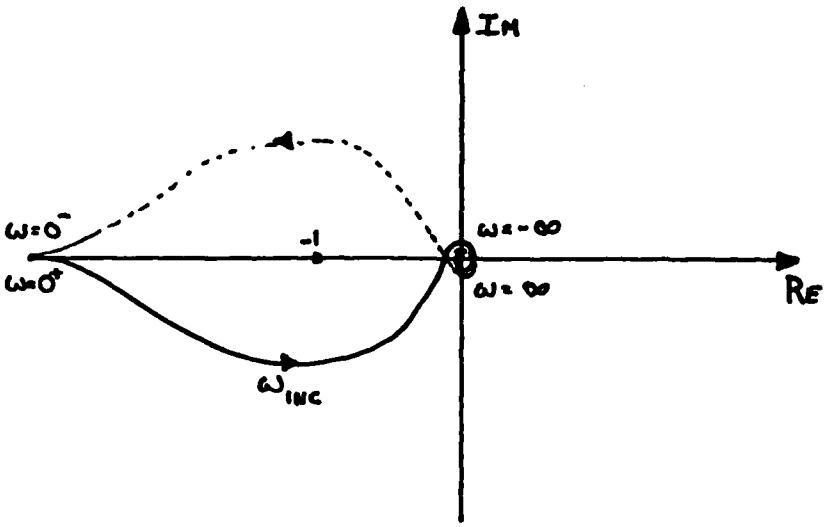

Fig.IV.6-4: Polar Plot of Loop Transmission with an Unstable Pole that is Stable for Unity Feedback

N = Number of clockwise encirclements of the -1 + j0 point.

P = Number of RHP poles.

Since P = 1 the -1 point must be circled -1 times (counterclockwise) in order for Z = 0. Since g_1 should contain minimum phase terms it is of the form:

$$g_1 = \frac{K \quad (\text{LHP zeros})}{(\text{LHP poles})} \qquad (4.6\text{-}12)$$

If $K > 0$ then only the minimum phase transfer functions can be used for a plant with one unstable pole and no RHP zeros. If $K < 0$ then the plants containing one RHP zero may be stable, but this implies that Q_{11} has a RHP zero which cannot be used with the form of QFT exploited in this thesis. This can be seen if a pole-zero plot of the system is made(Figure

IV.6-5). Using unity feedback and minimum phase compensation in the forward loop does not change the fact that a branch of the root locus starts at the open-loop RHP pole and migrates to the RHP zero as the gain is increased. The system is unstable for all positive(and most negative) gain. One of the possible stable loop transmissons(Figure IV.6-4) has a starting point of -180 degrees at $\omega = 0$. Since one pole is in the RHP, this means that this pole is included in L_1 ,thus giving the -180 degrees without any free integrations. This implies that L_1 is Type 0, and that some steady-state error to command inputs has to be tolerated. The amount of steady state error is dependent on the DC gain, the higher the better. But a high DC gain also means that several poles might have to be added to drop L_1 fast enough to just meet the bound at $\omega = 1$ to minimize the bandwidth. This results in the forced addition of several zeros just to bring L_1 to the right of the forbidden region. An L_1 with this shape is of fairly high order in both the numerator and denominator, leading to an even more complex g_1 . Also the system is conditionally stable at best, and a large gain change may drive the system unstable. On the other hand,an L_1 with a lower DC gain can be used to reduce the complexity of L_1 since no great drop has to occur to meet the bound at $\omega = 1$, but the steady state error increases. The smaller DC gain is chosen since the amount of steady state error which arises in the flight control system is felt to be tolerable.

compensator is cheaper to build using analog elements, and simpler to implement digitally.

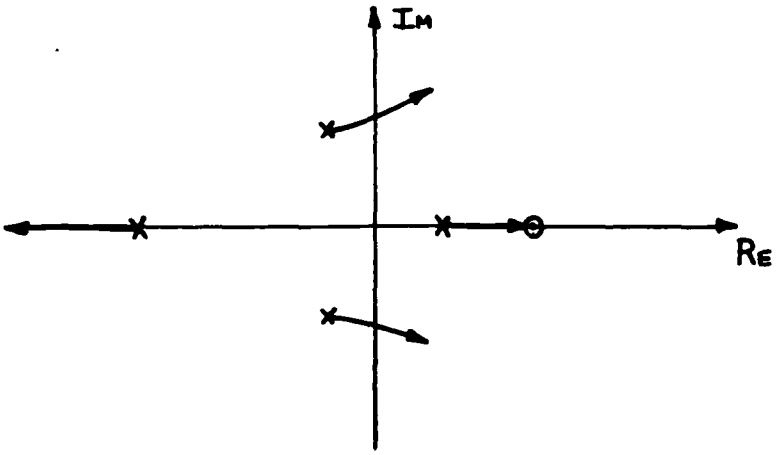

Fig.IV.6-5: Root Locus of Unstable Plant

When designing L_1 it is noted that that Q_{11} includes an unstable pole. This must be included in L_1 to avoid having an unstable compensator. One method for doing this is as follows. First L_1 is broken down into two parts:

$$L_1 = L_1' C \qquad (4.6\text{-}14)$$

TABLE IV.6-1

Original and Modified Difference Between b_{11} and a_{11} Tracking Bounds

Frequency ω (rad/s)	$Lm\{\Delta T(j\omega)\}$ (dB) Original	Modified
1.0	0.3677	0.3677
2.0	1.374	3.000
4.0	4.610	6.000
8.0	12.51	20.00
20.0	14.78	∞
40.0	20.89	∞
80.0	25.34	∞

wnere

$$C(s) = (s + 0.3851)/(s - 0.3851) \qquad (4.6\text{-}15)$$

C(s) contains the unstable pole. The zero could be placed anywhere, but placing it at the 'mirror' image of the unstable pole is analytically convenient. This can be seen from a frequency response plot of the above transfer function. C(jw) shows a straight line undergoing a 180 degree phase shift as $\omega \rightarrow \infty$ from -180° to 0°. This shifts L_1' from 0° to -180° at $\omega = 0$ to give the shape of L_1 required by the Nyquist stability criterion. L_1' is designed to start at 0° and satisfy the requirement that when it is multiplied by C(s) an L_1 is formed that satisfies all bounds. For the

bounds in Figure IV.6-3 , an L_{lo} that satisfies the bounds is

$$L_{lo} = \frac{1.515(10^6)(s + 0.3051)}{(s - 0.3851)(s + 0.2)(s + 200)(s + 600)} \qquad (4.6\text{-}16)$$

One can see how well L_{lo} meets its bounds by examining Figure IV.6-6 . L_{lo} is close to optimum at 1 rad/s and again at 20 rad/s, but far from the bounds at 2, 4, and 3 rad/s. To bring it in any closer at these points requires a much more complicated compensator which might not reduce the 3 dB bandwidth much from its current 13 rad/s position, and only gives slightly less high frequency response along with a higher resonant peak around 2 rad/s. Figure IV.6-7 is a Bode plot of L_{lo} (phase suppressed). For this L_{lo} the required compensator g_1 is

$$g_1 = \frac{2.37(10^5)(s+0.3851)(s+0.6067+j0.3576)}{(s+0.2)(s+200)(s+600)(s+0.6124)} \cdot \frac{(s+11.56)(s+53.88)(s+1.973)}{(s+1.153)(s+7.728)(s+22.25)} \qquad (4.6\text{-}17)$$

Figure IV.6-8 contains the frequency response of g_1 , and shows that it looks like a lead-lag filter. Looking at a root locus of the system, the for high compensator gain values the unstable open-loop pole migrates across the j axis to an open-loop zero. This again illustrates why a non-minimum phase zero cannot be used here. This zero is unaffected by feedback, and under high gain conditions an open-loop pole migrates to that zero, making the system unstable.

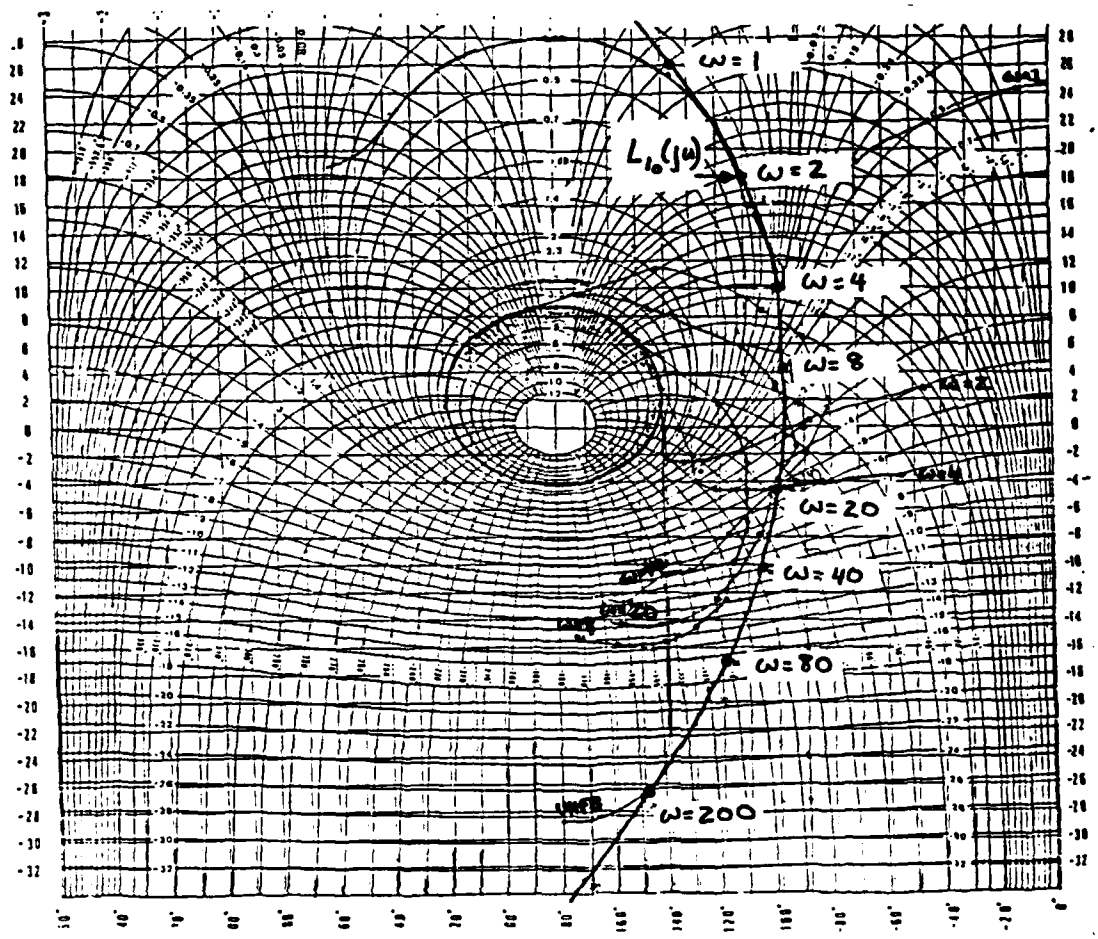

Fig.IV.6-6: Loop Transmission L_{1_0}

Using the method outlined in Chapter III and given in detail in reference[9]the prefilter f_{11} turns out to be a simple first order lag:

$$f_{11} = \frac{13.9}{(s + 4)} \qquad (4.5\text{-}18)$$

The frequency response of f_{11} is in Figure IV.6-9 showing its 3 dB bandwidth to be about 20 rad/s.

Even though g_1 leads to the desired loop transfer function it also leads to a complex compensator, being 6th over 7th order. From Figure IV.6-3 it seems as if

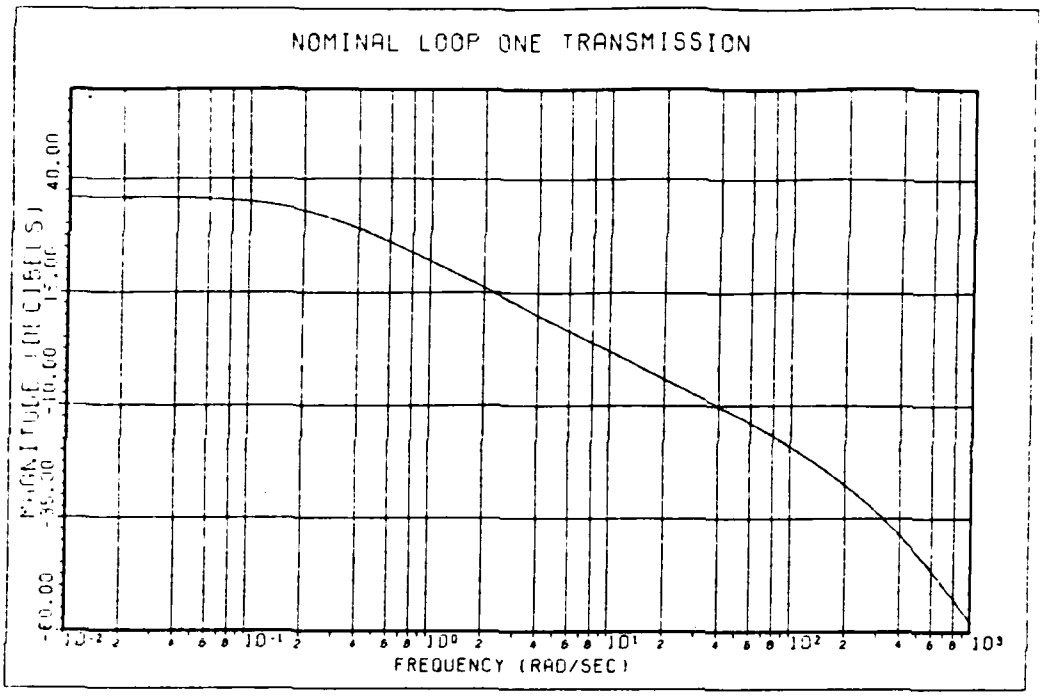

Fig.IV.6-7: Log Magnitude of L_{1o} Verses Frequency

the compensator can be simplified. A transfer function which mimics the shape of g_1 is:

$$g_1 = \frac{1.926(10^6)(s + 6)}{(s + 100)(s + 600)} \qquad (4.6\text{-}19)$$

This compensator leads to a greater bandwidth since it tends to have a greater gain at each frequency than the exact compensator. A comparison of the two AOA channel compensators is in Figure IV.6-10 . When the simplified compensator is multiplied by the nominal plant and the loop closed, the resulting bandwidth is 13 rad/s, higher as classical control theory predicts. The simpler compensation is used in the simulation to keep the order of the whole system at a minimum to reduce simulation costs and computer loading.

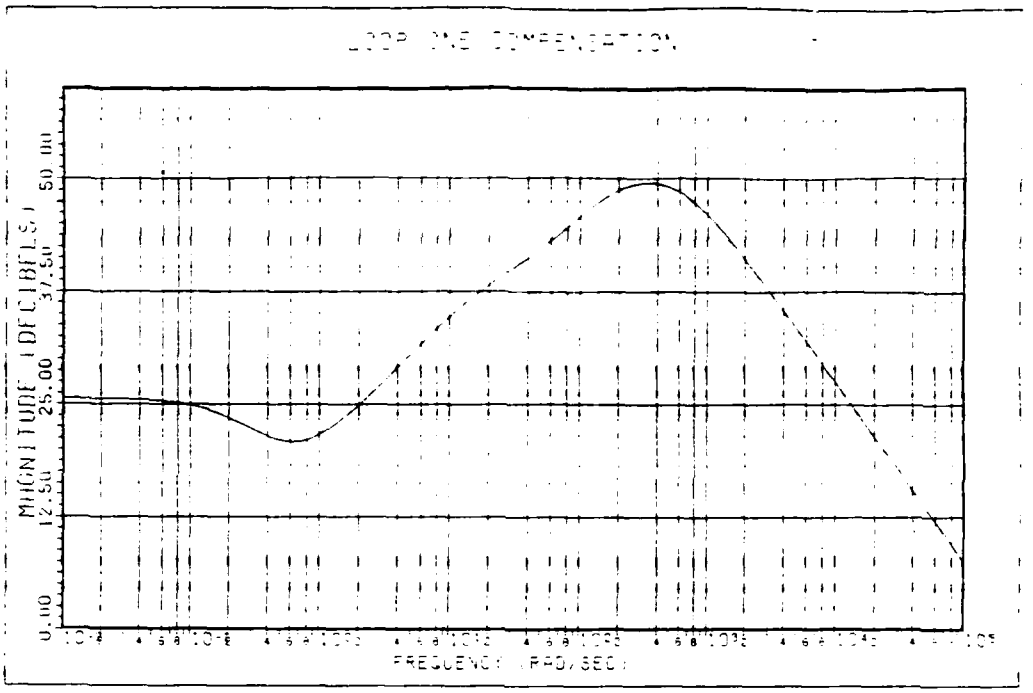

Fig.IV.6-8: Frequency response of Compensation, g_1

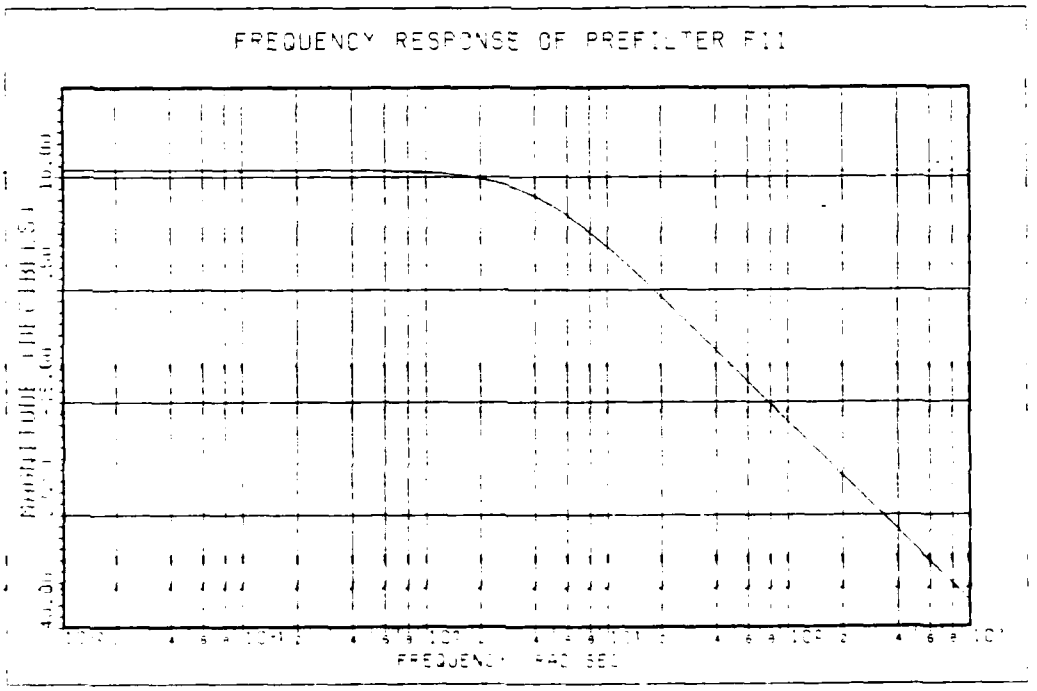

Fig.IV.6-9: Prefilter f_{11} Frequency Response

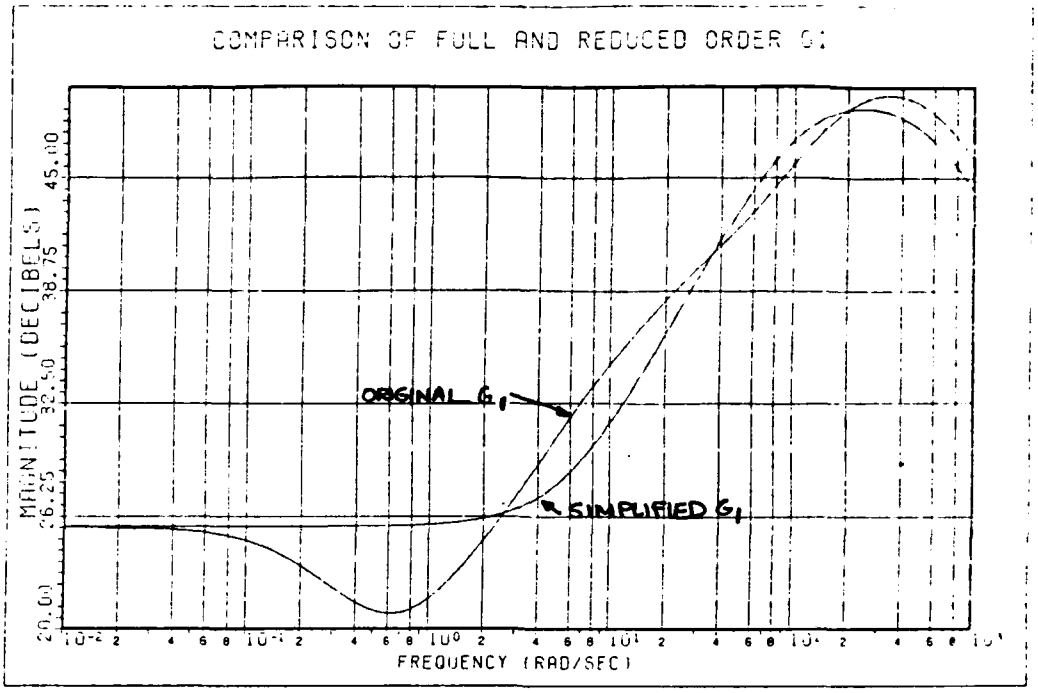

Fig.IV.6-10: Comparison of Full and Reduced Order Loop One Compensators

IV.7 Design of Second Loop Compensation

Once the first loop is designed, the knowledge of that first loop compensation is used to give more exact(more optimal in the sense of minimizing bandwidth) compensation for the second loop[18]. The exact equations for t_{12} and t_{11} are subsituted into the equations for t_{21} and t_{22} to give

$$t_{22} = f_{22} L_{2e}/(1 + L_{2e}) \qquad (4.7\text{-}1)$$

where

$$L_{2e} = g_2 Q_{22e}$$

$$= q_2 Q_{22} (1 + L_1)/(1 + L_1 - \gamma_1) \qquad (4.7\text{-}2)$$

with —

$$\gamma = Q_{11} Q_{22} / (Q_{12} Q_{21}) \qquad (4.7\text{-}3)$$

The Q_{22e} calculated using the first loop compensation are in Tables IV.7-1 through IV.7-3 , differing by flight condition. At low frequencies where $|L_{2e}| \gg 1$ this is approximated by

$$t_{22} = f_{22} \qquad (4.7\text{-}4)$$

When $|L_{2e}| \ll 1$ at higher frequencies the equation can be represented by

$$t_{22} = f_{22} L_{2e} \qquad (4.7\text{-}5)$$

At frequencies in between, the simplifications are not valid and the true relationships are used. The disturbance output t_{21} is now given by:

$$t_{21} = f_{11} L_1 / [Q_{21} (1 + L_{2e})(1 + L_1 - \gamma)] \qquad (4.7\text{-}6)$$

Again at ω such that $|L_1| \gg 1$, the response is

$$t_{21} = f_{11} / [Q_{21} (1 + L_{2e})] \qquad (4.7\text{-}7)$$

And at high frequencies where $|1 - \gamma| \gg |L_1|$, t_{21} is

$$t_{21} = f_{11} L_1 / [Q_{21} (1 + L_{2e})(1 - \gamma)] \qquad (4.7\text{-}8)$$

TABLE IV.7-1

Equivalent Q_{22} Plant Transfer Functions for Flight Condition One

---

No Failures:

$$\frac{191.3(s+0.3097\pm j0.4501)(s+13.24)(s+100)(s+59.67)}{(s+1.546)(s-0.2346)(s+21.07)(s+28.12)(s+49.77)(s+0.01397\pm j0.2508)}$$

Canard Failed:

$$\frac{789.3(s+0.3468\pm j0.4407)(s+13.24)(s+130)(s+53.28)}{(s-0.2846)(s+1.546)(s+20.16)(s+0.01826\pm j0.2567)(s+160\pm j130.4)}$$

Ailerons Failed:

$$\frac{304.3(s+0.3503\pm j0.4303)(s+13.24)(s+130)(s+60.93)(s+59.48)}{(s+0.0132\pm j0.256)(s+9.86,15.5)(s+128\pm j80.2)(s+1.546)(s-0.2346)}$$

Stabilator Failed:

$$\frac{210.7(s+0.357\pm j0.4401)(s+58.77)(s+13.24)(s+180)(s+60.93)}{(s+1.545)(s+0.2346)(s+0.0132\pm j0.257)(s+18\pm j7.96)(s+125\pm j44.1)}$$

Stabilator and Ailerons Failed:

$$\frac{401.5(s+0.3316\pm j0.5513)(s+5.407)(s+13.24)(s+180)}{(s+0.0183\pm j0.258)(s+80.3\pm j153)(s+1.546)(s-0.2046)(s+32.18)}$$

Stabilator and Canard Failed:

$$\frac{398.7(s+0.3316\pm j0.5516)(s+40.24\pm j20.52)(s+13.24)(s+180)}{(s+0.0183\pm j0.257)(s+13.6\pm j6.57)(s+126\pm j95.1)(s-0.2346)(s+1.546)}$$

TABLE IV.7-2

Equivalent Q_{22} Plant Transfer Functions for Flight Condition Two

---

No Failures:

$$\frac{107(s+0.0676+j0.259)(s+180)(s+40.39)}{(s+0.01407+j0.2181)(s+113.8+j55.38)(s+1.979)(s-0.3851)}$$

Canard Failed:

$$\frac{85.18(s+0.7124+j0.2019)(s+29.91,j19.08)(s+180)(s+232.6)}{(s+0.0147+j0.218)(s+111+j209)(s+1.98)(s-0.385)(s+28.7)(s+51)}$$

Ailerons Failed:

$$\frac{224.3(s+0.6696+j0.2279)(s+180)(s+23.77)(s+45.11)(s+13.24)}{(s+0.0147+j0.218)(s+20.5+j2.38)(s+121+j120)(s-0.385)(s+1.93)}$$

Stabilator Failed:

$$\frac{184.5(s+0.6124)(s+1.153)(s+7.728)(s+13.24)(s+130)(s+53.38)}{(s+0.0146+j0.218)(s+18.4+j7.94)(s+142+j113)(s+1.98)(s-0.385)}$$

Stabilator and Ailerons Failed:

$$\frac{738.8(s+0.5834+j0.3083)(s+15.39+j3.131)(s+180)(s+46.39)}{(s+0.0146+j0.218)(s+157+j189)(s+1.98)(s-0.385)(s+31.9)(s+33)}$$

Stabilator and Canard Failed:

$$\frac{433.1(s+.6496+j0.4263)(s+8.061)(s+13.24)(s+180)}{(s+0.01494+j0.2131)(s+114+j156)(s+1.979)(s-0.3851)(s+19.98)}$$

Bottom Vanes Failed:

$$\frac{222.8(s+0.6567+j0.2722)(s+180)(s+33.53)(s+95.98)}{(s+0.01411+j0.2173)(s+115+1.j160.7)(s+43.56)(s+1.979)(s-0.3851)}$$

TABLE IV.7-1

Equivalent Q_{22} Plant Transfer Functions for Flight Condition Three

---

No Failures:

$$\frac{411.2(s+0.4902+j1.107)(s+180)(s+46.07)(s+13.24)}{(s+0.00321+j0.109)(s+113+j97.51)(s+2.686)(s-0.4603)(s+21.61)}$$

Canard Failed:

$$\frac{260(s+0.456+j1.156)(s+42.95+j28.58)(s+13.24)(s+180)}{(s+0.00321+j0.109)(s+24.2+j3.16)(s+141+j129)(s+2.69)(s-0.461)}$$

Ailerons Failed:

$$\frac{286.7(s+0.3589+j1.069)(s+19.92+j9.679)(s+58.96)(s+13.24)}{(s+0.00321+j0.109)(s+22.2+j15.4)(s+2.69)(s+32.9)(s+95.7)(s-0.461)}$$

Stabilator Failed:

$$\frac{338.9(s+0.4468+j1.036)(s+38.55+j15.33)(s+13.24)(s+180)}{(s+0.00321+j0.109)(s+24.0+j4.40)(s+109+j94.4)(s+2.69)(s-0.461)}$$

Stabilator and Ailerons Failed:

$$\frac{343.6(s+0.3422+j1.001)(s+16.61+j11.13)(s+180)(s+14.31)}{(s+0.00321+j0.109)(s+17.4+j24.9)(s+121+j22.6)(s+2.69)(s-0.461)}$$

Stabilator and Canard Failed:

$$\frac{62.07(s+0.3961+j1.219)(s+75.21)(s+13.24)}{(s+0.00321+j0.109)(s+38.87)(s+2.69)(s+38.63)(s+38.63)}$$

Equations 4.7-1 through 4.7-8 are used to find both the tracking and disturbance bounds for the second loop. Notice that t_{22} contains only one term due to tracking response. The disturbance rejection has been "built in" by the time the second loop is designed.

The dominant bounds for the second loop are due to disturbance rejection at the low frequencies and tracking response at high frequencies. This differs from the first loop where the bounds are derived from tracking requirements only. Again this is due to the same reason, the derivation of $\underline{Q}$ from $\underline{P}'$ that made $|Q_{12}| > |Q_{11}|$ also made $|Q_{22}| > |Q_{21}|$. If $|L_1| >> 1$ then t_{21} is given by

$$t_{21} = f_{11}/[Q_{21}(1 + L_{2e}) \qquad (4.7\text{-}9)$$

which can be rearranged to the form

$$\left|1/(1 + L_{2e})\right| < \left|b_{21} Q_{21}/f_{11}\right| \qquad (4.7\text{-}10)$$

which for $|L_{2e}| >> 1$ is approximated as

$$|L_{2e}| > |f_{11}/(b_{21} Q_{21})| \qquad (4.7\text{-}11)$$

From this point forward L_{2e} is simply referred to as L_2. The plant templates for Q_{22e} are in Figure IV.7-1 . Notice that the uncertainty is increased from the first loop(Figure IV.6-5). As was done on the first loop, the lower tracking

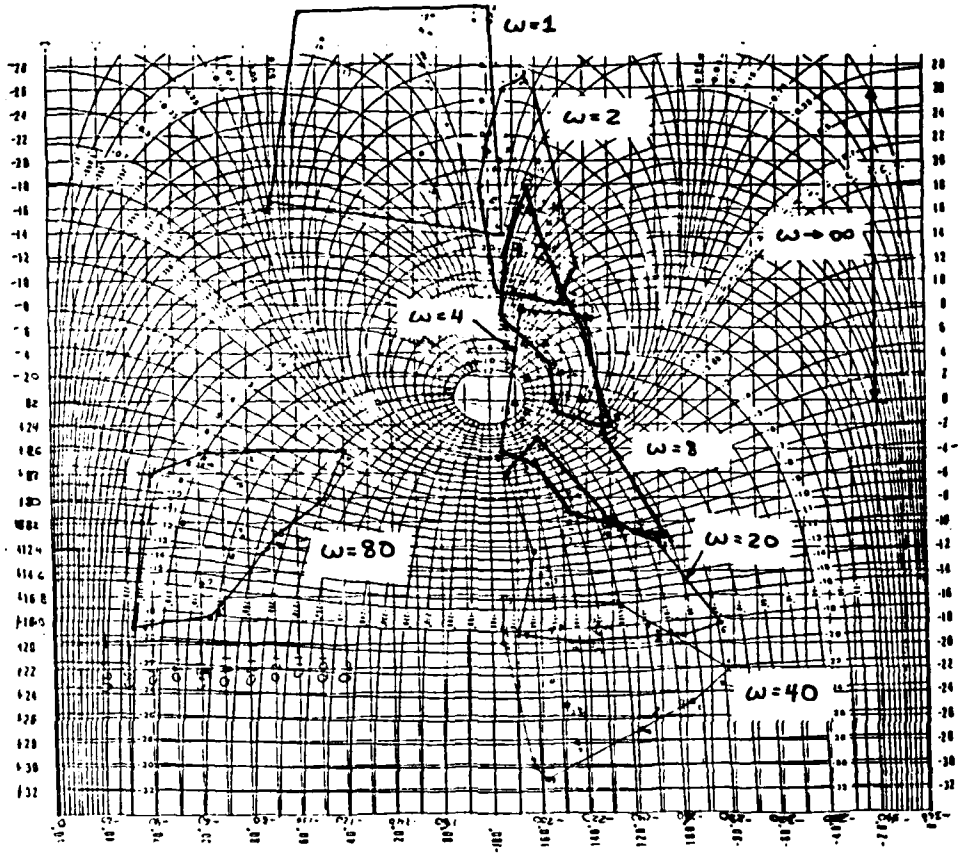

Fig.IV.7-1: Q_{22eq} Templates

bound is decreased at higher frequencies to provide bandwidth reduction. This is seen as an increase in $\Delta T(j\omega)$ which the templates must not violate. The tracking response can be restored by using the actual bound values when designing f_{22}. The original and modified $\Delta T(j\omega)$ bounds are listed in Table IV.7-4.

TABLE IV.7-4

Modified Tracking Bounds for L_2 Design

Frequency ω (rad/sec)	Exact $\lvert\Delta T(\omega)\rvert$	Modified $\lvert\Delta T(\omega)\rvert$
1.0	2.7	3.0
2.0	4.8	5.0
4.0	8.1	10.0
8.0	15.0	20.0
20	18	∞
40	21	∞
80	29	∞

Figure IV.7-2 shows the bounds for both tracking and disturbance rejection for loop two. Up to 20 rad/s disturbance rejection dominates, with the high frequency bounds determined both by tracking and disturbance considerations. The UHFB is a 26 dB vertical line. As before L_2 contains an unstable root and must start off at -180 degrees for stability. With the nominal plant again FC2:Canard Failed, an L_{2o} that satisfies the loop bounds with minimum bandwidth is:

$$L_{2o} = \frac{2.732(10^6)(s+0.3851)(s+25)}{(s+1)(s-0.3851)(s+300)(s+900)} \qquad (4.7\text{-}12)$$

L_{2o} is shown in both the Nichol's chart in Figure IV.7-3 and the frequency response in Figure IV.7-4 . Again some overdesign of L_{2o} is evident since the bounds are not "just met" at each specific frequency. As before, this is done to

limit the complexity of L_{2o}. The closed loop bandwidth is

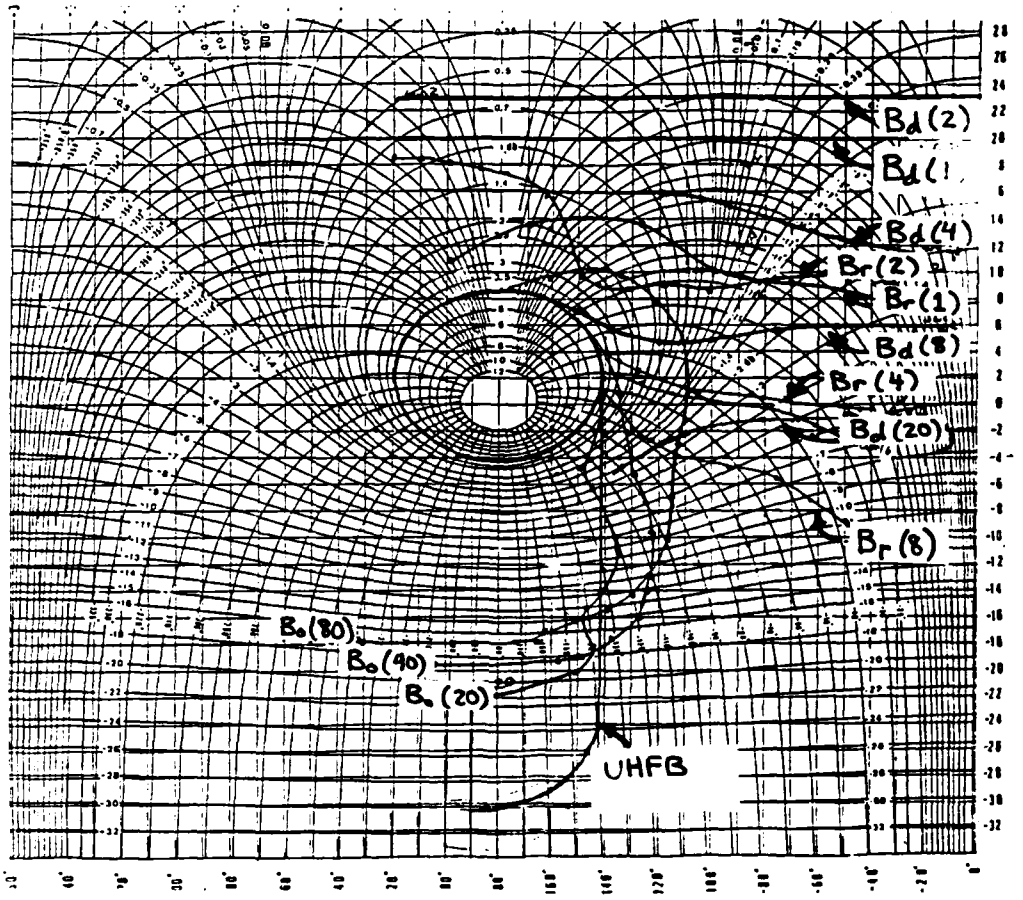

Fig.IV.7-2: Bounds on L_2

somewhat greater than L_{1o} at ω_o = 26 rad/s. With the nominal condition FC2:Stabilator Failed, the required loop compensation is:

$$g_2 = \frac{32250(s+31)(s+28.71)(s+17.26)(s+1.979)}{(s+1)(s+3)(s+300)(s+900)(s+0.7124+j0.2019)} \cdot \frac{(s+0.385)(s+25)(s+111+j208)(s+0.0146+j0.218)}{(s+29.9+j19.03)(s+232.5)(s+13.24)(s+180)} \quad (4.7\text{-}13)$$

The frequency response of g_2 is in Figure IV.7-5 . Notice

that the gain at DC is actually in the negative dBs, rising to a peak of 25 dB at ω = 1000 rad/sec. This value is too high, indicating that the loop transmission should be reshaped.

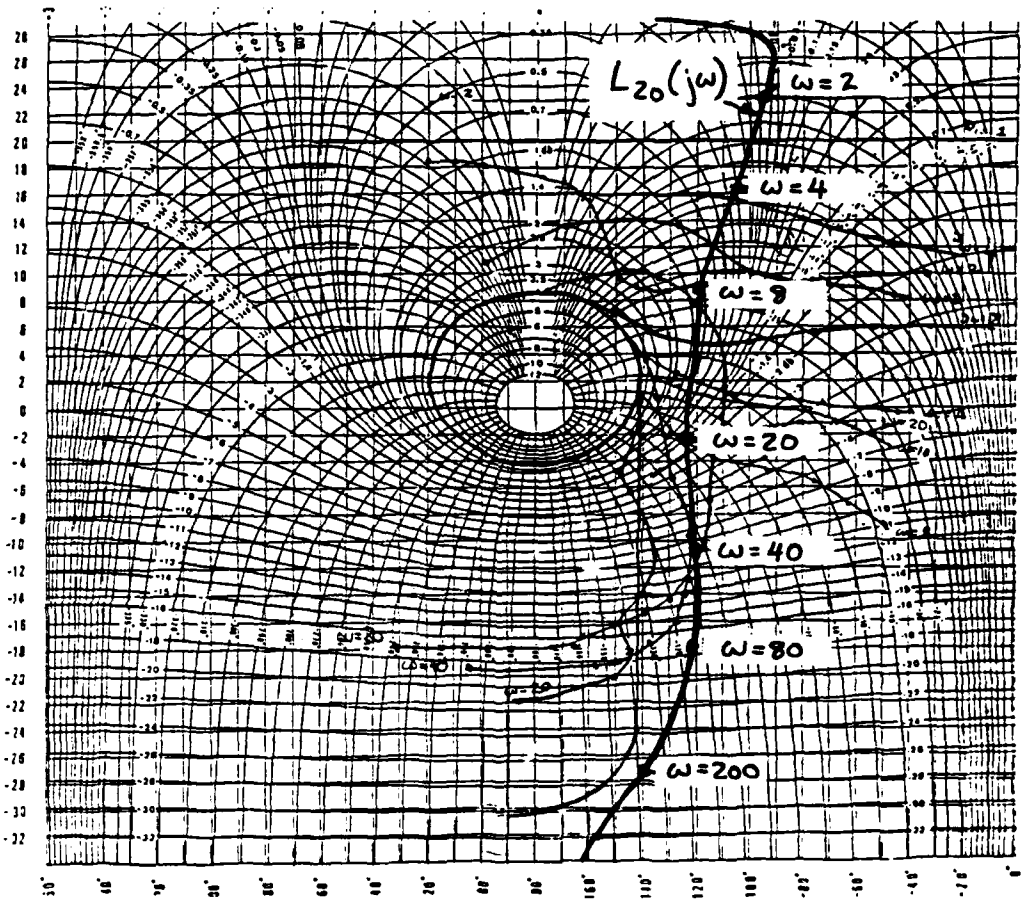

Fig.IV.7-3: Loop Transmission L_{20}

Again, if a slightly higher bandwidth can be tolerated, y_2 can be simplified. A simplified y_2 that mimics the full order y_2 is:

$$y_2 = \frac{20.72(s+0.2)(s+0.4)}{(s+2.0)(s+19)} \qquad (4.7\text{-}14)$$

A comparison between the full order and simplified g_2, Figure IV.7-6, shows the higher gain at some regions that leads to increased bandwidth, a price paid using the

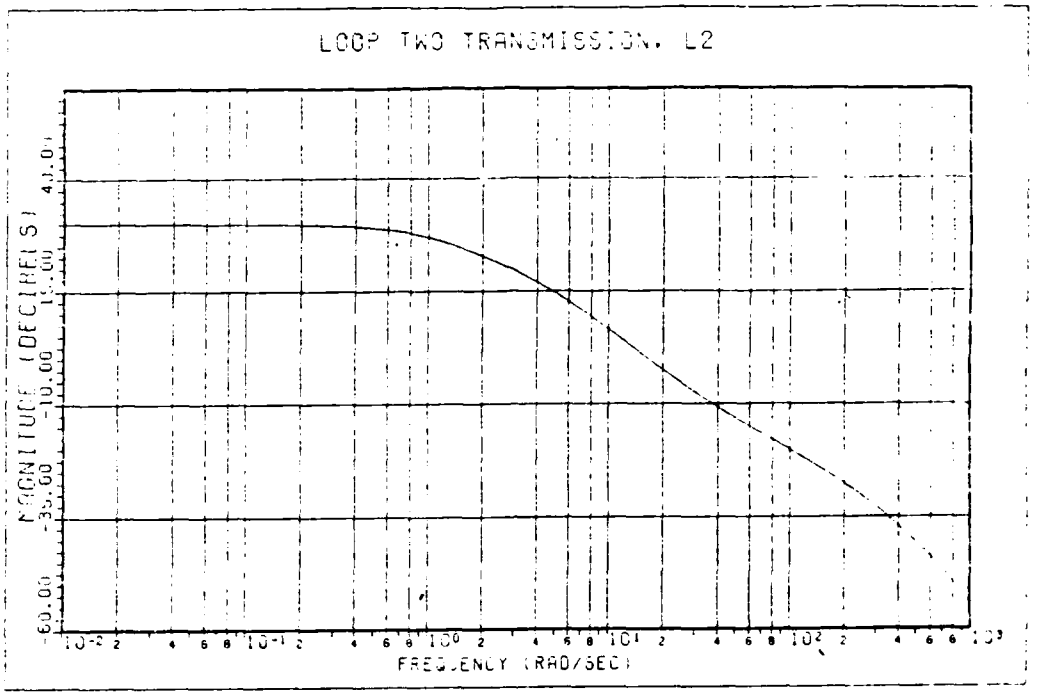

Fig.IV.7-4: Frequency Response of L_{2o}

simplification. The loop bandwidth with the simplified g_2 is approximately 35 rad/sec.

From the tracking bounds for loop two, an f_{22} that gives the desired frequency response is:

$$f_{22} = 4/(s+0.8) \qquad (4.7\text{-}15)$$

The frequency response of f_{22} is in Figure IV.7-7, showing a 3dB bandwidth of 5.7 rad/s.

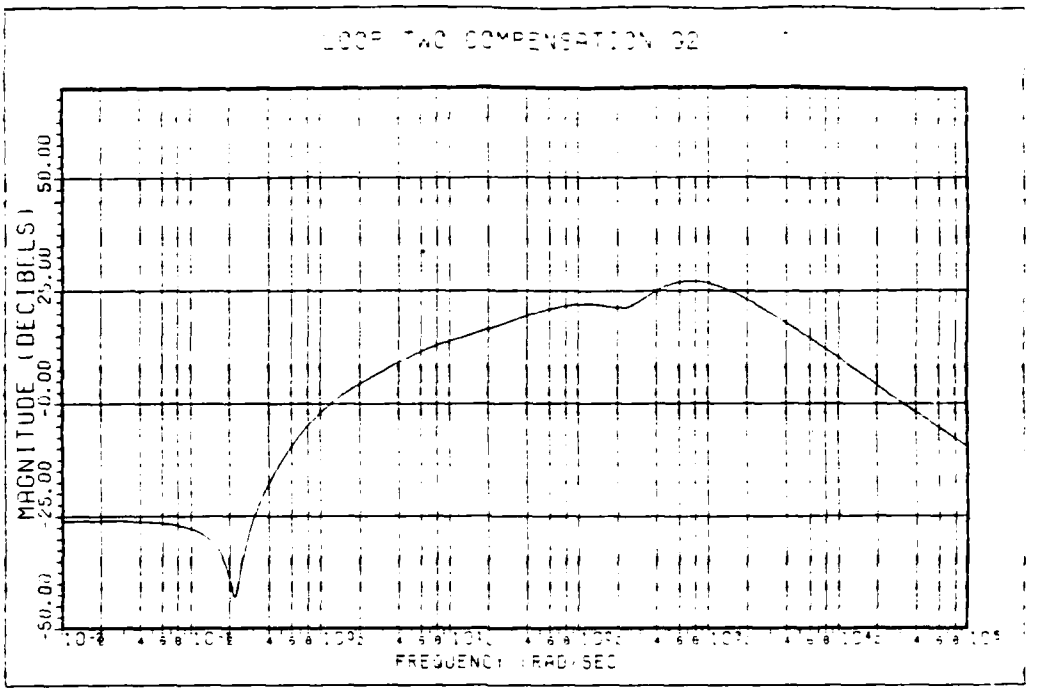

Fig.IV.7-5: Loop Two Compensation

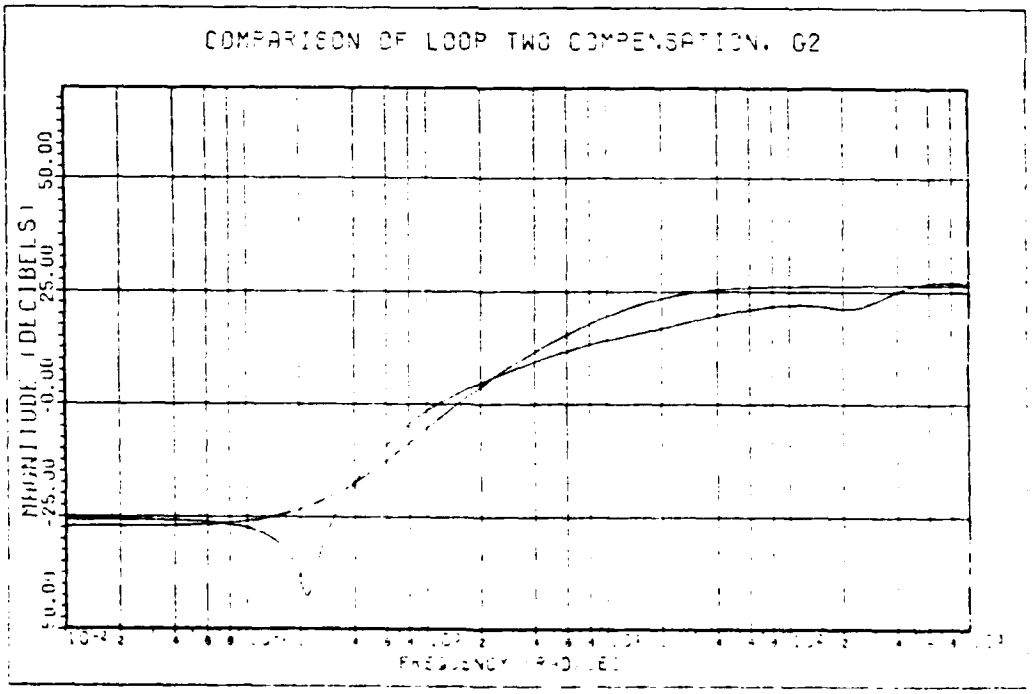

Fig.IV.7-6: Comparison of Full Order and Simplified Loop Two Compensators

IV.6 Summary

Using QFT, compensators for controlling the F-15 STOL aircraft AOA and velocity channels for three flight conditions with six separate surface failure conditions have been designed. Chapter V takes these control laws and

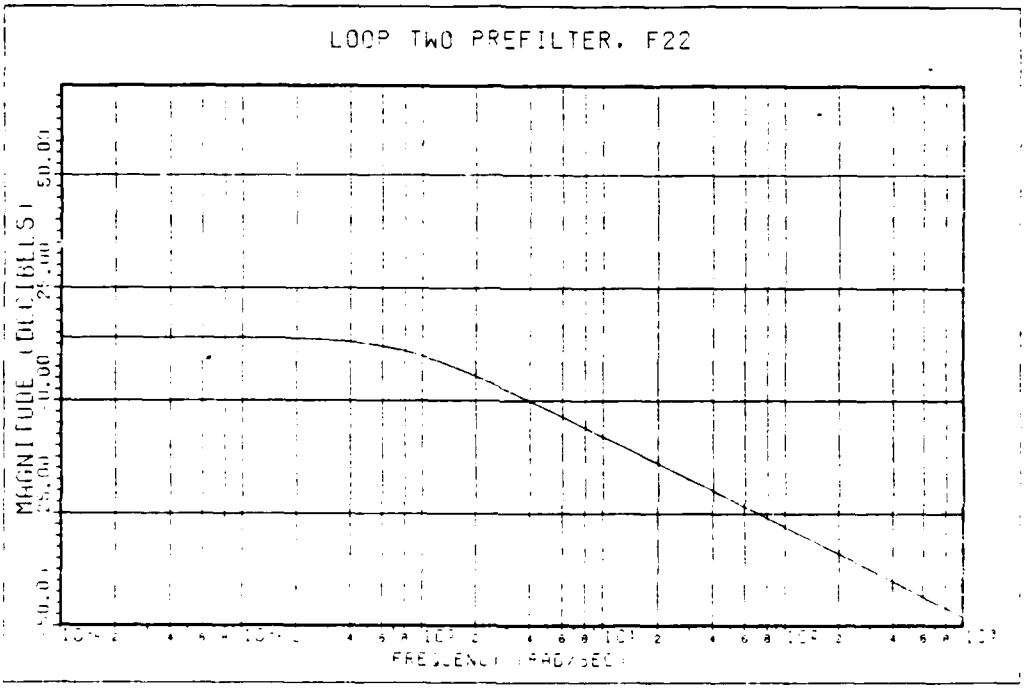

Fig.IV.7-7: Frequency Response of Prefilter f_{22}

integrates them into a digital simulation of the aircraft to check aircraft performance. Stability and tracking/disturbance rejection are guaranteed by QFT to meet the specifications; however, internal variables, such as the surface deflections and rates, require checking to see if they have exceeded physical bounds. This is not taken into account in the design since going beyond these bounds results in non-linear systems, not amenable to frequency domain

design techniques. To limit effects from saturations of internal elements, feedback paths around the saturating elements are required. QFT has been extended to handle feedback of internal variables, but that is beyond the thrust of this thesis[24]. After the system is designed, it is noticed that if L is shaped a bit differently then the gain can be saved at both low and high frequencies. This in turn reduces the closed-loop bandwidth. Unfortunately, this cannot be included in this chapter due to printing deadlines; however, the improved loops and their compensation are in Appendix H .

The original plan to control the flight path angle and velocity in the STOL landing scenario had to be modified to controlling the angle of attack and velocity in order to get minimum phase plants. QFT can be used in the control of non-minimum phase plants, but restrictions placed on the bandwidth of the loop transmission make it impractical to control the type of plant in this thesis containing both open loop RHP poles and zeros. Just controlling AOA implies that landing control is lost since the exact pitch angle is unknown . Thus, this control scheme cannot be used to effectively control landing since direct control of the decent is lost; however, it can be used to insure stability in the event of control surface failures. There is a chance, not investigated, that by expanding $\det\{\underline{P}\}$ vectors can be found that force the plant into minimum phase form. This is stated again in Chapter 6.

Before designing a MIMO control scheme using QFT one

should first form the determinant and determine the range of weightings which result in minimum phase plant matrices. Only then may QFT continue. The reversal of diagonal dominance seen in the equivalent plants could be caused by forcing the plant to be minimum phase, and does not seem to result from QFT directly.

Restating, using QFT, compensators are found which enables the system to meet the given performance tolerances. These higher order compensators are approximated by lower order compensators without significant error. Loop transmission bandwidths are 12 and 26 rad/sec for the AOA and velocity channel, respectively. Since development of these compensators, reshaping of the loop transmissions have significantly reduced the magnitude of y_1 and y_2 as a function of frequency. These improved compensators are in Appendix H.

V. Simulation Results

V.1 Introduction

This chapter presents the results of computer simulations of the compensated aircraft under normal and failure conditions. Nineteen separate cases over three flight conditions are examined. The commanded outputs are evaluated to see if performance tolerances are met. The control surfaces are examined to see if any physical limits not included in the controller synthesis have been exceeded, or saturated. Using these results, the practical application of the controller to an aircraft is examined, and any possible corrections or improvements are suggested.

V.2 Computer Model

The aircraft is simulated using the CAD package MATRIX X[25]. This program allows the system as a whole to be simulated in block form using transfer functions rather than transforming the entire system into state space. Individual control surface failures are simulated by removing connections between the specific blocks. Appendix G goes into further detail on the actual mechanics of the computer simulation.

Before simulation can occur the system must be modified to reflect the changes done during loop compensation design. The original signal flow chart for the control system is in Figure V.2-1 . Since the columns in $\underline{P}'$ are switched this

graph is no longer valid. The new system in Figure V.2-2 reflects the changes accomplished to compensate the system. The simulation uses the lower bandwidth compensators developed in Appendix H rather than the ones developed in Chapter IV. The first computer runs are made without taking into account surface rates or deflections. This is to verify

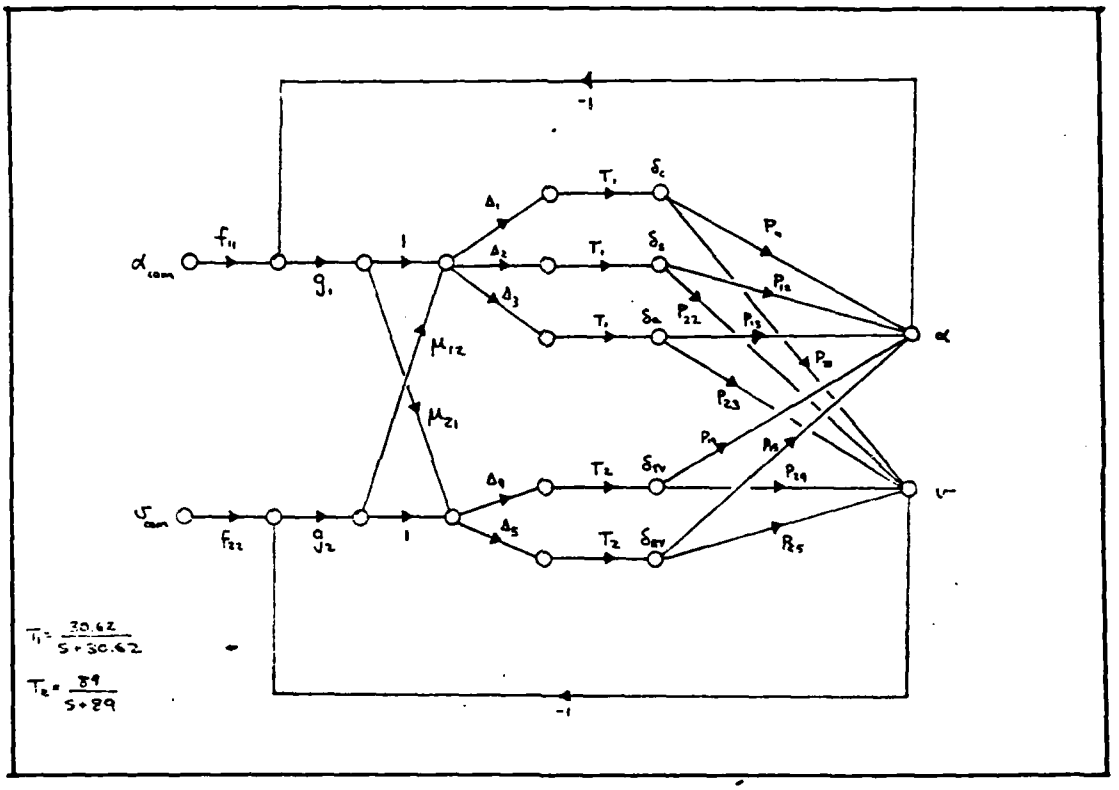

Fig.V.2-1: Signal Flow Graph of Original Plant

that the compensators designed using QFT did indeed force the plant to meet the performance tolerances. After this MATRIX X allows the designer to include saturations directly in tne plant model. Botn surface rate and deflection limits are introduced. The aerodynamic surfaces are limited to maximum deflections of ±20 degrees at rates up to 30 deg/sec. Of

course each type of surface has its own individual limits, but just one set of limits for all surfaces is chosen to simplify the simulation. The limits on the vanes have a faster deflection rate of 80 deg/sec, but since the vanes are very non-linear over large deflections within the range of their stops, their deflection is limited to ±8 degrees even though they can actually deflect much farther .

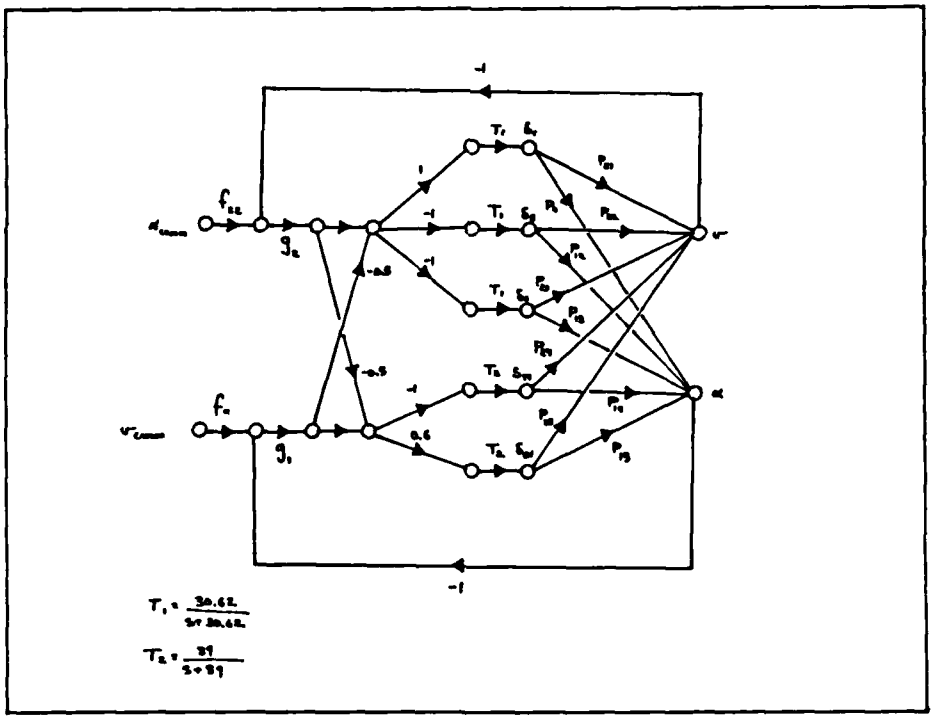

Fig.V.2-2: Modified Signal Flow Graph of Actual Plant Simulation

V.3 Simulation Results

Figures V.3-1a tnrough V.3-1d show the simulation results for all nineteen flight condition/failure combinations. Step inputs for both velocity and angle of attack are used. Figure V.3-1a is the AOA tracking response to an inch deflection stick input. Without error, an inch of stick deflection should result in a change of AOA by 3.5 degrees. QFT guarantees that the response is within the given response tolerances. The figure shows that all the transient parts of the responses except one lie within the bounds. Possible cause for the response lying just outside is the simplified compensators used. That response is underdamped and corresponds to a plant on the upper right hand side of tne plant template. The simplified compensation raises the frequency response of tne tracking output enougn to slightly exceed tne upper tracking bound. The increased overshoot is not very great, on the order of 2 percent, which should be tolerable. Since the system is Type 0, some steady state error is expected. The worst steady state tracking error is about 7 percent. The Figures of Merit for the AOA command input are contained in Table V.3-1 and lie within the specified ranges(see pages 64 and 68 for the ranges of the Figures of Merit for the two channels) except for FC1:Ailerons Failed case which shows the high overshoot noted previously. The disturbance output on the velocity channel for the step AOA command is in Figure V.3-1b. The largest deviation is -1 ft/sec with a steady state value of -0.9 .

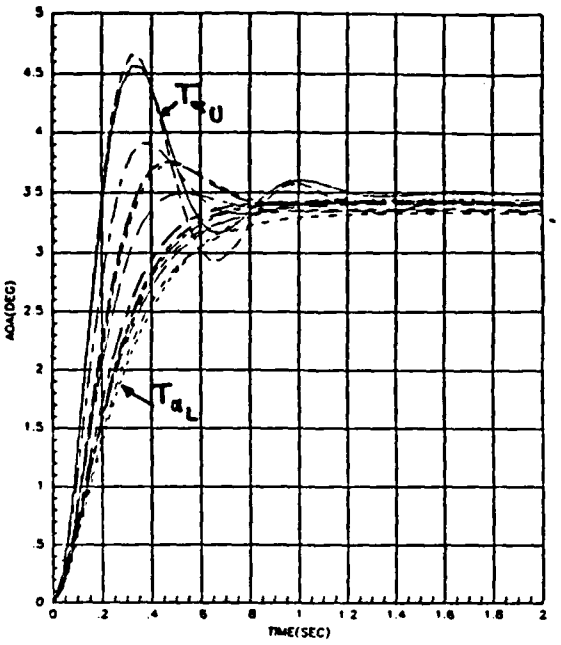

Fig.V.3-1a: AOA Response to AOA Step Input

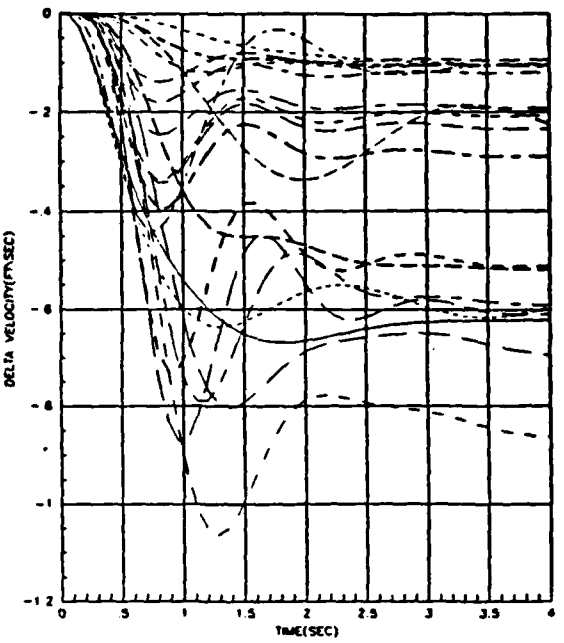

Fig.V.3-1b: Velocity Response to AOA Step Input

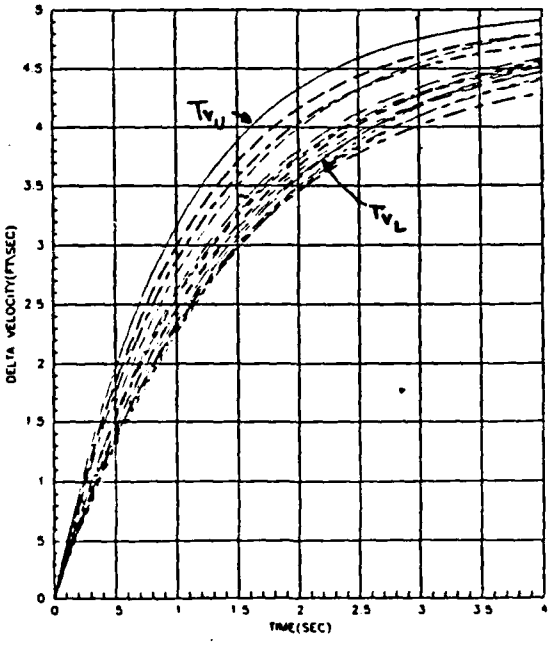

Fig.V.3-1c: Velocity Response to Velocity Step Input

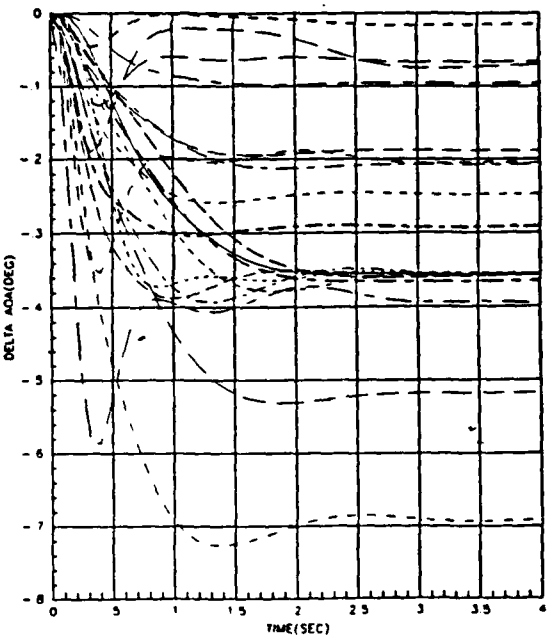

Fig.V.3-1d: AOA Response to Velocity Step Input

TABLE V.3-1

Figures of Merit for AOA Command with Linear Simulation

FC:	Failure	t_r	t_s	M_p	F_v	% Error
1	None	0.16	1.2	3.9	3.4	2.9
	Canard	0.17	1.1	3.7	3.4	2.9
	Ailerons	0.12	1.2	4.7	3.4	2.9
	Stabilator	0.48	0.65	3.4	3.4	2.9
	Stab/Ail	0.56	0.90	3.3	3.3	5.7
	Stab/Can	0.52	0.95	3.4	3.4	2.9
2	None	0.46	0.70	3.4	3.4	2.9
	Canard	0.58	1.1	3.3	3.3	5.7
	Ailerons	0.26	0.75	3.5	3.3	5.7
	Stabilator	0.46	0.70	3.3	3.3	5.7
	Stab/Ail	0.38	0.90	3.3	3.3	5.7
	Stab/Can	0.42	0.90	3.4	3.4	2.9
	Bot. Vanes	0.41	0.90	3.4	3.4	2.9
3	None	0.32	0.90	3.4	3.4	2.9
	Canard	0.40	1.0	3.4	3.4	2.9
	Stabilator	0.40	0.90	3.4	3.4	2.9
	Ailerons	0.17	1.1	3.7	3.4	2.9
	Stab/Ail	0.45	0.75	3.3	3.3	2.9
	Stab/Can	0.70	0.70	3.3	3.3	2.9

This corresponds to a DC gain of 12 dB down from the tracking response, within the -10 dB limit. This response is for the nominal plant P_o which is on the bottom of the plant template for most frequencies, and for which the DC gain and open loop bandwidth is at a minimum. Most of the plants exhibit much smaller variations which indicates greater loop gain and bandwidth leading to better disturbance rejection..

The tracking response for a velocity input is shown in Figure V.3-1c. A +5 ft/sec velocity change is commanded. All of the responses are initially within the previously described bounds, but at some time deviate since the steady state error is non-zero. The worst error is again for the nominal plant, FC2: Canard Failed with the lowest dc open-loop gain. The responses show the first order characteristics desired in the original specifications. Table V.3-2 contains the velocity response Figures of Merit, showing that the bounds are met for all cases. The AOA disturbance for the step velocity-command is in Figure V.3-1d. The 'worst' curve has a steady state value of 17 dB below the command input , well within the tolerances. This indicates that the loop transmission is overdesigned and can be decreased without violating the disturbance tolerances.

As a check of the QFT design proceedure, the system is simulated for FC2:Canard, Ailerons Failed and FC3:Canard, Ailerons Failed. Both of these plants have non-minimum phase Q_{ij} and should be unstable under high forward gain and negative feedback. Figures V.3-2a-d do indeed show the projected instability for both AOA and velocity step command inputs.

TABLE V.3-2

Figures of Merit for Velocity Command Using Linear Simulation

FC:Failures	t_r (sec)	t_s (sec)	M_p	F_v	% SSE
1 None	2.4	4.1	4.8	4.8	4
Canard	2.2	4.0	4.9	4.9	2
Stabilator	2.6	3.8	4.6	4.6	8
Aileron	3.0	4.6	4.6	4.6	8
Stab/Ail	3.0	4.6	4.5	4.5	10
Stab/Can	3.4	5.5	4.5	4.5	10
2 None	3.4	5.4	4.5	4.5	10
Canard	3.6	6.4	4.4	4.5	12
Stabilator	3.1	4.6	4.6	4.6	8
Aileron	3.0	4.5	4.6	4.6	8
Stab/Ail	3.2	4.8	4.6	4.6	8
Stab/Can	3.3	4.8	4.5	4.5	10
Bot.Vanes	3.1	4.5	4.6	4.6	8
3 None	2.4	4.1	4.8	4.8	4
Canard	3.5	5.6	4.6	4.6	8
Stabilator	3.6	5.4	4.7	4.7	6
Aileron	3.6	5.5	4.7	4.7	6
Stab/Ail	3.7	5.5	4.6	4.6	8
Stab/Can	3.7	5.6	4.6	4.6	8

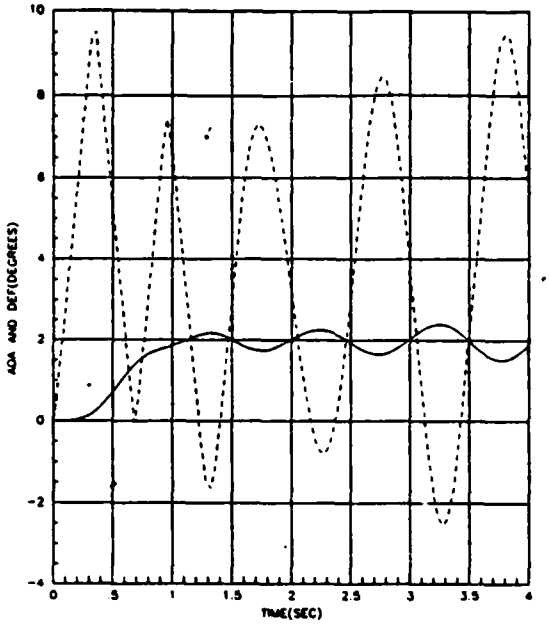

Fig.V.3-2a: AOA and Surface Deflections at FC2:Canards, Ailerons Failed

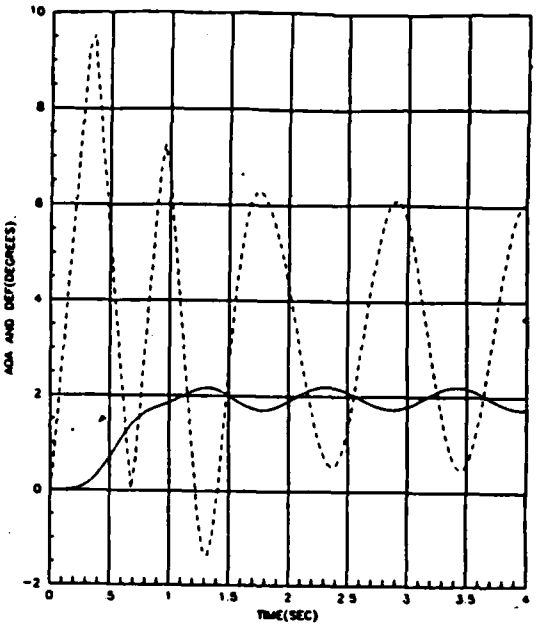

Fig.V.3-2b: Velocity and Surface Deflections at FC2:Canards, Ailerons Failed

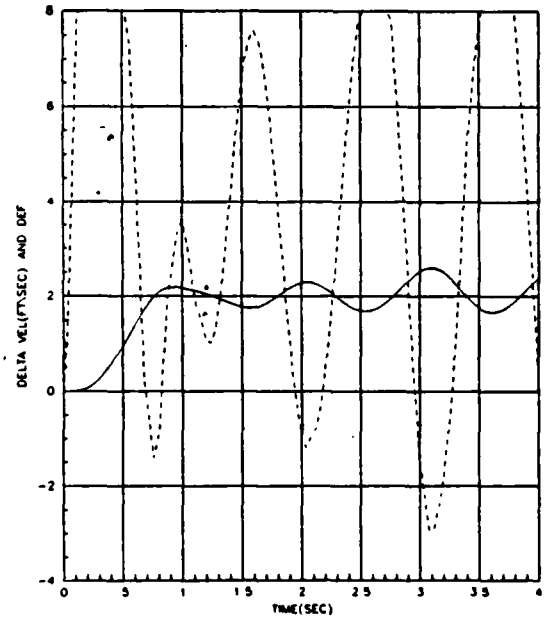

Fig.V.3-2c: AOA and Surface Deflections for FC3:Canards, Ailerons Failed

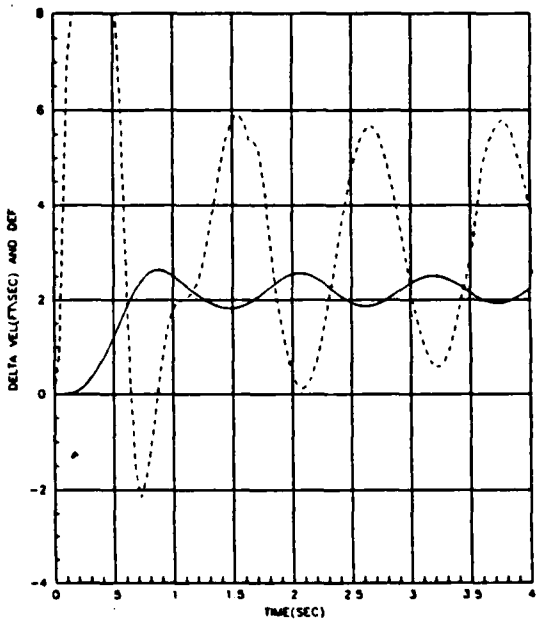

Fig.V.3-2d: Velocity and Surface Deflections for FC3:Canards, Ailerons Failed

The system has acted as predicted by QFT(and classical control theory).

In summary, the linear simulation shows that the control system satisfies the specifications over the range of uncertainty for which the design is made(is robust for the given control surface failures at the three flight conditions). This is guaranteed when QFT is applied correctly. What is not shown are the control surface deflections and rates. For a more realistic simulation these must be included. This is done in the next section.

V.4 System Simulation With Non-Linearities Included

The previous section shows that the system meets the desired performance tolerances for a wide variety of failure conditions asumming a linear plant. What is not shown are the internal variables of surface deflection and deflection rates which have definite limits. These internal variables must be examined to determine whether or not the controller works 'in the real world'. To do this the limits mentioned in Section V.2 are included directly in the simulation. The figures in this section contain plots of control surface movement. The two surfaces shown are the canard and top reversing vane. Given these responses, the response for the rest of the surfaces can be calculated using the $\underline{\Delta}$ vector. The other surfaces deflect the amount of degrees indicated on the plot times the Δ that premultiplies the particular surface. For instance, the stabilator deflection is -1 times the canard

deflection. The same procedure applies to calculate the bottom vane deflection from the top vane plot, the top vane deflection is multiplied by -0.6 . This is a bit misleading since not all surfaces saturate at the same deflection. Thus it gives the impression that all surfaces have saturated when there is actually some control authority left. The approximation is made to simplify the computer simulation.

Figures V.4-1a-d are graphs of the system response to a 3.5 degree AOA command. Figure V.4-1a is the AOA output and shows that most of the responses do approach 3.5 degrees, but a few, connected with single failure cases at each flight condition, have significant steady state error. The case FC2:Canard failed has the worst steady state error, over 20 percent. The reason these responses fail to meet the specifications could stem from the control surfaces saturating, failing to give the extra amount of control required to reach the desired value. Possibly simplifications made adding the saturation blocks, or in other places in the simulation, dropped the loop transmission enough that with these severe failures the dc gain dropped enough to increase steady state error. The system is unstable for all double failure cases(which makes sense since when all surfaces saturate the system becomes essentially 'open-loop', and the plant is open-loop unstable). This instability can be seen in Figure V.4-2 which plots the AOA output for the unstable cases. For the rest of the cases the output is acceptable, with the Figures of Merit in Table V.4-1. Single failure

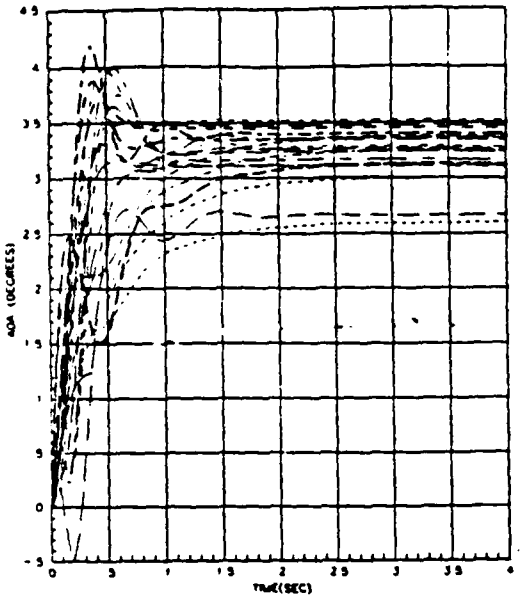

Fig.V.4-1a: AOA Response to AOA Step Input

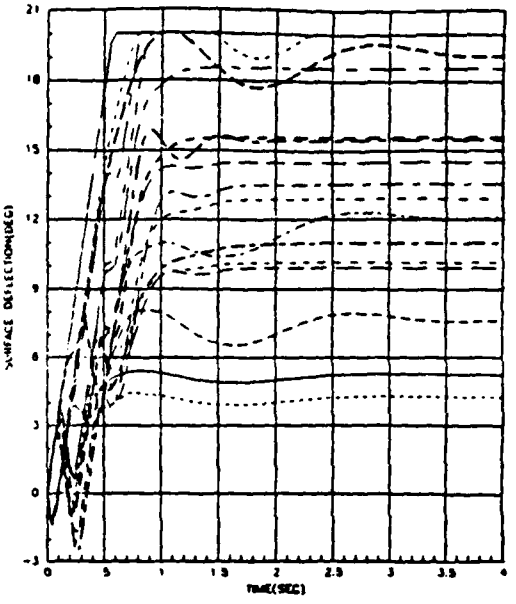

Fig.V. 4-1b: Aerodynamic Surface Deflections for AOA Step Input

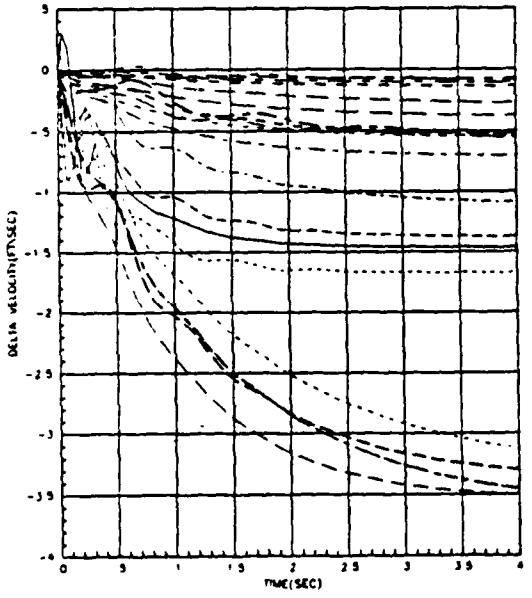

Fig.V.4-1c: Velocity Response to AOA Step Input

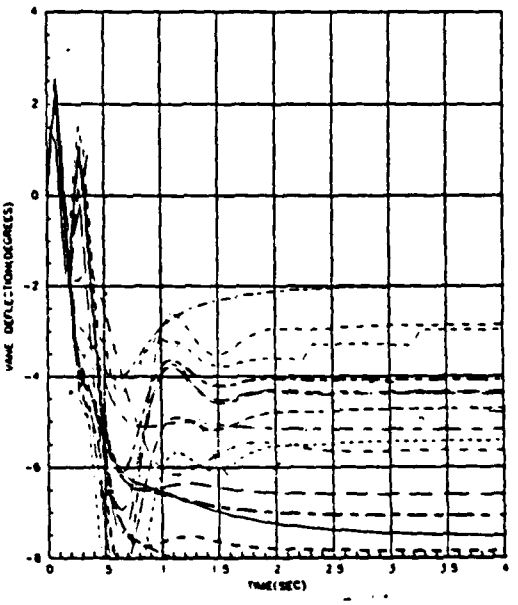

Fig.V.4-1d: Vane Deflection for AOA Step Input

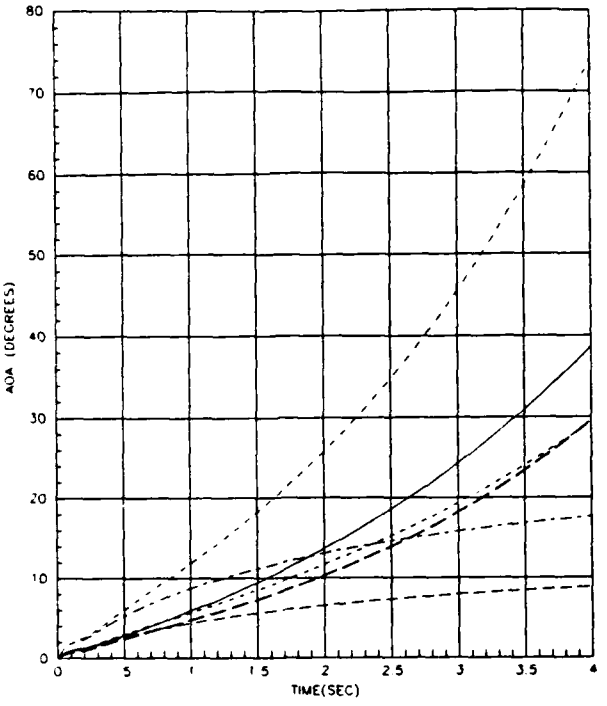

Fig.V.4-2: Unstable AOA Output for Step AOA input with Plants Containing Double Surface Failures

cases also increase the disturbance level, Note that in Figure V.4-1c the velocity drops as much as 3.5 ft/sec, the same amount as commanded(AOA), or 0 dB disturbance rejection. This can be disasterous, especially at V_{min}, since decelleration at that flight condition causes a stall. The rest of the cases experience changes in velocity within the -10 dB tolerance. Figures V.4-1b and V.4-1d are the deflections of the aerodynamic surfaces and thrust reversing vanes respectively. The surfaces 'hit the stops'(deflection saturation) for only the severe double failure conditions, causing instability; however, other cases undergo rate saturation. This rate saturation does not cause instability, possibly due to the small magnitude of the unstable root

TABLE V.4-1

Figures of Merit for AOA Command Including Saturations

FC:	Failure	t_r (sec)	t_s (sec)	M_p (deg)	F_v (deg)	% SSE
1:	None	0.26	0.75	3.7	3.4	3
	Canards	0.19	0.70	4.0	3.3	6
	Stabilator	0.25	0.75	3.6	3.4	3
	Ailerons	0.75	1.2	3.1	3.1	11
	Stab/Ail	----------Unstable System----------				
	Stab/Can	----------Unstable System----------				
2:	None	0.20	0.80	4.0	3.3	6
	Canards	1.1	1.8	2.5	2.5	29
	Stabilator	0.81	1.0	3.2	3.2	9
	Ailerons	0.37	0.95	3.4	3.1	11
	Stab/Ail	----------Unstable System----------				
	Stab/Can	----------Unstable System----------				
	Bot.Vanes	1.0	1.6	3.0	3.0	14
3:	None	0.25	0.75	4.0	3.4	3
	Canards	0.35	1.3	3.3	3.3	6
	Stabilator	0.75	1.3	3.2	3.2	9
	Ailerons	0.35	0.9	3.7	3.0	14
	Stab/Ail	----------Unstable System----------				
	Stab/Can	----------Unstable System----------				

(around .3) allowing the surface to deflect to the proper position for countering the unstable moments before they 'get out of hand'. However, even though the surfaces do not saturate for single failures in this simulation, the trim position of the surfaces has not been accounted for. Thus some of the previously non-saturated cases may actually be in saturation due to this. The reversing vanes show the same pattern of saturation, except they also saturate for FC2:Bottom Vanes failed.

The response of the system to a 5 ft/sec step velocity command is shown in Figures V.4-3a-d. The velocity response response in Figure V.4-3a shows that the velocity follows the input with only a slight increase in steady-state error except for the multiple failure cases. The Figures of Merit for the velocity command are in Table V.4-2. Multiple failures again cause instability. For some single failures the final velocity value is significantly less than desired. The loss of the control surfaces decreased the control authority to the point where the desired output is physically impossible(for that particular configuration). In Figure V.4-3c the disturbance rejection also stays below the -10 dB level(less than 1.6 degrees in magnitude) for most single failure cases and double failures(for which it is unstable). In the worse stable case, FC3:Stabilator Canard Failed, the 0 dB level is approached with the angle of attack decreasing 5 degrees for a 5 ft/sec velocity command input. From Figures V.4-3c,d the surface deflections saturate

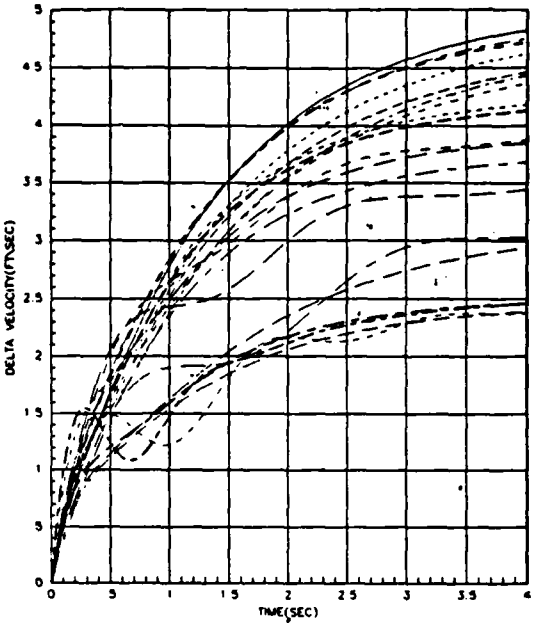

Fig.V.4-3a: Velocity Response for Velocity Step Input

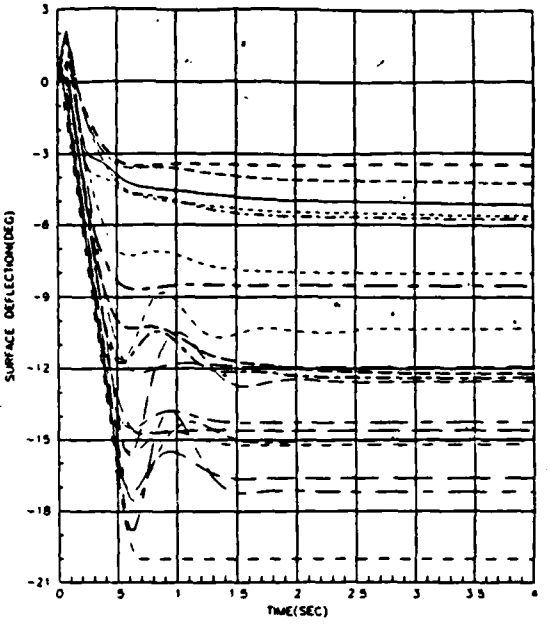

Fig.V.4-3b: Aerodynamic Surface Deflection for Velocity Step

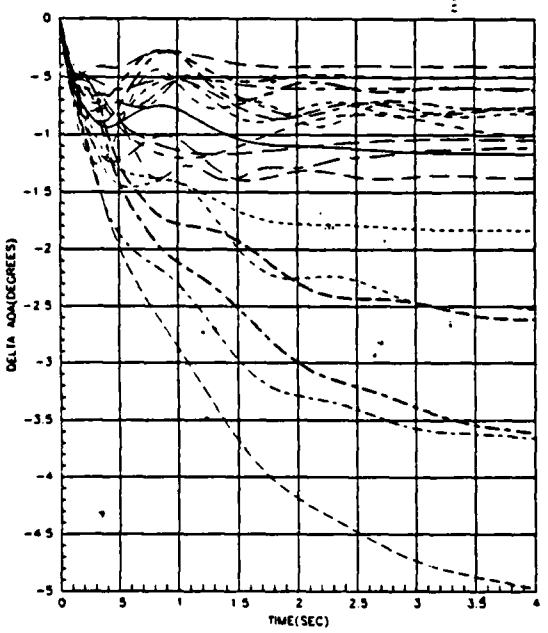

Fig.V.4-3c: AOA Response to Velocity Step Input

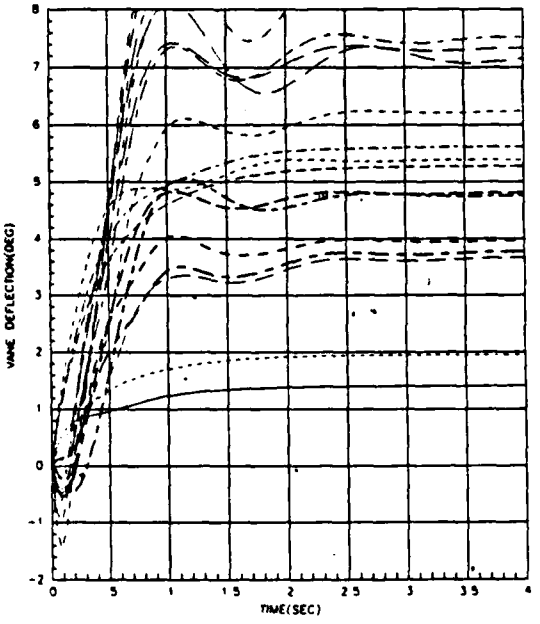

Fig.V.4-3d: Vane Deflection for Velocity Step Input

TABLE V.4-2

Figures of Merit for Velocity Command with Saturations

FC:Failures	t_r (sec)	t_s (sec)	M_p (deg)	F_v (deg)	%SSE
1:None	2.5	4.2	4.8	4.8	4
Canards	2.3	4.1	4.7	4.7	6
Stabilator	2.8	4.6	4.5	4.5	10
Ailerons	3.4	5.6	4.4	4.4	12
Stab/Ail	----------Unstable System----------				
Stab/Can	----------Unstable System----------				
2:None	3.4	5.5	4.6	4.6	8
Canards	3.7	5.4	4.4	4.4	12
Stabilator	3.3	5.3	4.3	4.3	14
Ailerons	3.2	4.8	4.2	4.2	16
Stab/Ail	----------Unstable System----------				
Stab/Can	----------Unstable System----------				
Bot.Vanes	3.4	5.6	3.8	3.3	24
3:None	3.0	4.6	4.9	4.9	2
Canards	3.6	5.6	4.2	4.2	16
Stabilator	3.5	5.5	4.0	4.0	20
Ailerons	4.0	5.9	3.4	3.4	32
Stab/Ail	----------Unstable System----------				
Stab/Can	----------Unstable System----------				

totally only for double failures. The vanes saturate for all double surface failure conditions.

The simulations including saturation effects show that the system remains stable and within performance tolerances for most single failure cases, but double failures lead to severe saturation and instability that certainly keeps the system from meeting the specifications.

V.5 Summary

For a linear system, the compensators developed using QFT meet the performance tolerances for the flight conditions and surface failures which they are designed for. This is not surprising since QFT guarantees the desired performance in the linear (nonsaturated) case. When saturations of control surfaces are included, the tolerances are met for the healthy aircraft and most single control surface failures. Double failures lead to instability due to the lack of available control authority. QFT has been extended to include, and compensate for, saturated elements in a SISO system, but has not yet been extended to the MIMO case. In other words, QFT provides a robust controller for this aircraft subjected to surface failures and changing flight conditions.

VI. Conclusions and Recommendations

VI.1 Discussion

This thesis has demonstrated the application of Quantitative Feedback Theory in designing control laws for a reconfigurable flight control system aircraft. Fixed compensation provides robust control for three different flight conditions with numerous control surface failures. The use of fixed compensation is important since it implies that identification of failures and/or scheduling for change of flight condition can be minimized, reducing identification failures, false alarms, required memory, and time delay. This compensation results from application of QFT(minimum phase technique) to the linearized, small perturbation equations of motion for an open-loop unstable aircraft(STOL F-15). The use of QFT is simple and straightforward once the plants are described properly, i.e. non-minimum phase terms are eliminated. In order to eliminate non-minimum phase terms proper control surface weightings, derived from an equation for the determinant of the plant, are used. QFT affords the designer insights on how wide the loop bandwidth should be for various failures and disturbance rejection levels. QFT enables the designer to eliminate those conditions which cause an unrealistically high loop bandwidth. Finally, QFT does the above from initial stages of the design effort(rather than finding out it "doesn't work" at the end of the design process).

VI.2 Conclusions

1. Quantitative Feedback Theory provides robust control for the complicated aircraft in this thesis. Fixed control laws for both healthy and damaged aircraft are designed such that performance is within the established tolerances using linear model simulation.

2. The original idea of controlling the flight path angle and velocity is modified to controlling the angle of attack and the velocity. This is due to the non-minimum phase plants associated with the flight path angle which limit the usefulness of QFT in this instance.

3. Control surfaces must be combined in such a fashion that the resulting plant matrices are minimum phase. This should be the first design step for problems having MIMO plants that are open-loop unstable, or exhibit non-minimum phase terms. Doing so ensures that the problem formulation is one that QFT can 'handle' without using the more involved "Singular G" method. Choosing the proper weightings requires examination of the influence of the individual surface weightings on the plant determinant.

4. Combination of surfaces using weighting factors designed to drive the plant minimum phase tended to reduce the control surface influence on some output variables and increase the effectiveness of others. In fact the effectiveness is reduced so much that the diagonal dominance reverses. The necessary process of eliminating RHP zeros appears to cause the reversal effect for this particular plant. Previous theses have not noticed this effect, possibly for two

reasons: one, the problems may be related to the particular plant, or two, the plants used in QFT theses up to this time have been open-loop stable (except for one channel of Arnold and Walkes use of Singular G on the X-29[23]) and the effect only shows up for open-loop unstable plants. The opinion of this thesis is that the particular plant data is to blame, not the technique.

5. When control surface rates and deflection limits are added to the simulation the surfaces saturate only for the double failure cases. Saturation in these cases leads to loss of aircraft control. This does not take into account any trim position the surface may be at before the command, thus saturation could occur for even lesser failure cases. In all single failure cases the system remains stable; however, for some instances the steady state tracking and disturbance rejection tolerances are not reached. One possible explaination of these effects could be the reduction of control surface effectiveness resulting from the desire to maintain minimum phase plants. Enough effectiveness seems to be reduced so that under double surface failures the aircraft does not have enough control authority left to remain stable while single surface failure reduces tracking response and increases disturbance output.

6. Reversing vane failure can only be tolerated at one flight condition, and that is only for the bottom vanes. For other conditions non-minimum phase plants resulted. This indicates that failure of these surfaces could cause

instability. Another failure case(Canards,Ailerons Failed) that QFT indicated would be unstable is checked and found unstable. This provides a check of QFT's ability to forcast cases it cannot compensate for.

7. Digitizing effects are not included in the loop transmission design. As with all future aircraft the STOL F-15 aircraft will have a digital flight control system. The digitizing effects introduce effective lags(as seen from the analog design), finite word lengtns, round-off errors, and maximum sampling rates. When using analog design proceedures for developing an eventual digital flight control system the designer might want to consider adding extra lead to the system to ensure stability when implimented. Dr. Horowitz has recently extended QFT into the discrete domain[26].

8. Loop compensation for both channels is high order, being 6th over 7th order in one case and 10th over 11th in the other. Approximate compensators with reduced order were found that mimiced the frequency response of the full order compensators. The full and reduced order compensators designed included considerable overdesign. Compensator designs with less bandwidth are included in Appendix H, and are used in the simulation.

9. The design of compensators using QFT would be much less time consuming if a computer aided design(CAD) package is implemented. With such a program the design of compensation for higher order plants(fourth on up) will be possible within the time allotted for a Masters Thesis. Doing

so allows more "realistic" design problems to be considered. For example, the STOL landing problem(as with any aircraft) is actually a six degree-of-freedom problem. Using a CAD package such thesis topics may become practical while using QFT. Current AFIT efforts include such a package, and these should be supported[27].

VI.3 Recommendations

1. The use of QFT to design robust reconfigurable flight control systems should be continued. Future problems should attempt the design of compensation for systems of third and higher orders, or as in this thesis, include more non-conventional control surfaces. In particular, redesign of the STOL F-15 aircraft for control of flight path angle, side velocity, forward velocity, and roll angle to provide increased landing control would be an useful extension of QFT design effort. Another extension of this thesis would be to retain the 2 X 2 equivalent plant matrix, but include control devices on the aircraft but omitted here such as flaps, thrust vectoring vanes, and engine throttle. This plant might also have more general frequency dependent $\underline{\Delta}$ terms for each surface, causing the surfaces to work together better than simple gains terms can accomplish. Including more control surfaces has the possibility of reducing or eliminating the problems with non-minimum phase plant matrices encountered in this thesis. This in turn could allow

the application of reconfigurability tneory in a greater extent than done here. A signal flow chart of this system is in Figure VI.3-1 . The use of internal loops to decrease the effects of saturation elements could also be investigated.

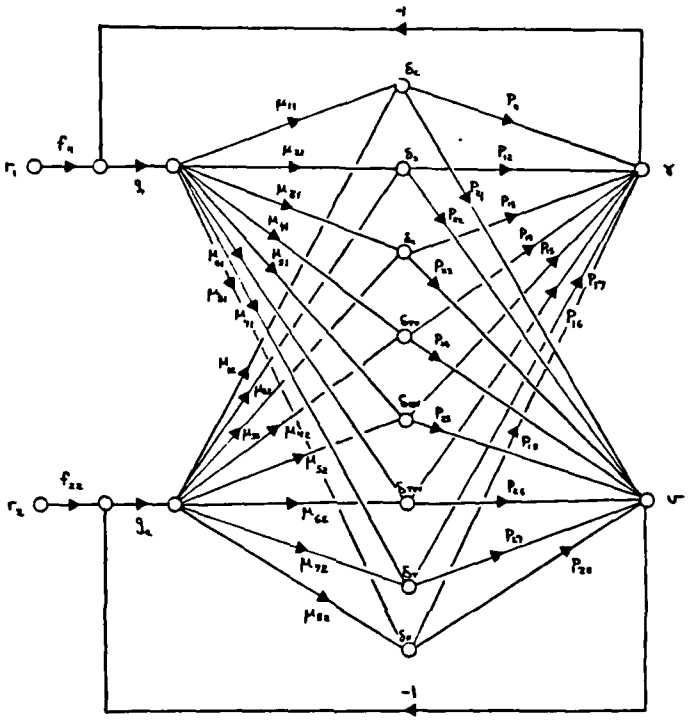

Fig.VI.3-1: 2X2 Signal Flow Graph for More General Control System of STOL F-15

Non-linear simulation of future designs using STOL F-15 models is available and should be used to validate the linear designs in the vicinity of the appropriate flignt condition's equilibrium point. This will provide a much greater check of the control system's roDustness.

2. When using QFT to design compensators for MIMO systems containing unstable poles and/or non-minimum phase zeros the first design step should be to expand out the expression for the plant determinant including the weignting terms. Then the

range of weighting terms leading to minimum phase plants must be established. Then working within this range concepts such as "control authority" and "effective use of surfaces" can be explored. Following this procedure could save the designer time and effort wasted on impractical plant configurations.

3. Digitizing effects should be included in future QFT flight control system designs using analog techniques. These could be as simple as first order lags. Current analog designs from QFT must be converted into difference equations for implementation in modern flight control systems. The sampling and processing delays within the flight control system should be included in the plant uncertainty to guarantee stability.

4. Future control system designs should also include at least a simple model of the most important part of the flight control system, the human pilot. Doing so will partially account for another source of time lag and possible instability.

5. A QFT CAD package should be implemented to provide SISO compensation design and MIMO system reduction into equivalent SISO plants. Doing so will result in a substantial decrease in time required for compensation design, and will allow the designer to contemplate more difficult problems.

6. Extension of QFT theory to the discrete domain for direct design of digital compensators, rather than analog design assuming fast-enough-sampling-rates, should be investigated. Future FCS will be digital, thus the design

method should reflect this and design directly in the sampled data domain. This could decrease problems encountered when implementing the control law design.

Appendix A

Flight Parameters and Aerodynamic Data Used to Obtain STOL Aircraft State Space Equations

The following tables contain the aerodynamic data used to obtain the state space equations for the STOL F-15. The data is provided by McDonnell Douglas Corporation. This data is preliminary, cursory, and experimental and should not be looked at as representing any finished aircraft. The stability derivatives are originally given in the aircraft body axis, but are converted to the stability axis for FCS design. Also some derivatives, especially those related to control surface deflections, have units per degree and are changed to a per radian measure. During simulation the output is converted back into a per degree measure.

TABLE A-1

Aerodynamic Data for Flight Condition One

Non-Dimensional Body Axis Stability Derivatives(1/deg)

CZA = -0.0613756	CZD3 = -0.00036784
CZQ = 0.0	CZD4 = -0.00036784
CZH = -0.000026124	CZD5 = 0.0016781
CZU = 0.011254	CZD6 = -0.0016781
CZD1= -0.001452119	CZD7 = 0.0016781
CZD2= -0.00549256	CZD8 = -0.0016781
CMA = 0.012469	CMD3 = 0.00096437
CMQ = -0.098561	CMD4 = -0.0012491
CMH = -0.0000346518	CMD5 = 0.0014572
CMU = -0.0115264	CMD6 = -0.0011263
CMD1= 0.0051492	CMD7 = 0.0014572
CMD2= -0.0098354	CMD8 = -0.0011263
CXA = 0.0025614	CXD3 = 0.001395584
CXQ = 0.0	CXD4 = 0.001395584
CXH = 0.00043821	CXD5 = -0.0045798
CXU = -0.173411	CXD6 = -0.0045798
CXD1= -0.00065298	CXD7 = -0.0045798
CXD2= -0.00099344	CXD8 = -0.0045798

TABLE A-2

Aerodynamic Data for Flight Condition Two

Non-Dimensional Body Axis Stability Derivatives(1/deg)

CZA =	-0.07062331	CZD3 =	-0.004384277
CZQ =	0.0	CZD4 =	-0.004515593
CZH =	-0.00001818665	CZD5 =	0.00135028
CZU =	0.006584185	CZD6 =	-0.00135028
CZD1=	-0.002571649	CZD7 =	0.00135028
CZD2=	-0.009552322	CZD8 =	-0.00135028
CMA =	0.009313564	CMD3 =	0.00112899
CMQ =	-0.169491	CMD4 =	-0.00214211
CMH =	-0.0000388546	CMD5 =	0.00129075
CMU =	-0.0140683	CMD6 =	-0.00137616
CMD1=	0.0052887	CMD7 =	0.00129075
CMD2=	-0.0107546	CMD8 =	-0.00137616
CXA =	0.00208763	CXD3 =	0.001365414
CXQ =	0.0	CXD4 =	0.000946581
CXH =	0.000681123	CXD5 =	-0.00340353
CXU =	-0.246589	CXD6 =	-0.00340353
CXD1=	-0.00153014	CXD7 =	-0.00340353
CXD2=	-0.002016566	CXD8 =	-0.00340353

TABLE A-3

Aerodynamic Data for Flight Condition Three

Non-Dimensional Body Axis Stability Derivatives(1/deg)

CZA = -0.07941805	CZD3 = -0.003408011
CZQ = 0.0	CZD4 = -0.003625448
CZH = -0.00006055214	CZD5 = 0.00196522
CZU = 0.013001412	CZD6 = -0.00196522
CZD1= -0.003086522	CZD7 = 0.00196522
CZD2= -0.010978221	CZD8 = -0.00196522
CMA = 0.004264454	CMD3 = -0.00362015
CMQ = -0.1564511	CMD4 = -0.00451965
CMH = -0.000027818	CMD5 = 0.00103652
CMU = -0.0049774	CMD6 = -0.00115411
CMD1= 0.0066521	CMD7 = 0.00103652
CMD2= -0.0125487	CMD8 = -0.00115411
CXA = -0.00095634	CXD3 = 0.000578922
CXQ = 0.0	CXD4 = 0.000354177
CXH = 0.000984122	CXD5 = -0.00201548
CXU = -0.193601	CXD6 = -0.00201548
CXD1= -0.000741196	CXD7 = -0.00201548
CXD2= -0.001530024	CXD8 = -0.00201548

Appendix B

State Space Models

This appendix contain the state space models used to derive the plant transfer functions. The three separate tables represent these state space models for the three flight conditions. The matrices are generated from the aerodynamic data in Appendix A by the program STOLCAT.FOR, a listing of which is in Appendix F. The state vector $\underline{x}$ is:

$$\underline{x} = \begin{bmatrix} v \\ q \\ \alpha \\ \theta \end{bmatrix} \qquad \text{(B-1)}$$

with the output vector y set equal to x. The state equations are of the form:

$$\dot{\underline{x}} = \underline{A}\,\underline{x} + \underline{B}\,\underline{u} \qquad \text{(B-2)}$$

$$\underline{y} = \underline{C}\,\underline{x} \qquad \text{(B-3)}$$

The input vector $\underline{u}$ represents the control surface deflections δ_i. The flight path angle γ is:

$$\gamma = \theta - \alpha = x_4 - x_3 \qquad \text{(B-4)}$$

TABLE B-1

State Space Matrix Model for Flight Condition One

$$\underline{A} = \begin{bmatrix} 0.0102576 & -50.3603 & 19.0236 & -30.7282 \\ 0.00184734 & -0.862621 & 0.872441 & 0.0 \\ -0.002003938 & 0.954293 & -0.446653 & -0.0571142 \\ 0.0 & 1.0 & 0.0 & 0.0 \end{bmatrix} =$$

$$= \begin{bmatrix} -1.48151 & 0.180446 & 1.44876 & -9.49654 & -9.49654 \\ 0.634746 & -1.17764 & -0.147179 & 0.79452 & -0.501398 \\ -0.027395 & -0.076598 & -0.027436 & 0.38909 & -.389091 \\ 0.0 & 0.0 & 0.0 & 0.0 & 0.0 \end{bmatrix}$$

$$\underline{\underline{I}} = \begin{bmatrix} 1.0 & 0.0 & 0.0 & 0.0 \\ 0.0 & 1.0 & 0.0 & 0.0 \\ 0.0 & 0.0 & 1.0 & 0.0 \\ 0.0 & 0.0 & 0.0 & 1.0 \end{bmatrix}$$

TABLE B-2

State Space Matrix Model for Flight

Condition Two

$$\underline{A} = \begin{bmatrix} -0.0017287 & -41.1037 & 2.42647 & -31.5195 \\ 0.00163094 & -0.987155 & 1.40620 & 0.0 \\ -0.00147934 & 0.978867 & -0.627584 & -0.0327601 \\ 0.0 & 1.0 & 0.0 & 0.0 \end{bmatrix}$$

$$\underline{B} = \begin{bmatrix} -2.49396 & -0.441907 & 1.51389 & -10.2305 & -10.0305 \\ 0.819132 & -1.49814 & -0.310057 & 0.75054 & -0.382174 \\ -0.021074 & -0.066476 & -0.036040 & 0.30321 & -.30381 \\ 0.0 & 0.0 & 0.0 & 0.0 & 0.0 \end{bmatrix}$$

$$\underline{C} = \begin{bmatrix} 1.0 & 0.0 & 0.0 & 0.0 \\ 0.0 & 1.0 & 0.0 & 0.0 \\ 0.0 & 0.0 & 1.0 & 0.0 \\ 0.0 & 0.0 & 0.0 & 1.0 \end{bmatrix}$$

TABLE B-3

State Space Matrix Model for Flight Condition Three

$$A = \begin{bmatrix} -0.0149226 & -20.5762 & 31.2520 & -32.1258 \\ 0.00137881 & -1.38385 & 2.45191 & 0.0 \\ -0.00066242 & 0.997696 & -0.832834 & -0.0072024 \\ 0.0 & 1.0 & 0.0 & 0.0 \end{bmatrix}$$

$$B = \begin{bmatrix} -2.53333 & -0.158766 & 0099 & -10.8721 & -10.8721 \\ 1.87981 & -2.96717 & -0.36601 & 0.75232 & -0.27378 \\ -0.028296 & -0.095538 & -0.058232 & 0.19892 & -.19892 \\ 0.0 & 0.0 & 0.0 & 0.0 & 0.0 \end{bmatrix}$$

$$C = \begin{bmatrix} 1.0 & 0.0 & 0.0 & 0.0 \\ 0.0 & 1.0 & 0.0 & 0.0 \\ 0.0 & 0.0 & 1.0 & 0.0 \\ 0.0 & 0.0 & 0.0 & 1.0 \end{bmatrix}$$

Appendix C

Control Surface Transfer Functions

This appendix contains the individual control surface deflection to response output transfer functions for the state space models in Appendix B. The transfer functions are calculated using the CAD package TOTAL[7]. The transfer functions are arranged according to the output variable, with the responses for a single output to all of the surfaces over the three flight conditions arranged in a single table. The output variables are the angle of attack α, pitch angle θ, and the forward velocity v. These transfer functions do not contain the servo poles.

TABLE C-1

Control Surface Input to Velocity Output Transfer Functions

Flight Condition One:

$$v/\delta_c = [-1.482(s+0.3051\pm j0.4095)(s+22.63)]/\beta_1$$

$$v/\delta_s = [0.1804(s+0.3733\pm j0.4441)(s+321.3)]/\beta_1$$

$$v/\delta_a = [1.449(s+0.2980\pm j0.5369)(s+5.469)]/\beta_1$$

$$v/\delta_{tv} = [-9.496(s+0.2328\pm j0.4762)(s+4.979)]/\beta_1$$

$$v/\delta_{bv} = [-9.469(s+0.5715\pm j0.1485)(s-2.415)]/\beta_1$$

$$\beta_1 = (s+1.546)(s-0.2846)(s+0.01897\pm j0.2508)$$

Flight Condition Two:

$$v/\delta_c = [-2.494(s+0.5869\pm j0.3159)(s+13.96)]/\beta_2$$

$$v/\delta_s = [-0.4419(s+0.7057\pm j0.1866)(s-138.8)]/\beta_2$$

$$v/\delta_a = [1.514(s+0.6460\pm j0.4218)\ \ +8.683)]/\beta_2$$

$$v/\delta_{tv} = [-10.03(s+0.3978\pm j0.5199)(s+3.887)]/\beta_2$$

$$v/\delta_{bv} = [-10.03(s+0.2861)(s+1.607)(s-1.837)]/\beta_2$$

$$\beta_2 = (s+1.979)(s-0.3851)(s+0.01104\pm j0.2081)$$

TABLE C-1 (continued)

Flight Condition Three:

$$v/\delta_c = [-2.533(s+0.3177\pm j1.006)(s+17.20)]/\beta_3$$

$$v/\delta_s = [-0.1588(s+0.4734\pm j1.136)(s-364.5)]/\beta_3$$

$$v/\delta_a = [1.201(s+0.3548\pm j1.202)(s+14.83)]/\beta_3$$

$$v/\delta_{tv} = [-10.87(s-0.07658\pm j0.7329)(s+3.736)]/\beta_3$$

$$v/\delta_{bv} = [-10.87(s+0.3564)(s-0.9588)(s+2.358)]/\beta_3$$

$$\beta_3 = (s+2.686)(s-0.4608)(s+0.003206\pm j0.1090)$$

TABLE C-2

Pitch Angle Response to Control Surface Input Transfer Functions

Flight Condition One:

$$\theta/\delta_c = [0.6347(s+0.1374)(s+0.2527)]/\beta_1$$

$$\theta/\delta_s = [-1.178(s+0.08939)(s+0.4035)]/\beta_1$$

$$\theta/\delta_a = [-0.1472(s+0.1011)(s+0.4798)]/\beta_1$$

$$\theta/\delta_{tv} = [0.7946(s+0.1556)(s+0.3015)]/\beta_1$$

$$\theta/\delta_{bv} = [-0.5014(s+0.03614)(s+0.5029)]/\beta_1$$

$$\beta_1 = (s+1.546)(s-0.2846)(s+0.01897\pm j0.2508)$$

Flight Condition Two:

$$\theta/\delta_c = [0.8191(s+0.01344)(s+0.5747)]/\beta_2$$

$$\theta/\delta_s = [-1.498(s+0.006778)(s+0.6854)]/\beta_2$$

$$\theta/\delta_a = [-0.3101(s+0.01372)(s+0.7711)]/\beta_2$$

$$\theta/\delta_{tv} = [0.7506(s+0.03004)(s+0.6343)]/\beta_2$$

$$\theta/\delta_{bv} = [-0.3822(s-0.02779)(s+0.8115)]/\beta_2$$

$$\beta_2 = (s+1.979)(s-0.3851)(s+0.01104\pm j0.2081)$$

TABLE C-2 (continued)

Flight Condition Three:

$$\theta/\delta_c = [1.880(s+0.04249)(s+0.7665)]/\beta_3$$

$$\theta/\delta_s = [-2.967(s+0.04023)(s+0.8865)]/\beta_3$$

$$\theta/\delta_a = [-0.8661(s+0.04034)(s+0.9704)]/\beta_3$$

$$\theta/\delta_{tv} = [0.7524(s+0.04998)(s+0.8427)]/\beta_3$$

$$\theta/\delta_{bv} = [-0.2738(s+0.01886)(s+1.062)]/\beta_3$$

$$\beta_3 = (s+2.686)(s-0.4608)(s+0.003206 \pm j0.1090)$$

TABLE C-3

ADA Response to Control Surface Input Transfer Functions

Flight Condition One:

$$\alpha/\delta_c = [-0.2740(s+0.01895\pm j0.2564)(s-21.41)]/\beta_1$$

$$\alpha/\delta_s = [-0.7660(s+0.01834\pm j0.2571)(s+15.49)]/\beta_1$$

$$\alpha/\delta_a = [-0.2744(s+0.01734\pm j0.2572)(s+6.045)]/\beta_1$$

$$\alpha/\delta_{tv} = [0.3890(s+0.01799\pm j0.2564)(s+20.80)]/\beta_1$$

$$\alpha/\delta_{bv} = [-0.3890(s+0.01900\pm j0.2583)(s+12.61)]/\beta_1$$

$$\beta_1 = (s+1.546)(s-0.2846)(s+0.01897\pm j0.2508)$$

Flight Condition Two:

$$\alpha/\delta_c = [-0.2107(s+0.01501+j0.2171)(s-37.26)]/\beta_2$$

$$\alpha/\delta_s = [-0.6648(s+0.01504\pm j0.2182)(s+23.01)]/\beta_2$$

$$\alpha/\delta_a = [-0.3604(s+0.01434\pm j0.2169)(s+9.444)]/\beta_2$$

$$\alpha/\delta_{tv} = [0.3032(s+0.01387\pm j0.2177)(s+25.68)]/\beta_2$$

$$\alpha/\delta_{bv} = [-0.3032(s+0.01719\pm j0.2195)(s+12.80)]/\beta_2$$

$$\beta_2 = (s+1.979)(s-0.3851)(s+0.01104\pm j0.2081)$$

TABLE C-3 (continued)

Flight Condition Three:

$$\alpha/\delta_c = [-0.2830(s+0.01037\pm j0.1445)(s-64.66)]/\beta_3$$

$$\alpha/\delta_s = [-0.9554(s+0.01066\pm j0.1445)(s+32.36)]/\beta_3$$

$$\alpha/\delta_a = [-0.5823(s+0.01030\pm j0.1485)(s+16.23)]/\beta_3$$

$$\alpha/\delta_{tv} = [0.1989(s+0.007381\pm j0.1466)(s+39.48)]/\beta_3$$

$$\alpha/\delta_{bv} = [-0.1989(s+0.01938\pm j0.1485)(s+14.73)]/\beta_3$$

$$\beta_3 = (s+2.686)(s-0.4608)(s+0.003206\pm j0.1090)$$

APPENDIX D

Equivalent Reconfigurable MIMO Plant Matrices and the Equivalent SISO Plant Matrices used in Designing the Aircraft FCS Compensation using QFT

In Chapter IV a set of P matrices are developed for three flight conditions and various control surface failures. Then using reconfigurable theory as discussed in Chapter III, the equivalent reconfigurable matrices P' are formed. The P' matrices are then transformed into the equivalent SISO system matrices Q. Tables D-1 through D-18 contain the P' matrices, while Tables D-19 through D-38 are the Q matrices used in FCS compensation design.

In the tables:

$$\Delta_1 = (S+1.546)(S-0.2846)(S+0.01897\pm j0.2508)(S+89)(S+30.62)$$

$$\Delta_2 = (S+1.979)(S-0.3851)(S+0.01104\pm j0.2081)(S+89)(S+30.62)$$

$$\Delta_3 = (S+2.686)(S-0.4608)(S+0.003206\pm j0.1090)(S+89)(S+30.62)$$

TABLE D-1

Plant Matrix for FCl No Failures

$$\underline{P}' = \frac{1}{\Delta_1} \begin{bmatrix} 28.87\ (S+0.01826\pm j0.2567)(S+19.29)(S+31.74) & -16.20\ (S+0.01827\pm j0.2568)(S+22.03)(S+35.87) \\ -216.6\ (S+0.3396 j0.4492)(S+32.02\pm j3.985) & 180.8\ (S+0.3432\pm j0.4449)(S+32.33)(S+53.28) \end{bmatrix}$$

TABLE D-2

Plant Matrix for FCl Canard Failed

$$\underline{P}' = \frac{1}{\Delta_1} \begin{bmatrix} 29.29\ (S+0.01823\pm j0.2568)(S+16.64)(S+32.64) & -17.03\ (S+0.01817\pm j0.2569)(S+15.24)(S+43.13) \\ -193.9\ (S+0.3491\pm j0.4590)(S+28.12\pm j8.148) & 134.4\ (S+0.3593\pm j0.4578)(S+38.28\pm j12.30) \end{bmatrix}$$

TABLE D-3

Plant Matrix for FCl Ailerons Failed

$$\underline{P}' = \frac{1}{\Delta_1} \begin{bmatrix} 28.45\ (S+0.01828\pm j0.2566)(S+20.59)(S+29.79) & -15.36\ (S+0.01831\pm j0.2567)(S+27.94\pm j4.878) \\ -194.5\ (S+0.3414\pm j0.4439)(S+29.17\pm j13.55) & 134.5\ (S+0.3459\pm j0.4371)(S+41.24\pm j20.52) \end{bmatrix}$$

TABLE D-4

Plant Matrix for FC1 Stabilator Failed

$$\underline{P}' = \frac{1}{\Delta_1} \begin{bmatrix} 27.27\ (S+0.01828\pm j0.2564)(S+20.31)(S+28.48) & -13.89\ (S+0.01832\pm j0.2567)(S+25.04\pm j7.554) \\ -213.9\ (S+0.3192+0.4502)(S+14.46)(S+43.13) & 174.3\ (S+0.3114\pm j0.4423)(S+14.25)(S+60.93) \end{bmatrix}$$

TABLE D-5

Plant Matrix for FC1 Stabilator and Aileron Failed

$$\underline{P}' = \frac{1}{\Delta_1} \begin{bmatrix} 28.12\ (S+0.01825\pm j0.2567)(S+15.10)(S+33.54) & -14.69\ (S+0.01808\pm j0.2566)(S+10.29)(S+39.16) \\ -191.7\ (S+0.3205\pm j0.4419)(S+18.24)(S+35.08) & 129.9\ (S+0.3124\pm j0.4250)(S+21.01)(S+47.60) \end{bmatrix}$$

TABLE D-6

Plant Matrix for FC1 Stabilator and Canard Failed

$$\underline{P}' = \frac{1}{\Delta_1} \begin{bmatrix} 28.12\ (S+0.01822\pm j0.2563)(S+16.87)(S+32.18) & -14.55\ (S+0.01821\pm j0.2569)(S+15.11)(S+35.91) \\ -191.2\ (S+0.3261\pm j0.4703)(S+11.58)(S+39.59) & 128.9\ (S+0.3192\pm j0.4893)(S+8.665)(S+33.68) \end{bmatrix}$$

TABLE D-10

Plant Matrix for FC2 Stabilator Failed

$$\underline{P}' = \frac{1}{\Delta_2} \begin{bmatrix} 44.75\ (S+0.01466\pm j0.2181)(S+20.34)(S+33.09) & -24.73\ (S+0.01471\pm j0.2182)(S+19.60)(S+38.95) \\ -374.3\ (S+0.6577\pm j0.3211)(S+23.16\pm j6.916) & 174.3\ (S+0.6819\pm j0.2773)(S+29.91\pm j19.08) \end{bmatrix}$$

TABLE D-11

Plant Matrix for FC2 Stabilator and Aileron Failed

$$\underline{P}' = \frac{1}{\Delta_2} \begin{bmatrix} 43.50\ (S+0.01462\pm j0.2181)(S+18.22)(S+32.99) & -22.24\ (S+0.01457\pm j0.2183)(S+13.77)(S+37.44) \\ -395.3\ (S+0.6072\pm j0.3609)(S+11.48)(S+35.54) & 301.3\ (S+0.65975j0.3404)(S+12.70)(S+48.89) \end{bmatrix}$$

TABLE D-12

Plant Matrix for FC2 Stabilator and Canard Failed

$$\underline{P}' = \frac{1}{\Delta_2} \begin{bmatrix} 43.73\ (S+0.01464\pm j0.2180)(S+19.98)(S+32.09) & -22.69\ (S+0.01462\pm j0.2183)(S+18.27)(S+35.49) \\ -380.3\ (S+0.6199\pm j0.3847)(S+10.06)(S+34.41) & 128.9\ (S+0.6275\pm j0.3960)(S+9.553)(S+43.13) \end{bmatrix}$$

TABLE D-13

Plant Matrix for FC2 Bottom Vanes Failed

$$\underline{P}' = \frac{1}{\Delta_3} \begin{bmatrix} 28.23\ (S+0.01414\pm j0.2178)\ (S+30.91\pm j3.114) & -14.74\ (S+0.01449\pm j0.2179)\ (S+33.98)(S+39.86) \\ -500.9\ (S+0.6073\pm j0.3696)\ (S+12.75)(S+30.66) & 332.4\ (S+0.6471\pm j0.3059)\ (S+29.54)(S+32.57) \end{bmatrix}$$

TABLE D-14

Plant Matrix for FC3 No Failures

$$\underline{P}' = \frac{1}{\Delta_3} \begin{bmatrix} 16.08\ (S+0.00993\pm j0.1463)\ (S+34.89\pm j9.739) & -10.92\ (S+0.01024\pm j0.1463)\ (S+40.60\pm j12.82) \\ -248.2\ (S+0.3492\pm j1.1.02)\ (S+27.61\pm j4.906) & 206.3\ (S+0.38465j1.105)\ (S+35.79)(S+46.07) \end{bmatrix}$$

TABLE D-15

Plant Matrix for FC3 Canard Failed

$$\underline{P}' = \frac{1}{\Delta_3} \begin{bmatrix} 15.30\ (S+0.00975\pm j0.1464)\ (S+27.14)(S+27.72) & -9.352\ (S+0.01003\pm j0.1467)\ (S+26.88)(S+47.16) \\ -225.4\ (S+0.3995\pm j1.148)\ (S+26.95\pm j18.19) & 160.6\ (S+0.4341\pm j1.153)\ (S+42.954\pm j28.54) \end{bmatrix}$$

TABLE D-16

Plant Matrix for FC3 Stabilators Failed

$$\underline{P}' = \frac{1}{\Delta_3}\begin{bmatrix} 14.62\,(S+0.00976\pm j0.1461)(S+32.31\pm j10.55) & -7.997\,(S+0.00999\pm j0.1460)(S+37.35\pm j19.29) \\ -250.6\,(S+0.2675+j1.060)(S+11.65)(S+40.53) & 211.1\,(S+0.3092+j1.066)S+14.82)(S+58.96) \end{bmatrix}$$

TABLE D-17

Plant Matrix for FC3 Ailerons Failed

$$\underline{P}' = \frac{1}{\Delta_3}\begin{bmatrix} 15.19\,(S+0.00991\pm j0.1461)(S+33.85+j12.59) & -9.139\,(S+0.01023\pm 0.1461)(S+41.84+j20.87) \\ -229.8\,(S+0.3482\pm j1.087)(S+25.67\pm j9.221) & 169.4\,(S+0.3888\pm j1.88)(S+38.55\pm j15.33) \end{bmatrix}$$

TABLE D-18

Plant Matrix for FC3 Stabilators, Ailerons Failed

$$\underline{P}' = \frac{1}{\Delta}\begin{bmatrix} 13.73\,(S+0.00971\pm 0.1459)(S+30.99\pm j13.27) & -6.124\,(S+0.00993\pm j0.1455)(S+32.97\pm j27.80) \\ -232.3\,(S+0.2467\pm j1.017)(S+10.90)(S+37.22) & 160.6\,(S+0.2935\pm j1.011)(S+14.81)(S+52.64) \end{bmatrix}$$

TABLE D-19

Plant Matrix for FC3 Stabilator, Canards

$$P = \frac{1}{\Delta_3} \begin{bmatrix} 15.05\,(S+0.009646\pm j0.1464)(S+24.59)(S+38.87) & -8.863\,(S+0.009785\pm j0.1469)(S+21.20)(S+48.56) \\ -211.9\,(S+0.2125\pm j1.104)(S+8.226)(S+34.16) & 133.5\,(S+0.2892\pm j1.165)(S+11.29)(S+43.70) \end{bmatrix}$$

TABLE D-20

Q Matrix for FC1 No Failures

$$Q = \Delta \begin{bmatrix} \dfrac{1}{180.8\ (S+0.3432\pm j0.4449)(S+32.33)(S+53.28)} & \dfrac{1}{16.20\ (S+0.01827\pm j0.2568)(S+22.03)(S+35.87)} \\ \dfrac{1}{216.6\ (S+0.3396\pm j0.449)(S+31.06\pm j3.985)} & \dfrac{1}{28.87\ (S+0.0183\pm j0.2567)(S+19.29)(S+31.74)} \end{bmatrix}$$

$$\Delta = 1269\ \frac{(S+0.3697\pm j0.4561)(S+17.52)(S+59.67)}{(S+1.546)(S-0.2846)}$$

TABLE D-21

Q Matrix for FC1 Canards Failed

$$Q = \Delta \begin{bmatrix} \dfrac{1}{134.4\ (S+0.3593\pm j0.4578)(S+0.3828\pm j12.30)} & \dfrac{1}{17.03\ (S+0.01817\pm j0.2569)(S+15.24)(S+43.13)} \\ \dfrac{1}{193.9\ (S+0.3491\pm j0.459)(S+28.12\pm j8.148)} & \dfrac{1}{29.29\ (S+0.0183\pm j0.2568)(S+16.64)(S+34.62)} \end{bmatrix}$$

$$\Delta = 3363\ \frac{(S+0.3468\pm j0.4407)(S+17.52)(S+59.67)}{(S+1.546)(S-0.2846)}$$

TABLE D-22

Q Matrix for FC1 Stabilators Failed

$$Q = \Delta \begin{bmatrix} \dfrac{1}{174.3\ (S+0.3114\pm j0.4423)(S+14.25)(S+60.93)} & \dfrac{1}{13.89\ (S+0.01832\pm j0.2567)(S+25.04\pm j7.554)} \\ \dfrac{1}{213.9\ (S+0.3192\pm j0.4502)(S+14.46)(S+43.13)} & \dfrac{1}{27.72\ (S+0.0182\pm j0.2566)(S+20.31)(S+28.48)} \end{bmatrix}$$

$$\Delta = 1674\ \frac{(S+0.357\pm j0.4401)(S+17.89)(S+58.77)}{(S+1.546)(S-0.2846)}$$

TABLE D-23

Q Matrix for FC1 Ailerons Failed

$$Q = \Delta \begin{bmatrix} \frac{1}{135.4\ (S+0.3459\pm j0.4371)(S+41.24\pm j20.52)} & \frac{1}{15.36\ (S+0.01831\pm j0.2568)(S+27.94\pm j4.878)} \\ \frac{1}{194.5\ (S+0.3414\pm j0.4439)(S+29.17\pm j13.55)} & \frac{1}{78.45\ (S+0.01828\pm j0.2567)(S+20.59)(S+29.79)} \end{bmatrix}$$

$$\Delta = 1732\ \frac{(S+0.3503\pm j0.4303)(S+18.01)(S+59.48)}{(S+1.546)(S\ 0.2846)}$$

TABLE D-24

Q Matrix for FC1 Stabilator Failed

$$Q = \Delta \begin{bmatrix} \frac{1}{174.3\ (S+0.3114\pm j0.4423)(S+14.25)(S+60.93)} & \frac{1}{13.89\ (S+0.01832\pm j0.2567)(S+25.04\pm j7.554)} \\ \frac{1}{213.9\ (S+0.3192\pm j0.4502)(S+14.46)(S+43.13)} & \frac{1}{27.72\ (S+0.01828\pm j0.2567)(S+20.31)(S+28.48)} \end{bmatrix}$$

$$\Delta = 1674\ \frac{(S+0.3570\pm j0.4401)(S+17.89)(S+58.77)}{(S+1.546)(S-0.2846)}$$

TABLE D-25

Q Matrix for FC1 Stabilato , Ailerons Failed

$$Q = \Delta \begin{bmatrix} \frac{1}{129.9\ (S+0.3124\pm j0.4250)(S+21.01)(S+47.60)} & \frac{1}{14.69\ (S+0.01808\pm j0.2566)(S+10.29)(S+39.16)} \\ \frac{1}{191.7\ (S+0.3205\pm j0.4419)(S+18.24)(S+35.08)} & \frac{1}{28.12\ (S+0.01822\pm j0.2567)(S+15.10)(S+33.54)} \end{bmatrix}$$

$$\Delta = 1673\ \frac{(S+0.3070\pm j0.4141)(S+16.55)(S+29.76)}{(S+1.546)(S-0.2846)}$$

TABLE D-26

Q Matrix for FCI Canard Failed

$$\underline{Q} = \Delta \begin{bmatrix} \dfrac{1}{128.9\ (S+0.3192 \pm j0.4893)(S+8.669)(S+33.68)} & \dfrac{1}{14.69\ (S+0.01821 \pm j0.2567)(S+15.11)(S+39.91)} \\ \dfrac{1}{191.2\ (S+0.3261 \pm j0.4703)(S+11.58)(S+39.59)} & \dfrac{1}{28.12\ (S+0.01825 \pm j0.2567)(S+16.87)(S+32.18)} \end{bmatrix}$$

$$\Delta = \frac{1630\ (S+0.3316 \pm j0.5518)(S+5.407)(S+18.10)}{(S+1.546)(S-0.2846)}$$

TABLE D-27

O Matrix for FC2 No Failures

$$Q = \begin{bmatrix} \frac{1}{287.8(S+0.6564\pm j0.2920)(S+32.37)(S+40.39)} & \frac{1}{24.08(S+0.01474\pm j0.2181)(S+29.37\pm j3.225)} \\ \frac{1}{411.7(S+0.644\pm j0.3225)(S+20.68)(S+30.71)} & \frac{1}{44.41(S+0.01467\pm j0.2181)(S+23.23)(S+30.19)} \end{bmatrix} \Delta$$

$$\Delta = \frac{1434(S+0.6678\pm j0.2590)(S+23.35)(S+30.45)}{(S+1.979)(S-0.3851)}$$

TABLE D-28

O Matrix for FC2 Canards

$$Q = \Delta \begin{bmatrix} \frac{1}{212.9(S+0.6819\pm j0.2773)(S+32.79\pm j15.45)} & \frac{1}{24.73(S+0.01471\pm j0.2182)(S+19.60)(S+28.41\pm j8.189)} \\ \frac{1}{374.3(S+0.6437\pm j0.3144)(S+24.31\pm j5.982)} & \frac{1}{43.88(S+0.01468\pm j0.2181)(S+26.44\pm j1.156)} \end{bmatrix}$$

$$\Delta = \frac{1664(S+0.6696\pm j0.2279)(S+23.77)(S+45.11)}{(S-0.3851)(S+1.979)}$$

TABLE D-29

O Matrix for FC2 Stabilators Failed

$$Q = \Delta \begin{bmatrix} \frac{1}{301.3\ (S+0.6067\pm j0.3576)(S+11.56)(S+53.88)} & \frac{1}{22.05\ (S+0.01467\pm j0.2180)(S+26.91\pm j6.349)} \\ \frac{1}{418.5\ (S+0.6011\pm j0.3676)(S+11.04)(S+38.78)} & \frac{1}{43.5\ (S+0.01462\pm j0.2181)(S+18.22)(S+32.99)} \end{bmatrix}$$

$$\Delta = \frac{1926\ (S+0.6124)(S+1.153)(S+7.728)(S+22.25)}{(S-0.3851)(S+1.979)}$$

TABLE D-30

Q Matrix for FC2 Stabilator, Ailerons Failed

$$Q = \Delta \begin{bmatrix} \frac{1}{285\ (S+0.5975\pm j0.3404)(S+12.7)(S+46.89)} & \frac{1}{22.24\ (S+0.01457\pm j0.283)(S+13.77)(S+37.44)} \\ \frac{1}{395.3\ (S+0.6072\pm j0.3609)(S+11.48)(S+35.54)} & \frac{1}{43.50\ (S+0.01462\pm j0.2181)(S+18.22)(S+32.99)} \end{bmatrix}$$

$$= \frac{2646\ (S+0.5834\pm j0.3083)(S+15.39\pm j3.131)}{(S+1.979)(S-0.3851)}$$

TABLE D-31

Q Matrix for FC2 Stabilator, Canard Failed

$$Q = \Delta \begin{bmatrix} \frac{1}{225.0\ (S+0.6275\pm j0.3960)(S+9.553)(S+43.13)} & \frac{1}{22.69\ (S+0.01462\pm j0.2182)(S+18.27)(S+35.49)} \\ \frac{1}{380.3\ (S+0.6199\pm j0.3847)(S+10.06)(S+34.41)} & \frac{1}{43.73\ (S+0.01494\pm j0.2181)(S+19.98)(S+32.09)} \end{bmatrix}$$

$$\Delta = \frac{1908\ (S+0.6496\pm j0.4263)(S+8.661)(S+23.25)}{(S+1.979)(S-0.3851)}$$

TABLE D-32

Q Matrix for FC2 Bottom Vanes Failed

$$Q = \Delta \begin{bmatrix} \frac{1}{332.4\ (S+0.6471\pm j0.3059)(S+29.54)(S+32.57)} & \frac{1}{14.74\ (S+0.01449\pm j0.2179)(S+35.98)(S+39.86)} \\ \frac{1}{500.9\ (S+0.6073\pm j0.3696)(S+12.75)(S+30.66)} & \frac{1}{28.23\ (S+0.01414\pm j0.2178)(S+30.91\pm j3.114)} \end{bmatrix}$$

$$\Delta = \frac{615\ (S+0.6567\pm j0.2744)(S+33.53)(S+95.98)}{(S+1.979)(S-0.3851)}$$

TABLE D-33

Q Matrix for FC3 No Failures

$$\underline{Q} = \Delta \begin{bmatrix} \dfrac{1}{206.3\ (S+0.3846\pm j1.105)\ (S+35.79)(S+46.07)} & \dfrac{1}{10.92\ (S+0.01024\pm j0.1463)\ (S+43.60\pm j12.82)} \\ \dfrac{1}{248.2\ (S+0.3492\pm j1.102)\ (S+27.61\pm j4.906)} & \dfrac{1}{16.08\ (S+0.009934\pm j0.1463)\ (S+34.89\pm j9.739)} \end{bmatrix}$$

$$\Delta = 1210\ \frac{(S+0.009478\pm j0.1462)(S+0.4902\pm j1.107)(S+36.75\pm j18.30)}{(S+2.686)(S-0.4608)(S+0.003206\pm j0.1090)}$$

TABLE D-34

Q Matrix for FC3 Canards Failed

$$\underline{Q} = \Delta \begin{bmatrix} \dfrac{1}{16[illegible].6\ (S+0.4341\pm j1.153)\ (S+42.95\pm j28.58)} & \dfrac{1}{9.352\ (S+0.01003\pm j0.1467)\ (S+26.88)(S+47.16)} \\ \dfrac{1}{225.4\ (S+0.3995\pm j1.148)\ (S+26.95\pm j18.19)} & \dfrac{1}{15.30\ (S+0.00975\pm j0.1464)\ (S+37.14)(S+27.72)} \end{bmatrix}$$

$$\Delta = 668.8\ \frac{(S+0.009557\pm j0.1462)(S+0.4561\pm j1.156)(S+29.30)(S+143)}{(S+0.003206\pm j0.1090)(S+2.686)(S-0.4608)}$$

TABLE D-35

Q Matrix for FC3 Stabilator Failed

$$\underline{Q} = \Delta \begin{bmatrix} \dfrac{1}{211.1\ (S+0.3092\pm j1.066)\ (S+14.82)(S+58.96)} & \dfrac{1}{7.997\ (S+0.009995\pm j0.1460)\ (S+37.35\pm j19.29)} \\ \dfrac{1}{250.6\ (S+0.2675\pm j1.060)\ (S+11.65)(S+40.53)} & \dfrac{1}{14.62\ (S+0.009755\pm j0.1461)\ (S+32.31\pm j10.55)} \end{bmatrix}$$

$$\Delta = 2052\ \frac{(S+0.009488\pm j0.1462)(S+0.3589\pm j1.069)(S+19.92\pm 9.679)}{(S+0.003206\pm j0.1090)(S+2.686)(S-0.4608)}$$

TABLE D-36

Q Matrix for FC3 Ailerons Failed

$$\underline{Q} = \Delta \begin{bmatrix} \dfrac{1}{169.4\ (S+0.3888\pm j1.088)(S+38.55\pm j15.33)} & \dfrac{1}{9.139\ (S+0.01023\pm j0.1461)(S+41.84\pm j20.87)} \\ \dfrac{1}{229.8\ (S+0.3482\pm j1.087)(S+25.67\pm j9.221)} & \dfrac{1}{15.19\ (S+0.009911\pm j0.1461)(S+33.85\pm j12.59)} \end{bmatrix}$$

$$\Delta = \frac{946.3\ (S+0.009471\pm j0.1462)(S+0.4468\pm j1.086)(S+34.39\pm j25.57)}{(S+0.003206\pm j0.1090)(S+2.686)(S-0.4608)}$$

TABLE D-37

Q Matrix for FC3 Stabilator, Ailerons

$$\underline{Q} = \Delta \begin{bmatrix} \dfrac{1}{174.3\ (S+0.2935\pm j1.011)(S+14.81)(S+52.64)} & \dfrac{1}{6.214\ (S+0.009928\pm j0.1455)(S+32.97\pm j27.80)} \\ \dfrac{1}{232.3\ (S+0.2467\pm j1.017)(S+10.90)(S+37.22)} & \dfrac{1}{13.73\ (S+0.009711\pm j0.1459)(S+30.99\pm j13.27)} \end{bmatrix}$$

$$\Delta = \frac{1899\ (S+0.009478\pm j0.1464)(S+0.3422\pm j1.001)(S+16.61\pm j11.13)}{(S+0.003206\pm j0.1090)(S+2.686)(S-0.4608)}$$

TABLE D-38

Q Matrix for FC3 Stabilators, Canards

$$\underline{Q} = \Delta \begin{bmatrix} \dfrac{1}{133.5\ (S+0.2892\pm j1.165)(S+11.29)(S+43.70)} & \dfrac{1}{8.863\ (S+0.009785\pm j0.1469)(S+21.20)(S+48.56)} \\ \dfrac{1}{211.9\ (S+0.2125\pm j1.104)(S+8.226)(S+34.16)} & \dfrac{1}{15.05\ (S+0.009646\pm j0.1464)(S+24.59)(S+38.87)} \end{bmatrix}$$

$$\Delta = \frac{263.7\ (S+0.009510\pm j0.1460)(S+0.3961\pm j1.219)(S+15.24)(S+75.21)}{(S+0.003206\pm j0.1090)(S+2.686)(S-0.4608)}$$

Appendix E

Upper and Lower Tracking Bounds for AOA and Velocity Channels

Appendix E contains the calculated frequency responses for the tracking bounds outlined in pages 60-69 of Chapter IV. Table E-1 is the AOA upper tracking bound(T_{α_U}), while Table E-2 is the lower tracking bound(T_{α_L}). Tables E-3 and E-4 are the upper and lower velocity bounds(T_{v_U}, T_{v_L}) respectively.

TABLE E-1

Upper Frequency Bound for AOA Channel T_{α_U}

W(RAD/SEC)	DECIBELS	DEGREES
0.	10.8854	0.
.100000E-01	10.8854	-.286667E-01
.200000E-01	10.8855	-.573336E-01
.300000E-01	10.8855	-.860009E-01
.400000E-01	10.8855	-.114669
.500000E-01	10.8856	-.143338
.600000E-01	10.8857	-.172007
.700000E-01	10.8858	-.200678
.800000E-01	10.8859	-.229351
.900000E-01	10.8860	-.258025
.100000	10.8861	-.286700
.200000	10.8881	-.573603
.300000	10.8915	-.860911
.400000	10.8962	-1.14883
.500000	10.9023	-1.43756
.600000	10.9097	-1.72730
.700000	10.9184	-2.01828
.800000	10.9285	-2.31068
.900000	10.9400	-2.60473
1.00000	10.9528	-2.90063
2.00000	11.1556	-6.01052
3.00000	11.4950	-9.56744
4.00000	11.9703	-13.8706
5.00000	12.5721	-19.3200
6.00000	13.2689	-26.4513
7.00000	13.9784	-35.9109
8.00000	14.5284	-48.2084
9.00000	14.6567	-63.0524
10.0000	14.1497	-78.7284
20.0000	1.12672	-133.185
30.0000	-6.13492	-134.329
40.0000	-10.6410	-130.767
50.0000	-13.8041	-126.703
60.0000	-16.1883	-122.963
70.0000	-18.0757	-119.709
80.0000	-19.6252	-116.926
90.0000	-20.9337	-114.552
100.000	-22.0633	-112.521

TABLE E-2

Lower Frequency Bound for AOA Channel T_{α_L}

W(RAD/SEC)	DECIBELS	DEGREES
0.	10.8814	0.
.100000E-01	10.8813	-.212813
.200000E-01	10.8812	-.425623
.300000E-01	10.8811	-.638430
.400000E-01	10.8809	-.851232
.500000E-01	10.8806	-1.06403
.600000E-01	10.8803	-1.27681
.700000E-01	10.8799	-1.48958
.800000E-01	10.8794	-1.70235
.900000E-01	10.8789	-1.91509
.100000	10.8783	-2.12782
.200000	10.8692	-4.25380
.300000	10.8540	-6.37610
.400000	10.8329	-8.49293
.500000	10.8058	-10.6025
.600000	10.7729	-12.7032
.700000	10.7342	-14.7932
.800000	10.6899	-16.8710
.900000	10.6402	-18.9352
1.00000	10.5851	-20.9843
2.00000	9.78131	-40.4057
3.00000	8.65155	-57.4954
4.00000	7.35993	-72.2553
5.00000	6.01007	-85.0303
6.00000	4.65594	-96.2078
7.00000	3.32246	-106.110
8.00000	2.01991	-114.981
9.00000	.751756	-123.000
10.0000	-.481476	-130.301
20.0000	-11.1086	-178.698
30.0000	-19.2908	-203.698
40.0000	-25.7721	-218.434
50.0000	-31.0726	-227.982
60.0000	-35.5304	-234.617
70.0000	-39.3655	-239.474
80.0000	-42.7248	-243.175
90.0000	-45.7106	-246.085
100.000	-48.3959	-248.430

TABLE E-3

Upper Frequency Bound for Velocity Channel T_{v_U}

W(RAD/SEC)	DECIBELS	DEGREES
0.	13.9794	0.
.100000E-01	13.9790	-.572939
.200000E-01	13.9777	-1.14576
.300000E-01	13.9755	-1.71836
.400000E-01	13.9725	-2.29061
.500000E-01	13.9686	-2.86241
.600000E-01	13.9638	-3.43363
.700000E-01	13.9582	-4.00417
.800000E-01	13.9517	-4.57392
.900000E-01	13.9444	-5.14276
.100000E+00	13.9362	-5.71059
.100000	13.9362	-5.71059
.200000	13.8091	-11.3099
.300000	13.6051	-16.6992
.400000	13.3348	-21.8014
.500000	13.0103	-26.5651
.600000	12.6440	-30.9638
.700000	12.2475	-34.9920
.800000	11.8310	-38.6598
.900000	11.4026	-41.9872
1.00000	10.9691	-45.0000
1.00000	10.9691	-45.0000
2.00000	6.98970	-63.4349
3.00000	3.97940	-71.5651
4.00000	1.67491	-75.9638
5.00000	-.170333	-78.6901
6.00000	-1.70262	-80.5377
7.00000	-3.01030	-81.8699
8.00000	-4.14973	-82.8750
9.00000	-5.15874	-83.6598
10.0000	-6.06381	-84.2894
10.0000	-6.06381	-84.2894
20.0000	-12.0520	-87.1376
30.0000	-15.5678	-88.0908
40.0000	-18.0645	-88.5679
50.0000	-20.0017	-88.8542
60.0000	-21.5848	-89.0452
70.0000	-22.9234	-89.1815
80.0000	-24.0831	-89.2838
90.0000	-25.1060	-89.3634
100.000	-26.0210	-89.4271

TABLE E-4

Lower Frequency Bound for Velocity Channel T_{v_L}

W(RAD/SEC)	DECIBELS	DEGREES
0.	13.9794	0.
.100000E-01	13.9782	-1.02360
.200000E-01	13.9746	-2.04666
.300000E-01	13.9685	-3.06867
.400000E-01	13.9601	-4.08909
.500000E-01	13.9492	-5.10741
.600000E-01	13.9360	-6.12312
.700000E-01	13.9205	-7.13570
.800000E-01	13.9026	-8.14467
.900000E-01	13.8824	-9.14955
.100000E+00	13.8600	-10.1499
.100000	13.8600	-10.1499
.200000	13.5200	-19.8099
.300000	13.0062	-28.6272
.400000	12.3752	-36.4390
.500000	11.6778	-43.2409
.600000	10.9529	-49.1211
.700000	10.2262	-54.2050
.800000	9.51361	-58.6207
.900000	8.82412	-62.4839
1.00000	8.16209	-65.8926
1.00000	8.16209	-65.8926
2.00000	2.97028	-86.9013
3.00000	-.560205	-98.8229
4.00000	-3.26769	-107.845
5.00000	-5.51138	-115.433
6.00000	-7.46130	-122.096
7.00000	-9.20749	-128.063
8.00000	-10.8020	-133.461
9.00000	-12.2770	-138.377
10.0000	-13.6538	-142.876
10.0000	-13.6538	-142.876
20.0000	-24.1164	-173.518
30.0000	-31.3371	-191.383
40.0000	-36.9527	-203.764
50.0000	-41.5976	-213.003
60.0000	-45.5769	-220.159
70.0000	-49.0625	-225.841
80.0000	-52.1633	-230.440
90.0000	-54.9544	-234.223
100.000	-57.4906	-237.381

Appendix F

Computer Aided Design(CAD) Package STOLCAT

STOLCAT, written by the author and Captain Greg Mandt(AFWAL/FIGX) takes body axis aerodynamic data and transforms it into lateral and longitudinal state space aircraft equations of motion in the stability axis. The form of these equations is in Appendix B. This thesis uses only tne longitudinal equations, but provides the lateral equations for other Air Force Institute of Technology students working with the same aircraft in their thesis. The stability axis is chosen as the output axis to make the other student's analysis simpler. The choice has little effect on this thesis since design is limited to the longitudinal mode. The program is in FORTRAN 77, and set up to run interactive, rather than batch.

```
      PROGRAM STOLCAT
C*************************************************************************
C
C     DECLARE VARIABLE TYPES
C
C*************************************************************************
      REAL ALPHA,Q,S,C,B,U,DTHETA,W,BIXX,BIYY,BIZZ,
     1BIXZ,DALPHA,DPR,VT,
     2CZA,CZQ,CZU,CZD1,CZD2,CZD3,CZD4,CZD5,CDZ6,CDZ7,CZD8,
     3CXA,CXQ,CXU,CXD1,CXD2,CXD3,CXD4,CXD5,CXD6,CXD7,CXD8,
     4CMA,CMQ,CMU,CMD1,CMD2,CMD3,CMD4,CMD5,CMD6,CMD7,CMD8,
     5Z1,ZA,ZH,ZQ,ZU,ZD1,ZD2,ZD3,ZD4,ZD5,ZD6,ZD7,ZD8,
     6XA,XH,XQ,XU,XD1,XD2,XD3,XD4,XD5,XD6,XD7,XD8,
     7M1,MA,MH,MQ,MU,MD1,MD2,MD3,MD4,MD5,MD6,MD7,MD8
      REAL CNB,CYB,CLB,L,N
      DIMENSION AMAT(4,4),BMAT(4,8)
      DIMENSION DIRMAT(5,5),DIRBMAT(5,9)
      CHARACTER*3 KEY, KEY1, DATA1, DATA2, DATA3, RUN
      CHARACTER*1 STAB1,STAB2
C*************************************************************************
C
C     INITIAL DATA VALUES FOR PROGRAM CHECK
C
C*************************************************************************
      DATA Q /48.1/,S /608./, C /15.94/, B /42.7/, U /201./
      DATA DTHETA /11.8030/, DALPHA /11.8030/,W /33576.14/
      DATA BIXX /23644./,BIYY /181847./,BIZZ /199674./,BIXZ /-3086./
      DATA CZA /-7.84976E-2/, CXA /1.5095276E-3/, CMA /9.574118E-3/
      DATA CZQ /0./, CXQ /0./, CMQ /-.16951603/
      DATA CZU /-1.06551597/, CXU /-6.1932E-3/, CMU /6.394289E-2/
      DATA CZH /-1.676463E-4/, CXH /6.662777E-4/, CMH /1.76622E-4/
      DATA CZD1 /-2.63634E-3/, CXD1 /-1.552420E-3/, CMD1 /5.57696E-3/
      DATA CZD2 /-8.31511E-3/, CXD2 /-2.749671E-4/, CMD2 /-1.02066E-2/
      DATA CZD3 /-5.59102E-3/, CXD3 /1.157373E-3/, CMD3 /8.52107E-4/
      DATA CZD4 /-4.50843E-3/, CXD4 /9.4211093E-4/, CMD4 /-2.11118E-3/
      DATA CZD5 /1.896349E-3/, CXD5 /-3.120989E-3/, CMD5 /2.55459E-3/
      DATA CZD6 /-7.422954E-4/, CXD6 /-3.595656E-3/, CMD6 /-1.30123E-3/
      DATA CZD7 /1.896349E-3/, CXD7 /-3.120989E-3/, CMD7 /2.55459E-3/
      DATA CZD8 /-7.422954E-4/, CXD8 /-3.595658E-3/, CMD8 /-1.30123E-3/
      DATA CLB /-2.973933E-3/, CNB /-5.5065055E-4/, CYB /-1.637941E-2/
      DATA CLP /-5.740524E-3/, CNP /-2.3099719E-3/, CYP / 0.000000000/
      DATA CLR / 3.902348E-3/, CNR /-9.6998151E-3/, CYR / 0.000000000/
      DATA CLD1/1.0017E-4/, CND1/-1.3256E-3/, CYD1/3.0606E-3/
      DATA CLD2/-1.14999E-4/, CND2/5.1323E-4/, CYD2/1.3139E-3/
      DATA CLD3/8.5104E-4/, CND3/4.4837E-4/, CYD3/-1.0623E-3/
      DATA CLD4/7.5284E-4/, CND4/7.6138E-5/, CYD4/-1.5235E-4/
      DATA CLD5/6.9959E-4/, CND5/0.00/, CYD5/0.00/
      DATA CLD6/9.6816E-5/, CND6/1.5934E-4/, CYD6/0.0/
      DATA CLD7/-3.7897E-5/, CND7/1.8357E-4 , CYD7/0.0/
      DATA CLD8/-9.6816E-5/, CND8/-1.5934E-4/, CYD8/0.0/
      DATA CLD9/3.7897E-5/, CND9/-1.8357E-4/, CYD9/0.0/
      DPR = 57.2957795
C*************************************************************************
C
C     SCREEN INFO PACKAGE
C
C*************************************************************************
      WRITE(*,5)
 5    FORMAT(1X,'*************************************************')
```

```
      WRITE(*,10)
 10   FORMAT(1X,'*** STABILITY DERIVATIVE TRANSFORMATION PROGRAM  ***')
      WRITE(*,20)
 20   FORMAT(1X,'*****************************************************')
      WRITE(*,100)
 100  FORMAT(1X,'ENTER BODY AXIS (NON-DIMENSIONALIZED) COEFFICIENTS ')
      WRITE(*,101)
 101  FORMAT(1X,'FOR TRANSFORMATION TO DIMENSIONALIZED BODY AXIS')
      WRITE(*,102)
 102  FORMAT(1X,'AND TO GENERATE STATE AND INPUT MATRICES.')
      WRITE(*,41)
 41   FORMAT(1X,'NOTE:  ALL COEFFICIENTS ARE REQUESTED WHEN COMPUTING')
 103  CONTINUE
      WRITE(*,30)
 30   FORMAT(1X,'*****************************************************')
      WRITE(*,106)
 106  FORMAT(1X,'TO TRANSFORM ONLY LONGITUDINAL DATA - TYPE LONG')
      WRITE(*,107)
 107  FORMAT(1X,'TO TRANSFORM ONLY LATERAL-DIRECTIONAL DATA - TYPE LAT')
      WRITE(*,108)
 108  FORMAT(1X,'TO TRANSFORM BOTH LONG AND LAT-DIR DATA - TYPE BOTH')
      WRITE(*,111)
 111  FORMAT(1X,'KEYWORD =   ')
      READ(*,109) KEY
 109  FORMAT(A3)
      IF(KEY .EQ. 'LAT') GO TO 104
      IF(KEY .EQ. 'LON') GO TO 104
      IF(KEY .EQ. 'BOT') GO TO 104
      IF(KEY .EQ. 'GAM') GO TO 596
      GO TO 103
C*********************************************************************
C
C       INPUT DATA
C
C*********************************************************************
 104  CONTINUE
      WRITE(*,500)
 500  FORMAT(1X,'*****************************************************')
      WRITE(*,510)
 510  FORMAT(1X,'Q  (DYNAMIC PRESSURE - LBS/FT**2) = ')
      READ(*,*) Q
      WRITE(*,520)
 520  FORMAT(1X,'S  (WING REFERENCE AREA - FT**2) = ')
      READ(*,*) S
      WRITE(*,530)
 530  FORMAT(1X,'C  (WING MEAN AERODYNAMIC CORD - FT) = ')
      READ(*,*) C
      WRITE(*,540)
 540  FORMAT(1X,'B  (WING SPAN - FT) = ')
      READ(*,*) B
      WRITE(*,550)
 550  FORMAT(1X,'VT (TRIM VELOCITY - FT/SEC) = ')
      READ (*,*) U
      VT=U
      WRITE(*,560)
 560  FORMAT(1X,'THETA (PITCH ANGLE - DEGS) = ')
      READ(*,*) DTHETA
      WRITE(*,570)
 570  FORMAT(1X,'W  (WEIGHT - LBS) = ')
      READ(*,*) W
```

```
      PROGRAM STOLCAT
C*************************************************************************
C
C     DECLARE VARIABLE TYPES
C
C*************************************************************************
      REAL ALPHA,Q,S,C,B,U,DTHETA,W,BIXX,BIYY,BIZZ,
     1BIXZ,DALPHA,DPR,VT,
     2CZA,CZQ,CZU,CZD1,CZD2,CZD3,CZD4,CZD5,CDZ6,CDZ7,CZD8,
     3CXA,CXQ,CXU,CXD1,CXD2,CXD3,CXD4,CXD5,CXD6,CXD7,CXD8,
     4CMA,CMQ,CMU,CMD1,CMD2,CMD3,CMD4,CMD5,CMD6,CMD7,CMD8,
     5Z1,ZA,ZH,ZQ,ZU,ZD1,ZD2,ZD3,ZD4,ZD5,ZD6,ZD7,ZD8,
     6XA,XH,XQ,XU,XD1,XD2,XD3,XD4,XD5,XD6,XD7,XD8,
     7M1,MA,MH,MQ,MU,MD1,MD2,MD3,MD4,MD5,MD6,MD7,MD8
      REAL CNB,CYB,CLB,L,N
      DIMENSION AMAT(4,4),BMAT(4,8)
      DIMENSION DIRMAT(5,5),DIRBMAT(5,9)
      CHARACTER*3 KEY, KEY1, DATA1, DATA2, DATA3, RUN
      CHARACTER*1 STAB1,STAB2
C*************************************************************************
C
C     INITIAL DATA VALUES FOR PROGRAM CHECK
C
C*************************************************************************
      DATA Q /48.1/,S /608./, C /15.94/, B /42.7/, U /201./
      DATA DTHETA /11.8030/, DALPHA /11.8030/,W /33576.14/
      DATA BIXX /23644./,BIYY /181847./,BIZZ /199674./,BIXZ /-3086./
      DATA CZA /-7.84976E-2/, CXA /1.5095276E-3/, CMA /9.574118E-3/
      DATA CZQ /0./, CXQ /0./, CMQ /-.16951603/
      DATA CZU /-1.06551597/, CXU /-6.1932E-3/, CMU /6.394289E-2/
      DATA CZH /-1.676463E-4/, CXH /6.662777E-4/, CMH /1.76622E-4/
      DATA CZD1 /-2.63634E-3/, CXD1 /-1.552420E-3/, CMD1 /5.57696E-3/
      DATA CZD2 /-8.31511E-3/, CXD2 /-2.749671E-4/, CMD2 /-1.02066E-2/
      DATA CZD3 /-5.59102E-3/, CXD3 /1.157373E-3/, CMD3 /8.52107E-4/
      DATA CZD4 /-4.50843E-3/, CXD4 /9.4211093E-4/, CMD4 /-2.11118E-3/
      DATA CZD5 /1.896349E-3/, CXD5 /-3.120989E-3/, CMD5 /2.55459E-3/
      DATA CZD6 /-7.422954E-4/, CXD6 /-3.595656E-3/, CMD6 /-1.30123E-3/
      DATA CZD7 /1.896349E-3/, CXD7 /-3.120989E-3/, CMD7 /2.55459E-3/
      DATA CZD8 /-7.422954E-4/, CXD8 /-3.595658E-3/, CMD8 /-1.30123E-3/
      DATA CLB /-2.973933E-3/, CNB /-5.5065055E-4/, CYB /-1.637941E-2/
      DATA CLP /-5.740524E-3/, CNP /-2.3099719E-3/, CYP / 0.000000000/
      DATA CLR / 3.902348E-3/, CNR /-9.6998151E-3/, CYR / 0.000000000/
      DATA CLD1/1.0017E-4/, CND1/-1.3256E-3/, CYD1/3.0606E-3/
      DATA CLD2/-1.14999E-4/, CND2/5.1323E-4/, CYD2/1.3139E-3/
      DATA CLD3/8.5104E-4/, CND3/4.4837E-4/, CYD3/-1.0622E-3/
      DATA CLD4/7.5284E-4/, CND4/7.6138E-5/, CYD4/-1.5235E-4/
      DATA CLD5/6.9959E-4/, CND5/0.00/, CYD5/0.00/
      DATA CLD6/9.6816E-5/, CND6/1.5934E-4/, CYD6/0.0/
      DATA CLD7/-3.7897E-5/, CND7/1.8357E-4/, CYD7/0.0/
      DATA CLD8/-9.6816E-5/, CND8/-1.5934E-4/, CYD8/0.0/
      DATA CLD9/3.7897E-5/, CND9/-1.8357E-4/, CYD9/0.0/
      DPR = 57.2957795
C*************************************************************************
C
C     SCREEN INFO PACKAGE
C
C*************************************************************************
      WRITE(*,5)
 5    FORMAT(1X,'*****************************************************')
```

```
      WRITE(*,10)
 10   FORMAT(1X,'*** STABILITY DERIVATIVE TRANSFORMATION PROGRAM  ***')
      WRITE(*,20)
 20   FORMAT(1X,'*****************************************************')
      WRITE(*,100)
 100  FORMAT(1X,'ENTER BODY AXIS (NON-DIMENSIONALIZED) COEFFICIENTS ')
      WRITE(*,101)
 101  FORMAT(1X,'FOR TRANSFORMATION TO DIMENSIONALIZED BODY AXIS')
      WRITE(*,102)
 102  FORMAT(1X,'AND TO GENERATE STATE AND INPUT MATRICES.')
      WRITE(*,41)
 41   FORMAT(1X,'NOTE:  ALL COEFFICIENTS ARE REQUESTED WHEN COMPUTING')
 103  CONTINUE
      WRITE(*,30)
 30   FORMAT(1X,'*****************************************************')
      WRITE(*,106)
 106  FORMAT(1X,'TO TRANSFORM ONLY LONGITUDINAL DATA - TYPE LONG')
      WRITE(*,107)
 107  FORMAT(1X,'TO TRANSFORM ONLY LATERAL-DIRECTIONAL DATA - TYPE LAT')
      WRITE(*,108)
 108  FORMAT(1X,'TO TRANSFORM BOTH LONG AND LAT-DIR DATA - TYPE BOTH')
      WRITE(*,111)
 111  FORMAT(1X,'KEYWORD =   ')
      READ(*,109) KEY
 109  FORMAT(A3)
      IF(KEY .EQ. 'LAT') GO TO 104
      IF(KEY .EQ. 'LON') GO TO 104
      IF(KEY .EQ. 'BOT') GO TO 104
      IF(KEY .EQ. 'GAM') GO TO 596
      GO TO 103
C*********************************************************************
C
C       INPUT DATA
C
C*********************************************************************
 104  CONTINUE
      WRITE(*,500)
 500  FORMAT(1X,'*****************************************************')
      WRITE(*,510)
 510  FORMAT(1X,'Q  (DYNAMIC PRESSURE - LBS/FT**2) = ')
      READ(*,*) Q
      WRITE(*,520)
 520  FORMAT(1X,'S  (WING REFERENCE AREA - FT**2) = ')
      READ(*,*) S
      WRITE(*,530)
 530  FORMAT(1X,'C  (WING MEAN AERODYNAMIC CORD - FT) = ')
      READ(*,*) C
      WRITE(*,540)
 540  FORMAT(1X,'B  (WING SPAN - FT) = ')
      READ(*,*) B
      WRITE(*,550)
 550  FORMAT(1X,'VT (TRIM VELOCITY - FT/SEC) = ')
      READ (*,*) U
      VT=U
      WRITE(*,560)
 560  FORMAT(1X,'THETA (PITCH ANGLE - DEGS) = ')
      READ(*,*) DTHETA
      WRITE(*,570)
 570  FORMAT(1X,'W  (WEIGHT - LBS) = ')
      READ(*,*) W
```

```
      WRITE(*,575)
  575 FORMAT(1X,'INERTIAS MUST BE INPUT IN BODY AXIS.')
      WRITE(*,580)
  580 FORMAT(1X,'IXX  (SLUG-FT**2) = ')
      READ(*,*) BIXX
      WRITE(*,585)
  585 FORMAT(1X,'IYY  (SLUG-FT**2) = ')
      READ(*,*) BIYY
      WRITE(*,590)
  590 FORMAT(1X,'IZZ  (SLUG-FT**2) = ')
      READ(*,*) BIZZ
      WRITE(*,595)
  595 FORMAT(1X,'IXZ  (SLUG-FT**2) = ')
      READ(*,*) BIXZ
  596 CONTINUE
      WRITE(*,597)
  597 FORMAT(1X,'*****************************************************')
      WRITE(*,610)
  610 FORMAT(16X,'AIRCRAFT PARAMETERS')
      WRITE(*,615) Q
  615 FORMAT(1X,'Q  (DYNAMIC PRESSURE - LBS/FT**2) = ',G13.6)
      WRITE(*,620) S
  620 FORMAT(1X,'S  (WING REFERENCE AREA - FT**2) = ',G13.6)
      WRITE(*,625) C
  625 FORMAT(1X,'C  (WING MEAN AERODYNAMIC CORD - FT) = ',G13.6)
      WRITE(*,630) B
  630 FORMAT(1X,'B  (WING SPAN - FT) = ',G13.6)
      WRITE(*,635) U
  635 FORMAT(1X,'VT (TRIM VELOCITY - FT/SEC) = ',G13.6)
      WRITE(*,640) DTHETA
  640 FORMAT(1X,'THETA = ',G13.6)
      WRITE(*,645) W
  645 FORMAT(1X,'W  (WEIGHT - LBS) = ',G13.6)
      WRITE(*,650) BIXX
  650 FORMAT(1X,'IXX  (SLUG-FT**2) = ',G13.6)
      WRITE(*,655) BIYY
  655 FORMAT(1X,'IYY  (SLUG-FT**2) = ',G13.6)
      WRITE(*,660) BIZZ
  660 FORMAT(1X,'IZZ  (SLUG-FT**2) = ',G13.6)
      WRITE(*,665) BIXZ
  665 FORMAT(1X,'IXZ  (SLUG-FT**2) = ',G13.6)
      WRITE(*,670)
  670 FORMAT(1X,'*****************************************************')
  600 CONTINUE
      WRITE(*,675)
  675 FORMAT(1X,'IS THE ENTERED DATA CORRECT ?  (YES/NO) ')
      READ(*,680) DATA3
  680 FORMAT(A3)
      WRITE(*,685)
  685 FORMAT(1X,'*****************************************************')
      IF(DATA3 .EQ. 'NO ') GO TO 104
      IF(DATA3 .EQ. 'YES') GO TO 686
      GO TO 600
  686 CONTINUE
      WRITE(*,105)
  105 FORMAT(1X,'ALPHA (DEG) = ')
      READ(*,*) DALPHA
C
C   CHANGE FROM DEGREES TO RADIANS
C
```

```
      THETA = DTHETA/DPR
      ALPHA = DALPHA/DPR
      IF(KEY .EQ. 'LAT')GO TO 446
      IF(KEY .EQ. 'GAM')GO TO 97
C
C    INPUT LONGITUDINAL VARIABLES
C
      WRITE(*,110)
 110  FORMAT (1X,'CZA = ')
      READ(*,*) CZA
      WRITE(*,120)
 120  FORMAT(1X,'CXA = ')
      READ(*,*) CXA
      WRITE(*,130)
 130  FORMAT(1X,'CMA = ')
      READ(*,*) CMA
      WRITE(*,140)
 140  FORMAT(1X,'CZQ = ')
      READ(*,*) CZQ
      WRITE(*,150)
 150  FORMAT(1X,'CXQ = ')
      READ(*,*) CXQ
      WRITE(*,160)
 160  FORMAT(1X,'CMQ = ')
      READ(*,*) CMQ
      WRITE(*,170)
 170  FORMAT(1X,'CZU = ')
      READ(*,*) CZU
      WRITE(*,180)
 180  FORMAT(1X,'CXU = ')
      READ(*,*) CXU
      WRITE(*,190)
 190  FORMAT(1X,'CMU = ')
      READ(*,*) CMU
      WRITE(*,191)
 191  FORMAT(1X,'CZH = ')
      READ(*,*) CZH
      WRITE(*,192)
 192  FORMAT(1X,'CXH = ')
      READ(*,*) CXH
      WRITE(*,193)
 193  FORMAT(1X,'CMH = ')
      READ(*,*) CMH
      WRITE(*,200)
 200  FORMAT(1X,'CZD1 = ')
      READ(*,*) CZD1
      WRITE(*,202)
 202  FORMAT(1X,'CXD1 = ')
      READ(*,*) CXD1
      WRITE(*,204)
 204  FORMAT(1X,'CMD1 = ')
      READ(*,*) CMD1
      WRITE(*,206)
 206  FORMAT(1X,'CZD2 = ')
      READ(*,*) CZD2
      WRITE(*,208)
 208  FORMAT(1X,'CXD2 = ')
      READ(*,*) CXD2
      WRITE(*,210)
 210  FORMAT(1X,'CMD2 = ')
```

```
      READ(*,*) CMD2
      WRITE(*,212)
212   FORMAT(1X,'CZD3 = ')
      READ(*,*) CZD3
      WRITE(*,214)
214   FORMAT(1X,'CXD3 = ')
      READ(*,*) CXD3
      WRITE(*,216)
216   FORMAT(1X,'CMD3 = ')
      READ(*,*) CMD3
      WRITE(*,218)
218   FORMAT(1X,'CZD4 = ')
      READ(*,*) CZD4
      WRITE(*,45)
45    FORMAT(1X,'CXD4 = ')
      READ(*,*) CXD4
      WRITE(*,50)
50    FORMAT(1X,'CMD4 = ')
      READ(*,*) CMD4
      WRITE(*,55)
55    FORMAT(1X,'CZD5 = ')
      READ(*,*) CZD5
      WRITE(*,60)
60    FORMAT(1X,'CXD5 = ')
      READ(*,*) CXD5
      WRITE(*,65)
65    FORMAT(1X,'CMD5 = ')
      READ(*,*) CMD5
      WRITE(*,70)
70    FORMAT(1X,'CZD6 = ')
      READ(*,*) CZD6
      WRITE(*,75)
75    FORMAT(1X,'CXD6 = ')
      READ(*,*) CXD6
      WRITE(*,80)
80    FORMAT(1X,'CMD6 = ')
      READ(*,*) CMD6
      WRITE(*,85)
85    FORMAT(1X,'CZD7')
      READ(*,*) CZD7
      WRITE(*,88)
88    FORMAT(1X,'CXD7')
      READ(*,*) CXD7
      WRITE(*,90)
90    FORMAT(1X,'CMD7 = ')
      READ(*,*) CMD7
      WRITE(*,92)
92    FORMAT(1X,'CZD8 = ')
      READ(*,*) CZD8
      WRITE(*,94)
94    FORMAT(1X,'CXD8 = ')
      READ(*,*) CXD8
      WRITE(*,96)
96    FORMAT(1X,'CMD8 = ')
      READ(*,*) CMD8
97    CONTINUE
      WRITE(*,225)
225   FORMAT(1X,'**************************************************')
      WRITE(*,230) DALPHA
230   FORMAT(15X,'ALPHA =',G13.6)
```

```
      WRITE(*,345)
  345 FORMAT(6X,'LONGITUDINAL NON-DIM BODY AXIS COEFFICIENTS(1/DEG)')
C
      CAL = COS(ALPHA)
      SAL = SIN(ALPHA)
      COSSQ = CAL**2
      SINSQ = SAL**2
      COSSIN = CAL*SAL
      CTH = COS(THETA)
      STH = SIN(THETA)
C
      WRITE(*,360) CZA,CMA,CXA
  360 FORMAT(3X,'CZA = ',G13.6,8X,'CMA = ',G13.6,5X,'CXA = ',G13.6)
      WRITE(*,390) CZQ,CMQ,CXQ
  390 FORMAT(3X,'CZQ = ',G13.6,8X,'CMQ = ',G13.6,5X,'CXQ = ',G13.6)
      WRITE(*,400) CZH,CMH,CXH
  400 FORMAT(3X,'CZH = ',G13.6,8X,'CMH = ',G13.6,5X,'CXH = ',G13.6)
      WRITE(*,410) CZU,CMU,CXU
  410 FORMAT(3X,'CZU = ',G13.6,8X,'CMU = ',G13.6,5X,'CXU = ',G13.6)
      WRITE(*,370) CZD1,CMD1,CXD1
  370 FORMAT(2X,'CZD1 = ',G13.6,7X,'CMD1 = ',G13.6,4X,'CXD1 = ',G13.6)
      WRITE(*,380) CZD2,CMD2,CXD2
  380 FORMAT(2X,'CZD2 = ',G13.6,7X,'CMD2 = ',G13.6,4X,'CXD2 = ',G13.6)
      WRITE(*,381) CZD3,CMD3,CXD3
  381 FORMAT(2X,'CZD3 = ',G13.6,7X,'CMD3 = ',G13.6,4X,'CXD3 = ',G13.6)
      WRITE(*,382) CZD4,CMD4,CXD4
  382 FORMAT(2X,'CZD4 = ',G13.6,7X,'CMD4 = ',G13.6,4X,'CXD4 = ',G13.6)
      WRITE(*,383) CZD5,CMD5,CXD5
  383 FORMAT(2X,'CZD5 = ',G13.6,7X,'CMD5 = ',G13.6,4X,'CXD5 = ',G13.6)
      WRITE(*,384) CZD6,CMD6,CXD6
  384 FORMAT(2X,'CZD6 = ',G13.6,7X,'CMD6 = ',G13.6,4X,'CXD6 = ',G13.6)
      WRITE(*,385) CZD7,CMD7,CXD7
  385 FORMAT(2X,'CZD7 = ',G13.6,7X,'CMD7 = ',G13.6,4X,'CXD7 = ',G13.6)
      WRITE(*,386) CZD8,CMD8,CXD8
  386 FORMAT(2X,'CZD8 = ',G13.6,7X,'CMD8 = ',G13.6,4X,'CXD8 = ',G13.6)
      WRITE(*,310)
  310 FORMAT(1X,'**************************************************')
  315 CONTINUE
      WRITE(*,320)
  320 FORMAT(1X,'IS THE ENTERED DATA CORRECT ?   (YES/NO)')
      READ(*,330) DATA1
  330 FORMAT(A3)
      IF(DATA1 .EQ. 'NO ') GO TO 686
      IF(DATA1 .EQ. 'YES') GO TO 340
      GO TO 315
C
C     START THE CALCULATIONS TO BUILD LONG. STATE SPACE MODEL
C
  340 CONTINUE
      WRITE(*,420)
  420 FORMAT(1X,'**************************************************')
      Z1 = (Q*S*32.2)/W
      A = C/(2.0*U)
      THETA = DTHETA/DPR
C
      ZA = Z1*CZA*DPR
      ZH = (Z1/U)*CZH
      ZQ = Z1*A*CZQ*DPR
      ZU = 2.*(Z1/U)*CZU
      ZD1 = Z1*CZD1*DPR
```

```
      ZD2 = Z1*CZD2*DPR
      ZD3 = Z1*CZD3*DPR
      ZD4 = Z1*CZD4*DPR
      ZD5 = Z1*CZD5*DPR
      ZD6 = Z1*CZD6*DPR
      ZD7 = Z1*CZD7*DPR
      ZD8 = Z1*CZD8*DPR
C
      XA = Z1*CXA*DPR
      XH = (Z1/U)*CXH
      XQ = Z1*A*CXQ*DPR
      XU = 2.*(Z1/U)*CXU
      XD1 = Z1*CXD1*DPR
      XD2 = Z1*CXD2*DPR
      XD3 = Z1*CXD3*DPR
      XD4 = Z1*CXD4*DPR
      XD5 = Z1*CXD5*DPR
      XD6 = Z1*CXD6*DPR
      XD7 = Z1*CXD7*DPR
      XD8 = Z1*CXD8*DPR
C
      M1 = (Q*S*C)/BIYY
C
      MA = M1*CMA*DPR
      MH = (M1/U)*CMH
      MQ = M1*A*CMQ*DPR
      MU = 2.*(M1/U)*CMU
      MD1 = M1*CMD1*DPR
      MD2 = M1*CMD2*DPR
      MD3 = M1*CMD3*DPR
      MD4 = M1*CMD4*DPR
      MD5 = M1*CMD5*DPR
      MD6 = M1*CMD6*DPR
      MD7 = M1*CMD7*DPR
      MD8 = M1*CMD8*DPR
C
C     WRITE THE DERIVATIVES
C
      WRITE(*,700)
 700  FORMAT (5X,'LONGITUDINAL AXIS DIMENSIONAL DERIVATIVES')
      WRITE(*,705)
 705  FORMAT (15X,'BODY AXIS (1/RAD)')
      WRITE(*,710) ZA,MA,XA
 710  FORMAT(4X,'ZA = ',G13.6,9X,'MA = ',G13.6,6X,'XA = ',G13.6)
      WRITE(*,720) ZQ,MQ,XQ
 720  FORMAT(4X,'ZQ = ',G13.6,9X,'MQ = ',G13.6,6X,'XQ = ',G13.6)
      WRITE(*,730) ZH,MH,XH
 730  FORMAT(4X,'ZH = ',G13.6,9X,'MH = ',G13.6,6X,'XH = ',G13.6)
      WRITE(*,740) ZU,MU,XU
 740  FORMAT(4X,'ZU = ',G13.6,9X,'MU = ',G13.6,6X,'XU = ',G13.6)
       WRITE(*,750) ZD1,MD1,XD1
 750  FORMAT(3X,'ZD1 = ',G13.6,8X,'MD1 = ',G13.6,5X,'XD1 = ',G13.6)
      WRITE(*,760) ZD2,MD2,XD2
 760  FORMAT(3X,'ZD2 = ',G13.6,8X,'MD2 = ',G13.6,5X,'XD2 = ',G13.6)
      WRITE(*,770) ZD3,MD3,XD3
 770  FORMAT(3X,'ZD3 = ',G13.6,8X,'MD3 = ',G13.6,5X,'XD3 = ',G13.6)
      WRITE(*,780) ZD4,MD4,XD4
 780  FORMAT(3X,'ZD4 = ',G13.6,8X,'MD4 = ',G13.6,5X,'XD4 = ',G13.6)
      WRITE(*,790) ZD5,MD5,XD5
 790  FORMAT(3X,'ZD5 = ',G13.6,8X,'MD5 = ',G13.6,5X,'XD5 = ',G13.6)
```

```
      WRITE(*,800) ZD6,MD6,XD6
  800 FORMAT(3X,'ZD6 = ',G13.6,8X,'MD6 = ',G13.6,5X,'XD6 = ',G13.6)
      WRITE(*,810) ZD7,MD7,XD7
  810 FORMAT(3X,'ZD7 = ',G13.6,8X,'MD7 = ',G13.6,5X,'XD7 = ',G13.6)
      WRITE(*,820) ZD8,MD8,XD8
  820 FORMAT(3X,'ZD8 = ',G13.6,8X,'MD8 = ',G13.6,5X,'XD8 = ',G13.6)
      WRITE(*,830)
  830 FORMAT(1X,'**************************************************')
C
C     DEVELOPMENT OF STATE MATRICIES
C
C     DEVELOPMENT OF THE PLANT MATRIX - A
C
      VT=U
      AMAT(1,1) = XU
      AMAT(1,2) = -VT*SAL
      AMAT(1,3) = XA
      AMAT(1,4) = -32.2*CTH
      AMAT(2,1) = MU
      AMAT(2,2) = MQ
      AMAT(2,3) = MA
      AMAT(2,4) = 0.0
      AMAT(3,1) = ZU/VT
      AMAT(3,2) = CAL
      AMAT(3,3) = ZA/VT
      AMAT(3,4) = -32.2*STH/VT
      AMAT(4,1) = 0.0
      AMAT(4,2) = 1.0
      AMAT(4,3) = 0.0
      AMAT(4,4) = 0.0
C
C     OK, LET'S WRITE THIS SUCKER OUT
C
      WRITE(*,*)
      WRITE(*,850)
  850 FORMAT('1',5X,'LONGITUDNAL STATE MATRIX(BODY AXIS)')
      WRITE(*,*)
      WRITE(*,842)
  842 FORMAT('0',2X,'FOR STATE1=U,STATE2=Q,STATE3=ALPHA,STATE4=THETA')
      WRITE(*,*)
      DO 855 I=1,4
      WRITE(*,860) (AMAT(I,J),J=1,4)
  855 CONTINUE
  860 FORMAT('0',2X,4(G13.6,4X))
      WRITE(*,*)
C
C     NOW WE'LL GET THE INPUT MATRIX - B
C
      BMAT(1,1) = XD1
      BMAT(1,2) = XD2
      BMAT(1,3) = XD3
      BMAT(1,4) = XD4
      BMAT(1,5) = XD5
      BMAT(1,6) = XD6
      BMAT(1,7) = XD7
      BMAT(1,8) = XD8
      BMAT(2,1) = MD1
      BMAT(2,2) = MD2
      BMAT(2,3) = MD3
      BMAT(2,4) = MD4
```

AD-A163 939 RECONFIGURABLE FLIGHT CONTROL SYSTEM FOR A STOL (SHORT 3/3
TAKE-OFF AND LANDI..(U) AIR FORCE INST OF TECH
WRIGHT-PATTERSON AFB OH SCHOOL OF ENGI.. B T CLOUGH
UNCLASSIFIED DEC 84 AFIT/GE/ENG/85D-8 F/G 1/3 NL

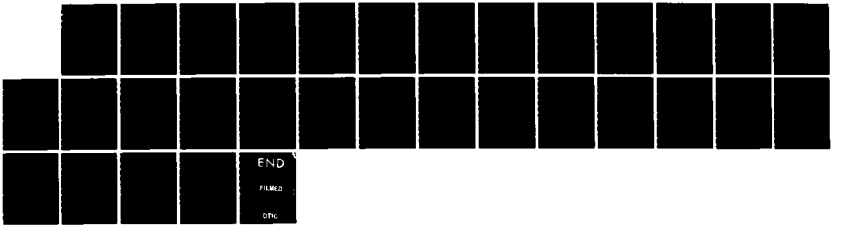

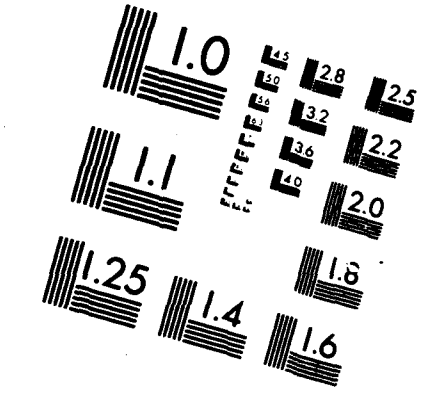

```
      BMAT(2,5) = MD5
      BMAT(2,6) = MD6
      BMAT(2,7) = MD7
      BMAT(2,8) = MD8
      BMAT(3,1) = ZD1/VT
      BMAT(3,2) = ZD2/VT
      BMAT(3,3) = ZD3/VT
      BMAT(3,4) = ZD4/VT
      BMAT(3,5) = ZD5/VT
      BMAT(3,6) = ZD6/VT
      BMAT(3,7) = ZD7/VT
      BMAT(3,8) = ZD8/VT
      DO 865 I=1,8
      BMAT(4,I) = 0.0
  865 CONTINUE
C
C     PRINT OUT THE LONG INPUT MATRIX
C
      WRITE(*,*)
      WRITE(*,870)
  870 FORMAT( '0',5X,'LONGITUDNAL INPUT MATRIX')
      WRITE(*,*)
      WRITE(*,868)
  868 FORMAT(2X,'FOR DEL1=CANARD,DEL2=STAB,DEL3=TEF,DEL4=DR AILERON')
      WRITE(*,869)
  869 FORMAT(2X,'    DEL5=RT RV, DEL6=RB RV, DEL7=LT RV, DEL8=LB RV')
      WRITE(*,*)
      WRITE(*,*)
      WRITE(*,871)
  871 FORMAT('0',5X,'ROW1',11X,'ROW2',11X,'ROW3',11X,'ROW4')
      WRITE(*,*)
      DO 872 I=1,8
      WRITE(*,880) (BMAT(J,I),J=1,4)
  872 CONTINUE
      WRITE(*,*)
  875 CONTINUE
      WRITE(*,873)
  873 FORMAT(1X,' DO YOU WANT STAB AXIS DATA FOR LONG?(Y/N)')
      READ(*,874) STAB1
  874 FORMAT(A1)
      IF ( STAB1 .EQ. 'Y' ) GO TO 877
      IF ( STAB1 .EQ. 'N' ) GO TO 857
      GO TO 875
  877 CONTINUE
C
C*************************************************************
C*                                                           *
C*           CONVERT BODY AXIS DATA TO STABILITY AXIS        *
C*             (FOR CHECK WITH MCAIR DATA)                   *
C*                                                           *
C*                                                           *
C*************************************************************
C
       SMU =( MU*CAL +   (MA/U)*SAL*CAL)
       SMH =( ( SMU / MU ) * MH )
       SMA =( MA * COSSQ - MU * U * SAL )
       SMQ = MQ
       SMD1 = MD1
       SMD2 = MD2
       SMD3 = MD3
```

```
      SMD4 = MD4
      SMD5 = MD5
      SMD6 = MD6
      SMD7 = MD7
      SMD8 = MD8
C
      SXU=XU*COSSQ+(ZA/U)*SINSQ*CAL+((XA/U)*CAL+ZU)*SAL*CAL
      SXH = (SXU/XU)*XH
      SXA = XA*CAL**3 -U*ZU*SINSQ - (U*XU - ZA*CAL)*CAL*SAL
      SXQ =( XQ*CAL + ZQ*SAL )
      SXD1 = (XD1*CAL + ZD1*SAL)
      SXD2 =( XD2*CAL + ZD2*SAL)
      SXD3 = (XD3*CAL + ZD3*SAL)
      SXD4 = (XD4*CAL + ZD4*SAL)
      SXD5 = (XD5*CAL + ZD5*SAL)
      SXD6 = (XD6*CAL + ZD6*SAL)
      SXD7 = (XD7*CAL + ZD7*SAL)
      SXD8 = (XD8*CAL + ZD8*SAL)
C
      SZU=ZU*COSSQ-(XA/U)*SINSQ*CAL-(XU-(ZA/U)*CAL)*SAL*CAL
      SZH = (SZU/ZU) * ZH
      SZA=ZA*CAL**3 + U*XU*SINSQ - (U*ZU + XA*CAL)*CAL*SAL
      SZQ = (ZQ*CAL - XQ*SAL)
      SZD1 = (ZD1*CAL - XD1*SAL)
      SZD2 = (ZD2*CAL - XD2*SAL)
      SZD3 = (ZD3*CAL - XD3*SAL)
      SZD4 = (ZD4*CAL - XD4*SAL)
      SZD5 = (ZD5*CAL - XD5*SAL)
      SZD6 = (ZD6*CAL - XD6*SAL)
      SZD7 = (ZD7*CAL - XD7*SAL)
      SZD8 = (ZD8*CAL - XD8*SAL)
      WRITE(*,701)
  701 FORMAT ('0',5X,'LONGITUDINAL AXIS DIMENSIONAL DERIVATIVES')
      WRITE(*,702)
  702 FORMAT (15X,' STABILITY AXIS (1/RAD) ')
      WRITE(*,711) SZA,SMA,SXA
  711 FORMAT(4X,'ZA = ',G13.6,9X,'MA = ',G13.6,6X,'XA = ',G13.6)
      WRITE(*,721) SZQ,SMQ,SXQ
  721 FORMAT(4X,'ZQ = ',G13.6,9X,'MQ = ',G13.6,6X,'XQ = ',G13.6)
      WRITE(*,731) SZH,SMH,SXH
  731 FORMAT(4X,'ZH = ',G13.6,9X,'MH = ',G13.6,6X,'XH = ',G13.6)
      WRITE(*,741) SZU,SMU,SXU
  741 FORMAT(4X,'ZU = ',G13.6,9X,'MU = ',G13.6,6X,'XU = ',G13.6)
      WRITE(*,751) SZD1,SMD1,SXD1
  751 FORMAT(3X,'ZD1 = ',G13.6,8X,'MD1 = ',G13.6,5X,'XD1 = ',G13.6)
      WRITE(*,761) SZD2,SMD2,SXD2
  761 FORMAT(3X,'ZD2 = ',G13.6,8X,'MD2 = ',G13.6,5X,'XD2 = ',G13.6)
      WRITE(*,771) SZD3,SMD3,SXD3
  771 FORMAT(3X,'ZD3 = ',G13.6,8X,'MD3 = ',G13.6,5X,'XD3 = ',G13.6)
      WRITE(*,781) SZD4,SMD4,SXD4
  781 FORMAT(3X,'ZD4 = ',G13.6,8X,'MD4 = ',G13.6,5X,'XD4 = ',G13.6)
      WRITE(*,791) SZD5,SMD5,SXD5
  791 FORMAT(3X,'ZD5 = ',G13.6,8X,'MD5 = ',G13.6,5X,'XD5 = ',G13.6)
      WRITE(*,800) SZD6,SMD6,SXD6
  801 FORMAT(3X,'ZD6 = ',G13.6,8X,'MD6 = ',G13.6,5X,'XD6 = ',G13.6)
      WRITE(*,811) SZD7,SMD7,SXD7
  811 FORMAT(3X,'ZD7 = ',G13.6,8X,'MD7 = ',G13.6,5X,'XD7 = ',G13.6)
      WRITE(*,820) SZD8,SMD8,SXD8
  821 FORMAT(3X,'ZD8 = ',G13.6,8X,'MD8 = ',G13.6,5X,'XD8 = ',G13.6)
      WRITE(*,830)
```

```
 880  FORMAT(2X,4(G13.6,2X))
C
C       CALCULATE 'A' MATRIX ELEMENTS
C
        AMAT(1,1) = SXU
        AMAT(1,2) = 0.0
        AMAT(1,3) = SXA
        AMAT(1,4) = -32.2*CTH
        AMAT(2,1) = SMU
        AMAT(2,2) = SMQ
        AMAT(2,3) = SMA
        AMAT(2,4) = 0.0
        AMAT(3,1) = SZU/U
        AMAT(3,2) = 1.0
        AMAT(3,3) = SZA/U
        AMAT(3,4) = -32.2*STH/U
        AMAT(4,1) = 0.0
        AMAT(4,2) = 1.0
        AMAT(4,3) = 0.0
        AMAT(4,4) = 0.0
C       WRITE(*,851)
C851    FORMAT('0',5X,'LONGITUDNAL STATE MATRIX (STAB AXIS)')
C       WRITE(*,*)
C       WRITE(*,842)
C       WRITE(*,*)
C       DO 856 I=1,4
C       WRITE(*,860) (AMAT(I,J),J=1,4)
C856    CONTINUE
 857    CONTINUE
        IF (KEY .EQ. 'BOT' ) GO TO 446
        IF (KEY .EQ. 'GAM' ) GO TO 1465
 421    CONTINUE
        WRITE(*,430)
 430    FORMAT(1X,'IS ANOTHER PROGRAM RUN DESIRED ?  (YES/NO)')
        READ(*.440) RUN
 440    FORMAT(A3)
        WRITE(*,445)
 445    FORMAT(1X,'*****************************************************')
        IF(RUN .EQ. 'NO ') GO TO 450
        IF(RUN .EQ. 'YES') GO TO 103
        GO TO 421
 446    CONTINUE
C
C       THIS IS WHERE THE LATERAL DIRECTIONAL STARTS
C
        WRITE(*,1110)
 1110 FORMAT(1X,'CLB (1/DEG) = ')
        READ(*,*) CLB
        WRITE(*,1120)
 1120 FORMAT(1X,'CNB (1/DEG) = ')
        READ(*,*) CNB
        WRITE(*,1130)
 1130 FORMAT(1X,'CYB (1/DEG) = ')
        READ(*,*) CYB
        WRITE(*,1140)
 1140 FORMAT(1X,'CLP (1/DEG) = ')
        READ(*,*) CLP
        WRITE(*,1150)
 1150 FORMAT(1X,'CNP (1/DEG) = ')
        READ(*,*) CNP
```

```
      WRITE(*,1160)
1160  FORMAT(1X,'CYP (1/DEG) = ')
      READ(*,*) CYP
      WRITE(*,1170)
1170  FORMAT(1X,'CLR (1/DEG) = ')
      READ(*,*) CLR
      WRITE(*,1180)
1180  FORMAT(1X,'CNR (1/DEG) = ')
      READ(*,*) CNR
      WRITE(*,1190)
1190  FORMAT(1X,'CYR (1/DEG) = ')
      READ(*,*) CYR
      WRITE(*,1200)
1200  FORMAT(1X,'CLD1 (1/DEG) = ')
      READ(*,*) CLD1
      WRITE(*,1210)
1210  FORMAT(1X,'CND1 (1/DEG) = ')
      READ(*,*) CND1
      WRITE(*,1220)
1220  FORMAT(1X,'CYD1 (1/DEG) = ')
      READ(*,*) CYD1
      WRITE(*,1230)
1230  FORMAT(1X,'CLD2 (1/DEG) = ')
      READ(*,*) CLD2
      WRITE(*,1240)
1240  FORMAT(1X,'CND2 (1/DEG) = ')
      READ(*,*) CND2
      WRITE(*,1250)
1250  FORMAT(1X,'CYD2 (1/DEG) = ')
      READ(*,*) CYD2
      WRITE(*,1260)
1260  FORMAT(1X,'CLD3 (1/DEG) = ')
      READ(*,*) CLD3
      WRITE(*,1270)
1270  FORMAT(1X,'CND3 (1/DEG) = ')
      READ(*,*) CND3
      WRITE(*,1280)
1280  FORMAT(1X,'CYD3 (1/DEG) = ')
      READ(*,*) CYD3
      WRITE(*,1290)
1290  FORMAT(1X,'CLD4 (1/DEG) = ')
      READ(*,*) CLD4
      WRITE(*,1300)
1300  FORMAT(1X,'CND4 (1/DEG) = ')
      READ(*,*) CND4
      WRITE(*,1310)
1310  FORMAT(1X,'CYD4 (1/DEG) = ')
      READ(*,*) CYD4
      WRITE(*,1320)
1320  FORMAT(1X,'CLD5 (1/DEG) = ')
      READ(*,*) CLD5
      WRITE(*,1330)
1330  FORMAT(1X,'CND5 (1/DEG) = ')
      READ(*,*) CND5
      WRITE(*,1340)
1340  FORMAT(1X,'CYD5 (1/DEG) = ')
      READ(*,*) CYD5
      WRITE(*,1350)
1350  FORMAT(1X,'CLD6 (1/DEG) = ')
      READ(*,*) CLD6
```

```
      WRITE(*,1360)
 1360 FORMAT(1X,'CND6 (1/DEG) = ')
      READ(*,*) CND6
      WRITE(*,1370)
 1370 FORMAT(1X,'CYD6 (1/DEG) = ')
      READ(*,*) CYD6
      WRITE(*,1380)
 1380 FORMAT(1X,'CLD7 (1/DEG) = ')
      READ(*,*) CLD7
      WRITE(*,1390)
 1390 FORMAT(1X,'CND7 (1/DEG) = ')
      READ(*,*) CND7
      WRITE(*,1400)
 1400 FORMAT(1X,'CYD7 (1/DEG) = ')
      READ(*,*) CYD7
      WRITE(*,1410)
 1410 FORMAT(1X,'CLD8 (1/DEG) = ')
      READ(*,*) CLD8
      WRITE(*,1420)
 1420 FORMAT(1X,'CND8 (1/DEG) = ')
      READ(*,*) CND8
      WRITE(*,1430)
 1430 FORMAT(1X,'CYD8 (1/DEG) = ')
      READ(*,*) CYD8
      WRITE(*,1440)
 1440 FORMAT(1X,'CLD9 (1/DEG) = ')
      READ(*,*) CLD9
      WRITE(*,1450)
 1450 FORMAT(1X,'CND9 (1/DEG) = ')
      READ(*,*) CND9
      WRITE(*,1460)
 1460 FORMAT(1X,'CYD9 (1/DEG) = ')
      READ(*,*) CYD9
 1465 CONTINUE
      WRITE(*,1470)
 1470 FORMAT('1',8X,'LAT-DIR BODY AXIS COEFFICIENTS')
      IF(KEY .EQ. 'LON') GO TO 1490
      IF(KEY .EQ. 'BOT') GO TO 1490
      WRITE(*,1480) DALPHA
 1480 FORMAT(15X,'ALPHA = ',G13.6)
 1490 CONTINUE
      WRITE(*,1500) CLB,CNB,CYB
 1500 FORMAT(3X,'CLB = ',G13.6,8X,'CNB = ',G13.6,5X,'CYB = ',G13.6)
      WRITE(*,1510) CLP,CNP,CYP
 1510 FORMAT(3X,'CLP = ',G13.6,8X,'CNP = ',G13.6,5X,'CYP = ',G13.6)
      WRITE(*,1520) CLR,CNR,CYR
 1520 FORMAT(3X,'CLR = ',G13.6,8X,'CNR = ',G13.6,5X,'CYR = ',G13.6)
      WRITE(*,1530) CLD1,CND1,CYD1
 1530 FORMAT(2X,'CLD1 = ',G13.6,7X,'CND1 = ',G13.6,4X,'CYD1 = ',G13.6)
      WRITE(*,1540) CLD2,CND2,CYD2
 1540 FORMAT(2X,'CLD2 = ',G13.6,7X,'CND2 = ',G13.6,4X,'CYD2 = ',G13.6)
      WRITE(*,1550) CLD3,CND3,CYD3
 1550 FORMAT(2X,'CLD3 = ',G13.6,7X,'CND3 = ',G13.6,4X,'CYD3 = ',G13.6)
      WRITE(*,1560) CLD4,CND4,CYD4
 1560 FORMAT(2X,'CLD4 = ',G13.6,7X,'CND4 = ',G13.6,4X,'CYD4 = ',G13.6)
      WRITE(*,1570) CLD5,CND5,CYD5
 1570 FORMAT(2X,'CLD5 = ',G13.6,7X,'CND5 = ',G13.6,4X,'CYD5 = ',G13.6)
      WRITE(*,1580) CLD6,CND6,CYD6
 1580 FORMAT(2X,'CLD6 = ',G13.6,7X,'CND6 = ',G13.6,4X,'CYD6 = ',G13.6)
      WRITE(*,1590) CLD7,CND7,CYD7
```

```
1590 FORMAT(2X,'CLD7 = ',G13.6,7X,'CND7 = ',G13.6,4X,'CYD7 = ',G13.6)
     WRITE(*,1600) CLD8,CND8,CYD8
1600 FORMAT(2X,'CLD8 = ',G13.6,7X,'CND8 = ',G13.6,4X,'CYD8 = ',G13.6)
     WRITE(*,1610) CLD9,CND9,CYD9
1610 FORMAT(2X,'CLD9 = ',G13.6,7X,'CND9 = ',G13.6,4X,'CYD9 = ',G13.6)
     WRITE(*,*)
     WRITE(*,1620)
1620 FORMAT(1X,'*****************************************************')
1625 CONTINUE
     WRITE(*,1630)
1630 FORMAT(1X,'IS THE ENTERED DATA CORRECT ?   (YES/NO)')
     READ(*,1640) DATA2
1640 FORMAT(A3)
     IF ( DATA2 .EQ. 'NO') GO TO 446
     IF ( DATA2 .EQ. 'YES' ) GO TO 1645
     GO TO 1625
1645 CONTINUE
     WRITE(*,1646)
1646 FORMAT(1X,'DO YOU WANT STAB AXIS DATA FOR LAT-DIR? (Y/N)')
     READ(*,1647) STAB2
1647 FORMAT(A1)
     IF ( STAB2 .EQ. 'N') GO TO 1801
     IF ( STAB2 .EQ. 'Y') GO TO 1648
     GO TO 1645
1648 CONTINUE
     BSALPH=-ALPHA
     CSA=COS(BSALPH)
     SSA=SIN(BSALPH)
     CS=CSA*CSA
     SS=SSA*SSA
C
     SCLP=CLP*CS + CNR*SS - (CLR + CNP)*CSA*SSA
     SCLR=CLR*CS - CNP*SS + (CLP - CNR)*CSA*SSA
     SCLB=CLB*CSA - CNB*SSA
     SCLD1=CLD1*CSA - CND1*SSA
     SCLD2=CLD2*CSA - CND2*SSA
     SCLD3=CLD3*CSA - CND3*SSA
     SCLD4=CLD4*CSA - CND4*SSA
     SCLD5=CLD5*CSA - CND5*SSA
     SCLD6=CLD6*CSA - CND6*SSA
     SCLD7=CLD7*CSA - CND7*SSA
     SCLD8=CLD8*CSA - CND8*SSA
     SCLD9=CLD9*CSA - CND9*SSA
C
     SCNP=CNP*CS - CLR*SS + (CLP - CNR)*CSA*SSA
     SCNR=CNR*CS + CLP*SS + (CLP + CNR)*CSA*SSA
     SCNB=CNB*CSA + CLB*SSA
     SCND1=CND1*CSA + CLD1*SSA
     SCND2=CND2*CSA + CLD2*SSA
     SCND3=CND3*CSA + CLD3*SSA
     SCND4=CND4*CSA + CLD4*SSA
     SCND5=CND5*CSA + CLD5*SSA
     SCND6=CND6*CSA + CLD6*SSA
     SCND7=CND7*CSA + CLD7*SSA
     SCND8=CND8*CSA + CLD8*SSA
     SCND9=CND9*CSA + CLD9*SSA
C
     SCYP=CYP*CSA - CYR*SSA
     SCYR=CYR*CSA + CYP*SSA
     SCYB=CYB
```

```
      WRITE(*,1471)
 1471 FORMAT(8X,'LAT-DIR STAB AXIS COEFFICIENTS')
      WRITE(*,1501) SCLB,SCNB,SCYB
 1501 FORMAT(3X,'CLB = ',G13.6,8X,'CNB = ',G13.6,5X,'CYB = ',G13.6)
      WRITE(*,1511) SCLP,SCNP,SCYP
 1511 FORMAT(3X,'CLP = ',G13.6,8X,'CNP = ',G13.6,5X,'CYP = ',G13.6)
      WRITE(*,1521) SCLR,SCNR,SCYR
 1521 FORMAT(3X,'CLR = ',G13.6,8X,'CNR = ',G13.6,5X,'CYR = ',G13.6)
      WRITE(*,1531) SCLD1,SCND1,CYD1
 1531 FORMAT(2X,'CLD1 = ',G13.6,7X,'CND1 = ',G13.6,4X,'CYD1 = ',G13.6)
      WRITE(*,1541) SCLD2,SCND2,CYD2
 1541 FORMAT(2X,'CLD2 = ',G13.6,7X,'CND2 = ',G13.6,4X,'CYD2 = ',G13.6)
      WRITE(*,1551) SCLD3,SCND3,CYD3
 1551 FORMAT(2X,'CLD3 = ',G13.6,7X,'CND3 = ',G13.6,4X,'CYD3 = ',G13.6)
      WRITE(*,1561) SCLD4,SCND4,CYD4
 1561 FORMAT(2X,'CLD4 = ',G13.6,7X,'CND4 = ',G13.6,4X,'CYD4 = ',G13.6)
      WRITE(*,1571) SCLD5,SCND5,CYD5
 1571 FORMAT(2X,'CLD5 = ',G13.6,7X,'CND5 = ',G13.6,4X,'CYD5 = ',G13.6)
      WRITE(*,1581) SCLD6,SCND6,CYD6
 1581 FORMAT(2X,'CLD6 = ',G13.6,7X,'CND6 = ',G13.6,4X,'CYD6 = ',G13.6)
      WRITE(*,1591) SCLD7,SCND7,CYD7
 1591 FORMAT(2X,'CLD7 = ',G13.6,7X,'CND7 = ',G13.6,4X,'CYD7 = ',G13.6)
      WRITE(*,1601) SCLD8,SCND8,CYD8
 1601 FORMAT(2X,'CLD8 = ',G13.6,7X,'CND8 = ',G13.6,4X,'CYD8 = ',G13.6)
      WRITE(*,1611) SCLD9,SCND9,CYD9
 1611 FORMAT(2X,'CLD9 = ',G13.6,7X,'CND9 = ',G13.6,4X,'CYD9 = ',G13.6)
      WRITE(*,*)
C
      SIXX=BIXX*COSSQ + BIZZ*SINSQ - BIXZ*SIN(2*ALPHA)
      SIYY=BIYY
      SIZZ=BIZZ*COSSQ + BIXX*SINSQ + BIXZ*SIN(2*ALPHA)
      SIXZ=BIXZ*COS(2*ALPHA) + .5*(BIXX - BIZZ)*SIN(2*ALPHA)
C
      SN = DPR*(Q*S*B)/SIZZ
      SL = DPR*(Q*S*B)/SIXX
      SB = B/(2.0*U)
      SY = DPR*(Q*S*32.2)/W
      SNB = SN*SCNB
      SNP = SN*SB*SCNP
      SNR = SN*SB*SCNR
      SND1 = SN*SCND1
      SND2 = SN*SCND2
      SND3 = SN*SCND3
      SND4 = SN*SCND4
      SND5 = SN*SCND5
      SND6 = SN*SCND6
      SND7 = SN*SCND7
      SND8 = SN*SCND8
      SND9 = SN*SCND9
C
      SLB = SL*SCLB
      SLP = SL*SB*SCLP
      SLR = SL*SB*SCLR
      SLD1 = SL*SCLD1
      SLD2 = SL*SCLD2
      SLD3 = SL*SCLD3
      SLD4 = SL*SCLD4
      SLD5 = SL*SCLD5
      SLD6 = SL*SCLD6
      SLD7 = SL*SCLD7
```

```
      SLD8 = SL*SCLD8
      SLD9 = SL*SCLD9
C
      SYB = SY*SCYB
      SYR = SY*SB*SCYR
      SYP = SY*SB*SCYP
      SYD1 = SY*SCYD1
      SYD2 = SY*SCYD2
      SYD3 = SY*SCYD3
      SYD4 = SY*SCYD4
      SYD5 = SY*SCYD5
      SYD6 = SY*SCYD6
      SYD7 = SY*SCYD7
      SYD8 = SY*SCYD8
      SYD9 = SY*SCYD9
C
      WRITE(*,1661)
 1661 FORMAT(5X,'LAT-DIR STAB AXIS DIMENSIONAL DERIVATIVES(1/RAD)')
      WRITE(*,1671) SNB,SLB,SYB
 1671 FORMAT(4X,'NB = ',G13.6,9X,'LB = ',G13.6,5X,'YB = ',G13.6)
      WRITE(*,1681) SNP,SLP,SYP
 1681 FORMAT(4X,'NP = ',G13.6,9X,'LP = ',G13.6,5X,'YP = ',G13.6)
      WRITE(*,1691) SNR,SLR,SYR
 1691 FORMAT(4X,'NR = ',G13.6,9X,'LR = ',G13.6,5X,'YR = ',G13.6)
      WRITE(*,1701) SND1,SLD1,SYD1
 1701 FORMAT(3X,'ND1 = ',G13.6,8X,'LD1 = ',G13.6,4X,'YD1 = ',G13.6)
      WRITE(*,1711) SND2,SLD2,SYD2
 1711 FORMAT(3X,'ND2 = ',G13.6,8X,'LD2 = ',G13.6,4X,'YD2 = ',G13.6)
      WRITE(*,1721) SND3,SLD3,SYD3
 1721 FORMAT(3X,'ND3 = ',G13.6,8X,'LD3 = ',G13.6,4X,'YD3 = ',G13.6)
      WRITE(*,1731) SND4,SLD4,SYD4
 1731 FORMAT(3X,'ND4 = ',G13.6,8X,'LD4 = ',G13.6,4X,'YD4 = ',G13.6)
      WRITE(*,1741) SND5,SLD5,SYD5
 1741 FORMAT(3X,'ND5 = ',G13.6,8X,'LD5 = ',G13.6,4X,'YD5 = ',G13.6)
      WRITE(*,1751) SND6,SLD6,SYD6
 1751 FORMAT(3X,'ND6 = ',G13.6,8X,'LD6 = ',G13.6,4X,'YD6 = ',G13.6)
      WRITE(*,1761) SND7,SLD7,SYD7
 1761 FORMAT(3X,'ND7 = ',G13.6,8X,'LD7 = ',G13.6,4X,'YD7 = ',G13.6)
      WRITE(*,1771) SND8,SLD8,SYD8
 1771 FORMAT(3X,'ND8 = ',G13.6,8X,'LD8 = ',G13.6,4X,'YD8 = ',G13.6)
      WRITE(*,1781) SND9,SLD9,SYD9
 1781 FORMAT(3X,'ND9 = ',G13.6,8X,'LD9 = ',G13.6,4X,'YD9 = ',G13.6)
C
      WRITE(*,1650)
 1650 FORMAT(1X,'*****************************************************')
 1801 CONTINUE
      N = DPR*(Q*S*B)/BIZZ
      L = DPR*(Q*S*B)/BIXX
      BB = B/(2.0*U)
      Y = DPR*(Q*S*32.2)/W
      BNB = N*CNB
      BNP = N*BB*CNP
      BNR = N*BB*CNR
      BND1 = N*CND1
      BND2 = N*CND2
      BND3 = N*CND3
      BND4 = N*CND4
      BND5 = N*CND5
      BND6 = N*CND6
      BND7 = N*CND7
```

```
      BND8 = N*CND8
      BND9 = N*CND9
C
      BLB = L*CLB
      BLP = L*BB*CLP
      BLR = L*BB*CLR
      BLD1 = L*CLD1
      BLD2 = L*CLD2
      BLD3 = L*CLD3
      BLD4 = L*CLD4
      BLD5 = L*CLD5
      BLD6 = L*CLD6
      BLD7 = L*CLD7
      BLD8 = L*CLD8
      BLD9 = L*CLD9
C
      BYB = Y*CYB
      BYR = Y*BB*CYR
      BYP = Y*BB*CYP
      BYD1 = Y*CYD1
      BYD2 = Y*CYD2
      BYD3 = Y*CYD3
      BYD4 = Y*CYD4
      BYD5 = Y*CYD5
      BYD6 = Y*CYD6
      BYD7 = Y*CYD7
      BYD8 = Y*CYD8
      BYD9 = Y*CYD9
C
      WRITE(*,1660)
 1660 FORMAT(5X,'LAT-DIR BODY AXIS DIMENSIONAL DERIVATIVES(1/RAD)')
      WRITE(*,1670) BNB,BLB,BYB
 1670 FORMAT(4X,'NB = ',G13.6,9X,'LB = ',G13.6,5X,'YB = ',G13.6)
      WRITE(*,1680) BNP,BLP,BYP
 1680 FORMAT(4X,'NP = ',G13.6,9X,'LP = ',G13.6,5X,'YP = ',G13.6)
      WRITE(*,1690) BNR,BLR,BYR
 1690 FORMAT(4X,'NR = ',G13.6,9X,'LR = ',G13.6,5X,'YR = ',G13.6)
      WRITE(*,1700) BND1,BLD1,BYD1
 1700 FORMAT(3X,'ND1 = ',G13.6,8X,'LD1 = ',G13.6,4X,'YD1 = ',G13.6)
      WRITE(*,1710) BND2,BLD2,BYD2
 1710 FORMAT(3X,'ND2 = ',G13.6,8X,'LD2 = ',G13.6,4X,'YD2 = ',G13.6)
      WRITE(*,1720) BND3,BLD3,BYD3
 1720 FORMAT(3X,'ND3 = ',G13.6,8X,'LD3 = ',G13.6,4X,'YD3 = ',G13.6)
      WRITE(*,1730) BND4,BLD4,BYD4
 1730 FORMAT(3X,'ND4 = ',G13.6,8X,'LD4 = ',G13.6,4X,'YD4 = ',G13.6)
      WRITE(*,1740) BND5,BLD5,BYD5
 1740 FORMAT(3X,'ND5 = ',G13.6,8X,'LD5 = ',G13.6,4X,'YD5 = ',G13.6)
      WRITE(*,1750) BND6,BLD6,BYD6
 1750 FORMAT(3X,'ND6 = ',G13.6,8X,'LD6 = ',G13.6,4X,'YD6 = ',G13.6)
      WRITE(*,1760) BND7,BLD7,BYD7
 1760 FORMAT(3X,'ND7 = ',G13.6,8X,'LD7 = ',G13.6,4X,'YD7 = ',G13.6)
      WRITE(*,1770) BND8,BLD8,BYD8
 1770 FORMAT(3X,'ND8 = ',G13.6,8X,'LD8 = ',G13.6,4X,'YD8 = ',G13.6)
      WRITE(*,1780) BND9,BLD9,BYD9
 1780 FORMAT(3X,'ND9 = ',G13.6,8X,'LD9 = ',G13.6,4X,'YD9 = ',G13.6)
      WRITE(*,1790)
 1790 FORMAT(1X,'*****************************************************')
      WRITE(*,1800)
 1800 FORMAT(1X,'*****************************************************')
C
```

```
C
C     CONVERSION OF DATA INTO STATE SPACE FORM
C
C
      D = 1.0 - ((BIXZ*BIXZ)/(BIXX*BIZZ))
      R1 = BIXZ/BIZZ
      R2 = BIXZ/BIXX
C
      PBNB = (BNB + R1*BLB)/D
      PBNP = (BNP + R1*BLP)/D
      PBNR = (BNR + R1*BLR)/D
      PBND1 = (BND1 + R1*BLD1)/D
      PBND2 = (BND2 + R1*BLD2)/D
      PBND3 = (BND3 + R1*BLD3)/D
      PBND4 = (BND4 + R1*BLD4)/D
      PBND5 = (BND5 + R1*BLD5)/D
      PBND6 = (BND6 + R1*BLD6)/D
      PBND7 = (BND7 + R1*BLD7)/D
      PBND8 = (BND8 + R1*BLD8)/D
      PBND9 = (BND9 + R1*BLD9)/D
      PBLB = (BLB + R2*BNB)/D
      PBLP = (BLP + R2*BNP)/D
      PBLR = (BLR + R2*BNR)/D
      PBLD1 = (BLD1 + R2*BND1)/D
      PBLD2 = (BLD2 + R2*BND2)/D
      PBLD3 = (BLD3 + R2*BND3)/D
      PBLD4 = (BLD4 + R2*BND4)/D
      PBLD5 = (BLD5 + R2*BND5)/D
      PBLD6 = (BLD6 + R2*BND6)/D
      PBLD7 = (BLD7 + R2*BND7)/D
      PBLD8 = (BLD8 + R2*BND8)/D
      PBLD9 = (BLD9 + R2*BND9)/D
C
      PBYB = BYB/U
      PBYP = SAL
      PBYR = -CAL
      PBYPHI = 32.2*CTH/U
      PBYD1 = BYD1/U
      PBYD2 = BYD2/U
      PBYD3 = BYD3/U
      PBYD4 = BYD4/U
      PBYD5 = BYD5/U
      PBYD6 = BYD6/U
      PBYD7 = BYD7/U
      PBYD8 = BYD8/U
      PBYD9 = BYD9/U
C
C        LATERAL DIRECTIONAL STATE MATRIX
C
C
      DO 1805 I=1,5
        DO 1806 J=1,5
 1806     DIRMAT(I,J)=0.0
 1805 CONTINUE
      DIRMAT(1,3)=1.0
      DIRMAT(2,1)=PBYPHI
      DIRMAT(2,2)=PBYB
      DIRMAT(2,3)=PBYP
      DIRMAT(2,4)=PBYR
      DIRMAT(2,5)=32.2*STH/U
```

```
      DIRMAT(3,2)=PBLB
      DIRMAT(3,3)=PBLP
      DIRMAT(3,4)=PBLR
      DIRMAT(4,2)=PBNB
      DIRMAT(4,3)=PBNP
      DIRMAT(4,4)=PBNR
      DIRMAT(5,4)=1.0
C
C
C       OUTPUT THE STATE MATRIX
C
C
      WRITE(*,830)
      WRITE(*,1810)
 1810 FORMAT('1',2X,'LATERAL DIRECTIONAL STATE MATRIX')
      WRITE(*,1820)
 1820 FORMAT('0',5X,'STATES = PHI,BETA,P,R,PSI')
      WRITE(*,*)
      WRITE(*,1825) (DIRMAT(1,I),I=1,5)
      WRITE(*,1825) (DIRMAT(2,I),I=1,5)
      WRITE(*,1825) (DIRMAT(3,I),I=1,5)
      WRITE(*,1825) (DIRMAT(4,I),I=1,5)
      WRITE(*,1825) (DIRMAT(5,I),I=1,5)
      WRITE(*,*)
 1825 FORMAT('0',2X,5(G11.4,4X) )
C
C       LATERAL DIRECTIONAL INPUT MATRIX
C
C
      DO 1830 I=1,9
      DIRBMAT(1,I)=0.0
      DIRBMAT(5,I)=0.0
 1830 CONTINUE
      DIRBMAT(2,1)=PBYD1
      DIRBMAT(2,2)=PBYD2
      DIRBMAT(2,3)=PBYD3
      DIRBMAT(2,4)=PBYD4
      DIRBMAT(2,5)=PBYD5
      DIRBMAT(2,6)=PBYD6
      DIRBMAT(2,7)=PBYD7
      DIRBMAT(2,8)=PBYD8
      DIRBMAT(2,9)=PBYD9
      DIRBMAT(3,1)=PBND1
      DIRBMAT(3,2)=PBND2
      DIRBMAT(3,3)=PBND3
      DIRBMAT(3,4)=PBND4
      DIRBMAT(3,5)=PBND5
      DIRBMAT(3,6)=PBND6
      DIRBMAT(3,7)=PBND7
      DIRBMAT(3,8)=PBND8
      DIRBMAT(3,9)=PBND9
      DIRBMAT(4,1)=PBLD1
      DIRBMAT(4,2)=PBLD2
      DIRBMAT(4,3)=PBLD3
      DIRBMAT(4,4)=PBLD4
      DIRBMAT(4,5)=PBLD5
      DIRBMAT(4,6)=PBLD6
      DIRBMAT(4,7)=PBLD7
      DIRBMAT(4,8)=PBLD8
      DIRBMAT(4,9)=PBLD9
```

```
C
C     PRINT OUT THE INPUT MATRIX
C
      WRITE(*,1850)
 1850 FORMAT('0',2X,'LATERAL DIRECTIONAL INPUT MATRIX')
      WRITE(*,1860)
 1860 FORMAT('0',4X,'FOR INPUTS: DEL1=RUDDER,DEL2=DIFF CAN')
      WRITE(*,1870)
 1870 FORMAT( 6X,'DEL3=DIFF STAB, DEL4=DIFF AIL, DEL5=DIFF TEF')
      WRITE(*,1880)
 1880 FORMAT(6X,'DEL6 TO 9 ARE REVERSER VANE PORTS')
      WRITE(*,1890)
 1890 FORMAT('0',5X,'ROW1',11X,'ROW2',11X,'ROW3',11X,'ROW4',11X,'ROW5')
      DO 1900 I=1,9
      WRITE(*,1825) (DIRBMAT(J,I),J=1,5)
 1900 CONTINUE
      GO TO 421
  450 CONTINUE
      END
```

Appendix G

Simulation Set-Up

To simulate the response of the STOL aircraft the system in Figure V.3-2 was constructed using the CAD package MATRIX X[25]. MATRIX X allows the designer to construct the system several ways, including state-space and transfer functions. Transfer function representation for simulation is a "natural" since the required transfer functions already exist from the QFT design method. Using the "System Build" option the individual transfer functions can be entered as "blocks" of a larger "Super Block". These Super Blocks can be nested as parts of a larger Super Block. This is how the STOL simulation is constructed. Figure G-1 is a connection diagram of the system. The highest level Super Block, **STOL15**, has two inputs(commands) and four outputs(two output variables and two 'equivalent' surface deflections) and contains six other Super Blocks:

1) **prefil** contains both prefilters and the feedback loop summing junctions.
2) **servo** contains two Super Blocks(both shown as transfer functions, but actually are Super Blocks) **servo1** and **servo2** both of which contain servo transfer function, rate and deflection saturations as outlined in Super Block **stuff** .
3) **compen** contains both g_1 and g_2 along with the reconfigurable terms (Block 'Recof').

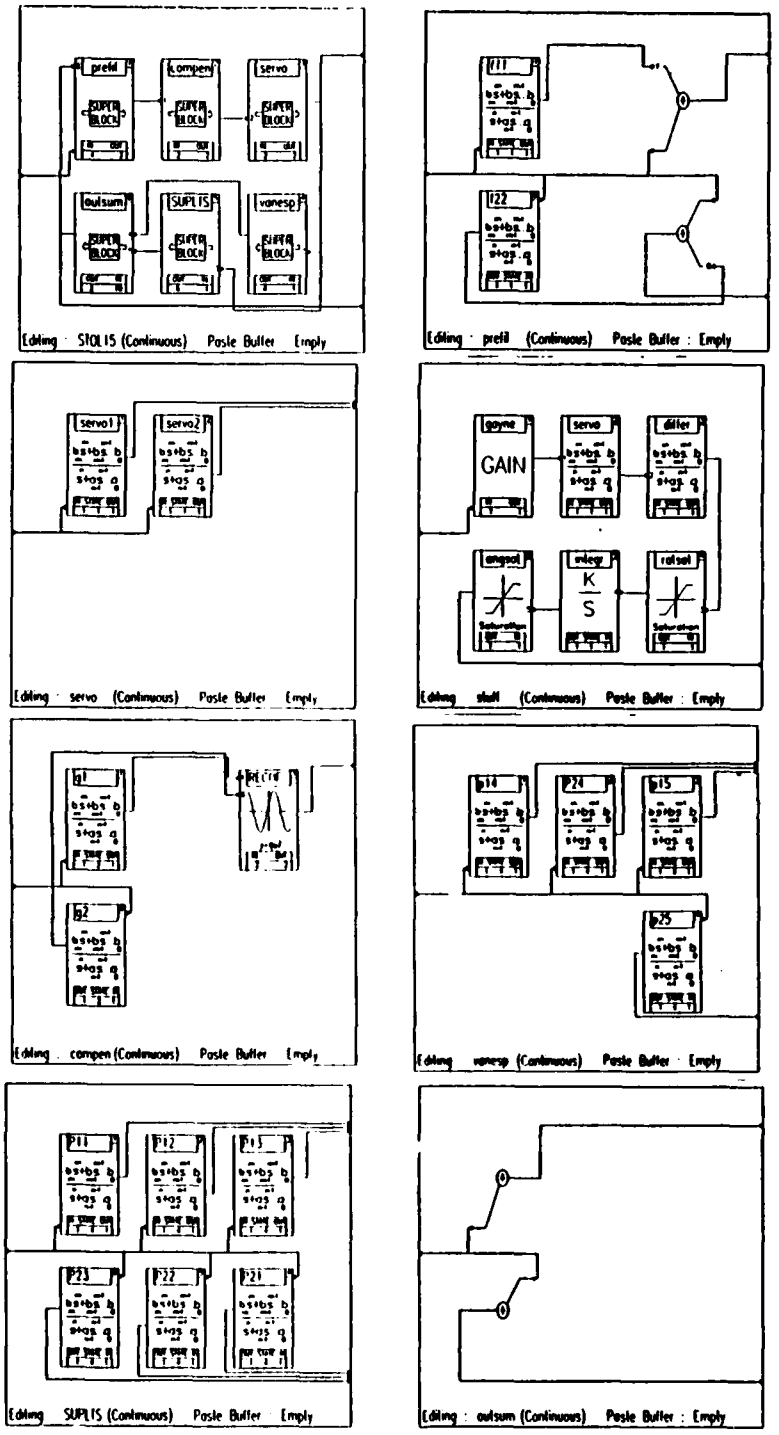

Fig.G-1: MATRIX X Simulation of STOL Aircraft

4) **vanesp** contains the plant transfer functions relating vane deflections to the outputs.

5) **SUPLTS** contains the plant transfer functions relating aerodynamic surface deflection to the outputs.

6) **outsum** contains the summing junctions that add together the outputs of the plant transfer functions, constructing the system outputs.

The MATRIX X CAD package used is hosted on a VAX computer with a VMS operating system. For simulation the CAD package takes the transfer functions, algebraic equations, and non-linear elements(such as saturations) and builds a state-space model to represent the entire system. For this simulation the state-space vector is of dimension 64. Needless to say, simulation is very slow. In order to decrease the computation time change the default integration routine from the Variable Step Kutta-Merson to the Implicit Stiff System Solver. Both are variable step methods; however, the MATRIX X manual states that making this change will decrease computational times for systems containing algebraic loops and/or dynamic systems. This it does markedly, sometimes by an order of three or more depending on the VAX load.

MATRIX X significantly reduced the time spent on the simulation part of this thesis. Previous theses used CAD packages that are not as powerful as MATRIX X, or they wrote their own simulation routines. In the authors opinion MATRIX X is the "best" control system design CAD package at the time

of this writing. AFIT administrators should expedite purchase of the CAD package to host on AFIT computer resourses. Doing so will reduce time, frustration, and stress level of future AFIT Controls Sequence students.

APPENDIX H

Reshaping of the Loop Transmissions

The loop transmissions developed in Chapter IV are overdesigned since they do not lie on the bounds at each frequency. This results in the magnitudes of the loop compensations g_1 and g_2 being greater than necessary over the entire frequency spectrum. This is especially noticable at higher frequencies. In order to reduce the overdesign and associated problems with wide bandwidth such as unmodelled pole excitation and noise, both loop transmissions are redesigned to be as close as possible to the bounds and to decrease in magnitude faster at high frequencies.

The redesign of loop one starts with the plotting of plant templates for frequencies of 200 and 400 rad/sec. These extra bounds are required when the new L_1 is shaped so no penetration of the maximum desired M_m contour(Forbidden Region) occurs in the range of 80 - 1000 rad/sec . The UHFB is again approximated by using the bound at $\omega = 1000$. The resulting bounds for the modified loop transmission are in Figure H-1. The initial form for L_{1o} includes just the unstable pole

$$L_{1o} = \frac{K(0.3851)}{(s - 0.3851)} \qquad \text{(H-1a)}$$

For $K > 0$ the system must remain stable and must drop in magnitude as fast as practically possible. To keep the loop

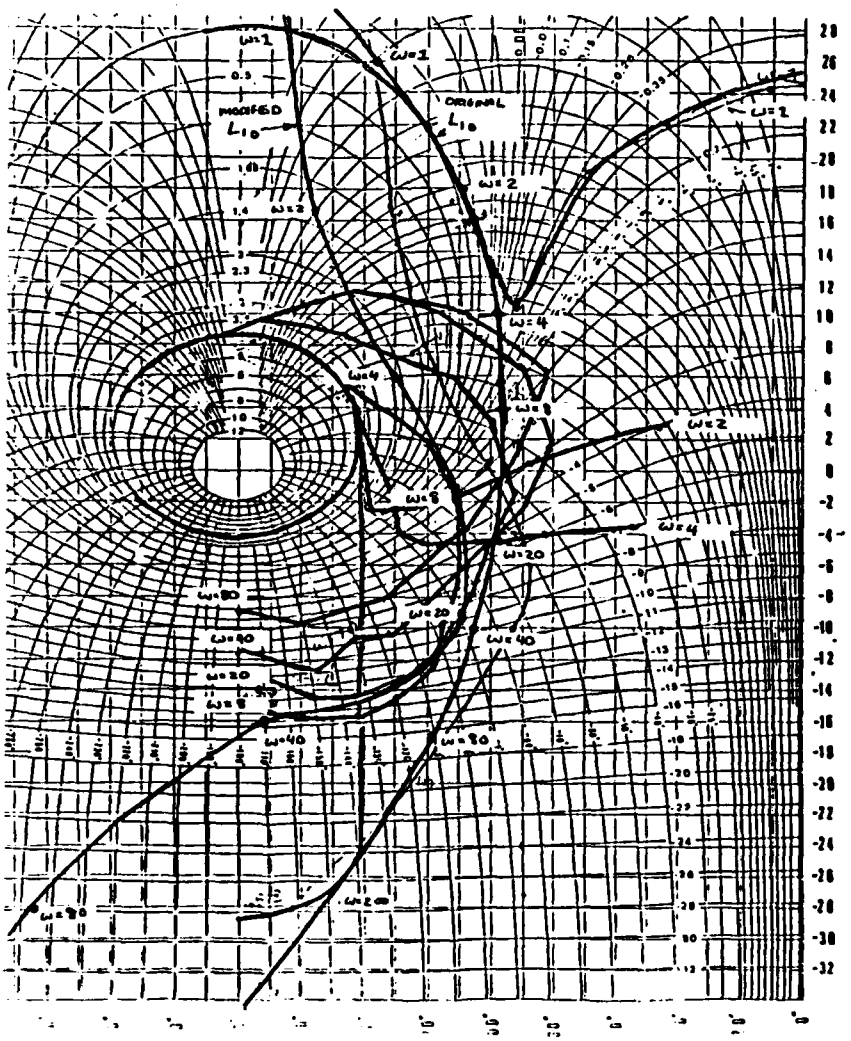

Fig.H-1: Loop One bounds and the reshaped Loop One Transmission

transmission as close as possible to the -180 degree line without crossing it (causing a conditionally stable system), and to increase the rolloff, a pole is added at -0.3851. To meet the bound at $\omega = 1$ the gain is increased by 200(46 dB). Using trial and error along with experience, the rest of the loop transmission is shaped; however, this time the bound at $\omega = 1000$ is crossed at a much lower frequency to increase the

phase angle and drop-off rate of L_{1o} much faster than the original L_{1o}. During the process the loop transmission is required to stay outside the bounds at ω = 20, 40, 80, 200, and 400 rad/sec. The result of this loop shaping is an L_{1o} that has a greatly lowered high frequency gain verses the original L_{1o}. The resulting transfer function is:

$$L_{1o} = \frac{3.211(10^{6})(s+3.81)(s+19.3)}{(s-0.3851)(s+0.3851)(s+16\pm j35)(s+79)(s+117)} \qquad (H-1b)$$

Figure H-1 is a plot of the bounds and L_{1o} on the Nichol's chart. The new L_{1o} is much closer to the bounds and drops off much sooner. This decreases the compensation bandwidth. The -3 dB bandwidth is approximately 10 rad/sec as compared to the 12 rad/sec of the original L_{1o}. With the nominal plant at FC2:Canard Failed, the required compensation is:

$$g_1 = \frac{5.023(10^{5})(s+3.81)(s+0.6067\pm j0.3579)(s+11.56)}{(s+0.3851)(s+0.6124)(s+1.153)(s+7.728)(s+22.25)} * \frac{(s+19.3)(s+1.979)(s+53.88)}{(s+22.25)(s+16\pm j35)(s+79)(s+117)} \qquad (H-2)$$

A comparison between the original compensator and the one above is shown in Figure H-2 . The high frequency gain is decreased by over 40 dB, showing the considerable overdesign present in the original g_1. The prefilter required for the new loop compensation is:

$$f_{11} = \frac{17.3}{(s+5)} \qquad (H-3)$$

Since the loop one compensation is changed new plant templates for Q_{22eq} are required. Using equations (4.7-1)

through (4.7-11) new Q_{22eq} are derived. The new plant templates closely resemble the previous ones. This is not surprising since most of the uncertainty in Q_{22eq} lies in Q_{22} which does not change with the new L_{1o}.

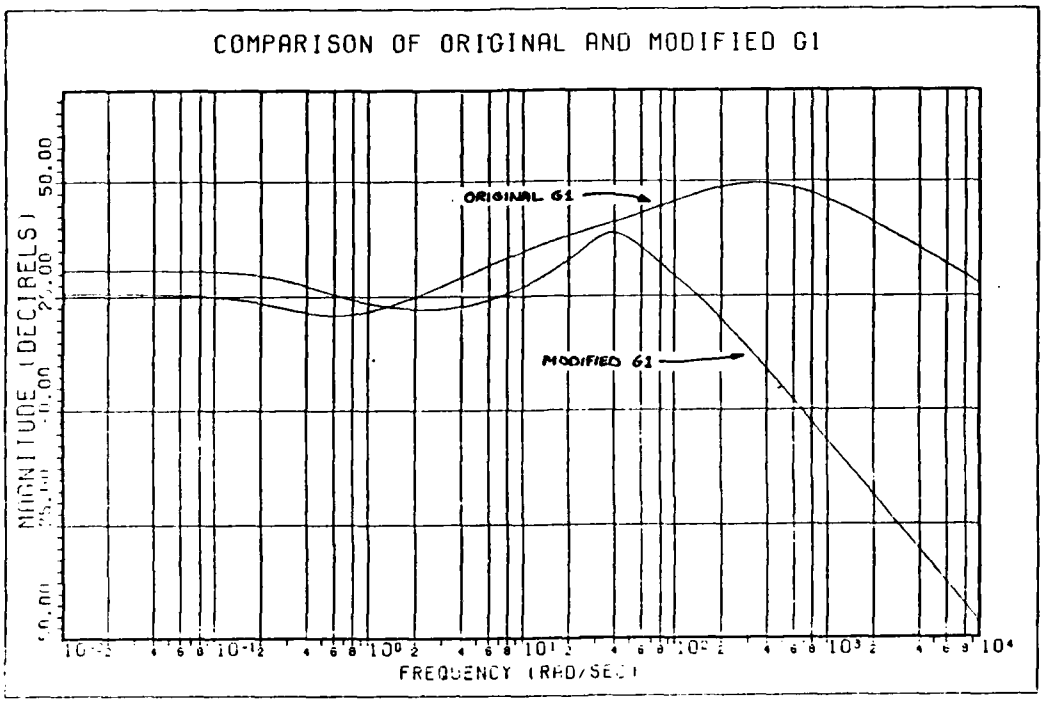

Fig.H-2: Comparison of New and Old Compensators G1

The new bounds for the second loop are shown in Figure H-3. Again the loop transmission contains the unstable pole at 0.3851 and cuts through the UHFB, outside(or above) the respective bounds at each frequencies, keeping the plant template outside the Forbidden Region. The shaped L_{2o} is:

$$L_{2o} = \frac{6.6154(10^5)(s+15)}{(s+0.3851)(s-0.3851)(s+60\pm j119)(s+220)} \quad \text{(H-4)}$$

and is shown also in Figure H-3 along with the original L_{2o}.

The -3 dB bandwidth is 34 rad/sec, 10 rad/sec greater than the -3 dB bandwidth of the earlier design. The increase in bandwidth is due to the loop bounds for distrurbance rejection shifting upward. The required loop compensation is:

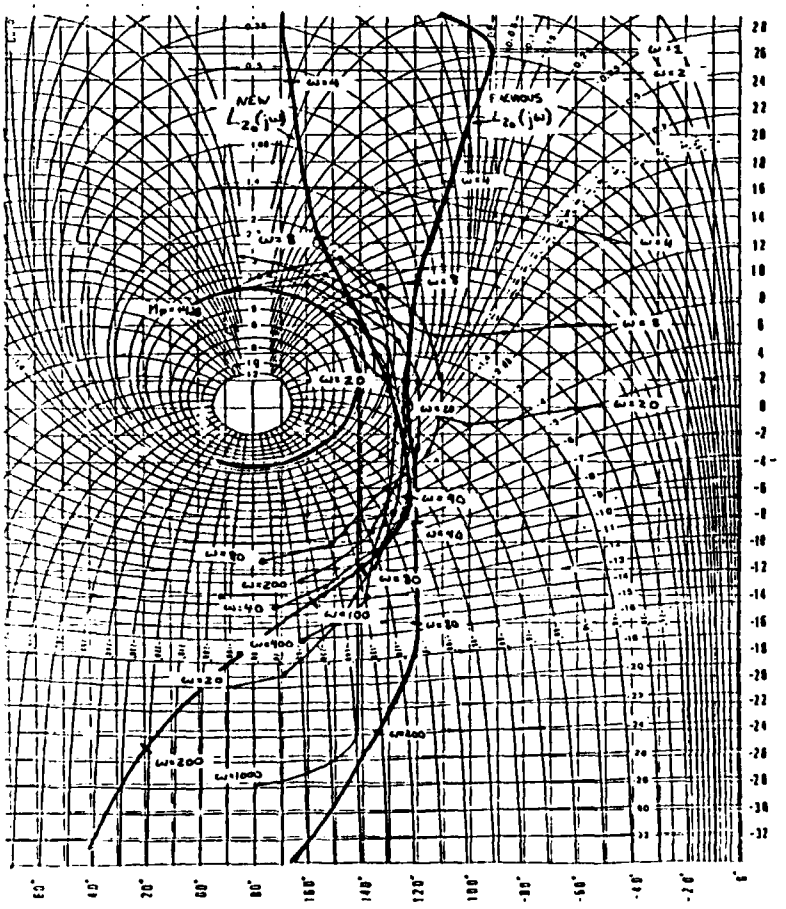

Fig.H-3: L_{2o} and Respective Bounds

$$g_2 = \frac{60742(s+15)(s+0.7631)(s+3.715)(s+24.31)}{(s+0.3851)(s+0.7124\pm j0.2019)(s+232.6)(s+22.49)} * \frac{(s+36.25)(s+0.6217\pm j0.2283)(s+1.979)}{(s+60.j119)(s+1.126)(s+5.677)(s+18.74)} * \frac{(s+20.34)(s+33.09)}{(s+41.71)(s+220)} \quad \text{(H-5)}$$

Figure H-4 shows the difference between the old and new g_2. Notice the decrease in high frequency gain, 30 dB at 10 rad/sec , 14 dB at 100 rad/sec, and over 50 dB at 1000 rad/sec.

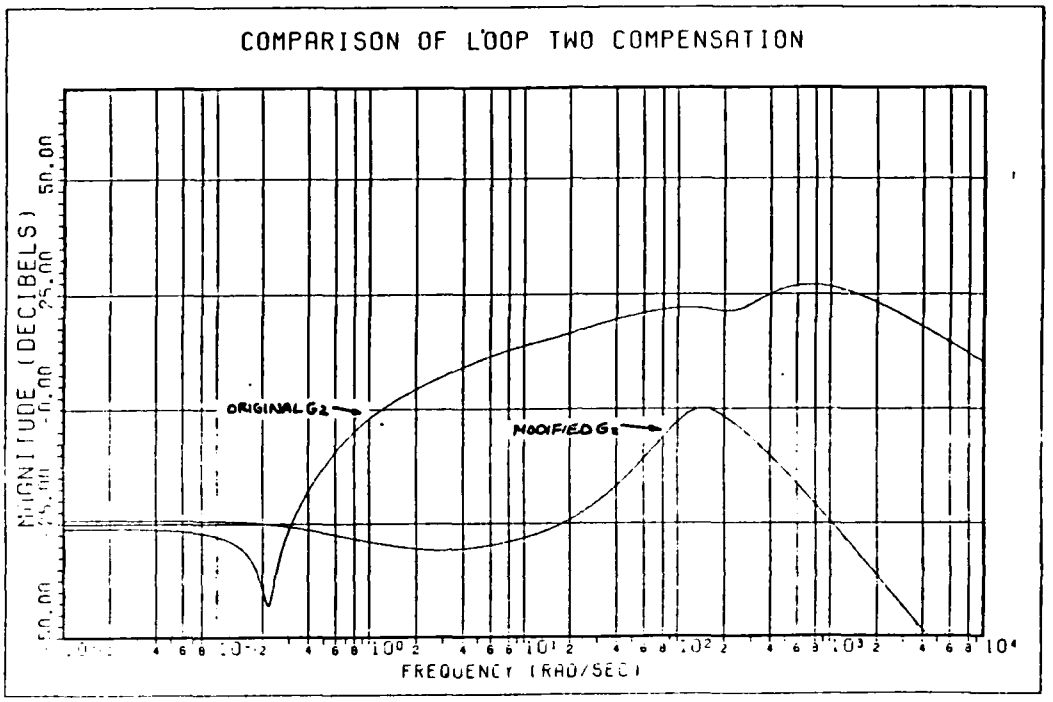

Fig.H-4: Comparison of Old and New Loop Two Compensation

The prefilter f_{22} does not have to be changed to give the desired tracking performance, thus:

$$f_{22} = \frac{4}{(s+0.8)} \qquad \text{(H-6)}$$

These compensations and prefilters, leading to loop transmissions having much smaller high frequency gain than the previously designed ones, are used in the simulations in Chapter V.

Appendix I

Derivation of Expanded Plant Determinant Equations

The determinant of the 2 X 2 aircraft plant P' is:

$$\det\{P'\} = \begin{bmatrix} P'_{11} P'_{22} - P'_{12} P'_{21} \end{bmatrix} \qquad (I-1)$$

From Eq(2.3-10) (A-1) can be expanded to

$$(\tilde{P}_{11} + \mu_{21} \tilde{P}_{12})(\tilde{P}_{22} + \mu_{12} \tilde{P}_{21}) - (\tilde{P}_{12} + \mu_{12} \tilde{P}_{11})(\tilde{P}_{21} + \mu_{21} \tilde{P}_{22}) \qquad (I-2)$$

Multiplying this expression out and collecting the terms results in:

$$(1 - \mu_{12} \mu_{21})(\tilde{P}_{11} \tilde{P}_{22} + \tilde{P}_{12} \tilde{P}_{21}) \qquad (I-3)$$

Ignoring the first quantity since its just a constant, the terms in the second quantity are expanded using Eq(2.3-9):

$$(\Delta P_{1\,11} + \Delta P_{2\,12} + \Delta P_{3\,13})(\Delta P_{4\,24} + \Delta P_{5\,25})$$

$$- (\Delta P_{1\,21} + \Delta P_{2\,22} + \Delta P_{3\,23})(\Delta P_{4\,14} + \Delta P_{5\,15}) \qquad (I-4)$$

When (A-4) is multiplied out and grouped according to the Δ_4 and Δ_5 values it can be expressed as:

$$\Delta_1 \Delta_4 (P_{11\,24} P_{14\,21} - P_{11\,24} P_{14\,21}) + \Delta_1 \Delta_5 (P_{25\,11} P_{15\,21} - P_{25\,11} P_{15\,21})$$

$$\Delta_2 \Delta_4 (P_{12\,24} P_{14\,22} - P_{12\,24} P_{14\,22}) + \Delta_2 \Delta_5 (P_{12\,25} P_{15\,22} - P_{12\,25} P_{15\,22})$$

$$\Delta_3 \Delta_4 (P_{13\,24} P_{14\,23} - P_{13\,24} P_{14\,23}) + \Delta_3 \Delta_5 (P_{13\,25} P_{15\,23} - P_{13\,25} P_{15\,23}) \qquad (I-5)$$

If the expression is divided by Δ_1 and Δ_4 it can be written as:

$$(P_{11}P_{24} - P_{21}P_{14}) + \psi(P_{25}P_{11} - P_{15}P_{21})$$
$$+ (\Delta_2/\Delta_1)(P_{12}P_{24} - P_{14}P_{22}) + \psi(P_{25}P_{12} - P_{15}P_{22})$$
$$+ (\Delta_3/\Delta_1)(P_{13}P_{24} - P_{14}P_{23}) + \psi(P_{25}P_{13} - P_{15}P_{23}) \qquad (I\text{-}6)$$

where $\psi = \Delta_5/\Delta_4$.

This is Eq(4.5-12) in Chapter IV of this thesis.

Bibliography

1. Arnold, Phillip B. Flight Control System Reconfiguration Design Using Quantitative Feedback Theory. MS Thesis . Air Force Institute of Technology(AU). Wright-Patterson AFB OH, December 1984.

2. Russel, Harvey H. Design of Robust Controllers for a Multiple Input-Multiple Output Control System with Uncertain Parameters Application to the Lateral and Longitudinal Modes of the KC-135 Transport Aircraft . MS Thesis. Air Force Institute of Technology(AU). Wright-Patterson AFB OH, December 1984.

3. Segner, D. L. Design of a Multiple Input-Multiple Output Flight Control System Containing Uncertain Parameters. MS Thesis. Air Force Institute of Technology(AU). Wright-Patterson AFB OH, September 1984.

4. Betzold, Robert. Multiple Input-Multiple Output Flight Control Design with Highly Uncertain Parameters; Applications to the C-135 Aircraft. MS Thesis. Air Force Institute of Technology(AU). Wright-Patterson AFB OH , December 1983.

5. Chandler, Phillip R. Self-Repairing Flight Control System Reliability and Maintainability. Program Plan. Air Force Wright Aeronautical Laboratories. Wright-Patterson AFB OH, February 1984.

6. McDonnell Aircraft Co. Data Package for STOL Approach. Memo SMTP-HSR011, March 1985.

7. Larimer, S. J. An Interactive Computer-Aided Design Program for Digital and Continuous System Analysis and Syntnesis(TOTAL). MS Thesis. Air Force Institute of Technology(AU). Wright-Patterson AFB OH, December 1978.

8. Conversation with Capt. Greg Mandt, Air Force Wright Aeronautial Laboratories Flight Control Division, Advanced Control Systems Development Branch. March 1985.

9. Horowitz, Isaac and Marcel Sidi. "Synthesis of Feedback Systems with Large Plant Ignorance for Prescribed Time-Domain Tolerances", International Journal of Control, 16 (2): 287-309 (1972).

10. Horowitz, Isaac. A Quantitive Inherent Reconfigurability Theory for a Class of Systems. Universal Energy Systems, Inc., Dayton OH, July 1984 (F33615-82-C-3000).

11. Horowitz, Isaac and Marcel Sidi. "Optimum Synthesis of Nonminimum Phase Feedback Systems with Plant Uncertainty" International Journal of Control, 27 (3): 361-386 (1978).

12. Horowitz, Isaac. "Quantitative Feedback Theory", IEEE Proceedings; Control Theory and Applications, 129 Part D (6): 215-226 (November 1982).

13. Horowitz, Isaac. Synthesis of Feedback Systems. New York: Academic Press, 1963.

14. Horowitz, Isaac, et al. Research in Advanced Flight Control Designs. AFFDL-TR-79-3120, Department of Applied Mathematics, The Weizmann Institute of Science, Rehovot, Isreal, January 1980.

15. QFT has been extended to SISO saturation(International Journal of Control, 38 : 169-187 (1983) and 40 : 1215-1229 (1984)) but not yet to MIMO system saturation.

16. Horowitz, Isaac. Lecture for Air Force Institute of Technology Class EE7:08, Spring 1985.

17. Horowitz, Isaac. "Quantitative Synthesis of Uncertain Multiple Input-Multiple Output Feedback Systems" , International Journal of Control, 30 (1): 81-106 (1979).

18. Horowitz, Isaac. "Improved Design Technique for Uncertain Multiple Input-Multiple Output Feedback Systems", International Journal of Control, 36 (6): 977-988 (1982).

19. Horowitz, Isaac and T. Kopelman. Multivariable Flight Control Design with Uncertain Parameters. Department of Applied Mathematics, The Weizmann Intitute of Science, Rehovot, Isreal, Final Report, October 1981.

20. Horowitz, Isaac and Claytin Loecher. "Design of a 3x3 Multivariable Feedback System with Large Plant Uncertainty", International Journal of Control, 30 (1): 677-699 (April 1981).

21. Horowitz, Isaac. Lecture for Air Force Institute of Technology Class EE7:08, Spring 1985.

22. Conversation with Capt Greg Manut, AFWAL/FIGX, June 1985.

23. Walke, Jon G. Design of Longitudinal Flight Control System Using the Singular "G" Method. MS Thesis. Air Force Institute of Technology(AU). Wright-Patterson AFB OH, December 1983.

24. Conversation with Dr. Isaac Horowitz, Department of Electrical Engineering, University of Colorado. September and October 1985.

25. MATRIX X Users Guide. Integrated Systems Inc. Palo Alto CA, September 1984.

26. Horowitz, Isaac. Unpublished Notes. Air Force Institute of Technology(AU). Wright-Patterson AFB OH. November 1985.

27. Conversation with Dr. Constantine H. Houpis, Department of Electrical and Computer Engineering, Air Force Institute of Technology(AU). December 1985.

Vita

First Lieutenant Bruce T. Clough attended the University of Akron from September 1977 until May 1982. He graduated Magna Cum Lauda with the degree of Bachelor of Science in Electrical Engineering, and received a reserve commission through Air Force ROTC in June 1982. From July 1982 to June 1984 he served as an Advanced Electronic Warfare Techniques Analyst at the Air Force Electronic Warfare Center, Electronic Security Command , coming to the Air Force Institute of Technology(AFIT) in June 1984.

Lieutenant Clough is a member of The Institute of Electrical and Electronics Engineers(IEEE), Sigma Pi Fraternity , Eta Kappa Nu , Tau Beta Pi, and Phi Eta Sigma honorary fraternities. Following graduation from AFIT his next assignment will be with the Air Force Flight Dynamics Laboratory.

UNCLASSIFIED

SECURITY CLASSIFICATION OF THIS PAGE

AD-A163939

REPORT DOCUMENTATION PAGE

1a. REPORT SECURITY CLASSIFICATION	1b. RESTRICTIVE MARKINGS
2a. SECURITY CLASSIFICATION AUTHORITY UNCLASSIFIED	3. DISTRIBUTION/AVAILABILITY OF REPORT Approved for public release; Distribution unlimited.
2b. DECLASSIFICATION/DOWNGRADING SCHEDULE	
4. PERFORMING ORGANIZATION REPORT NUMBER(S) AFIT/GE/ENG/85D-8	5. MONITORING ORGANIZATION REPORT NUMBER(S)
6a. NAME OF PERFORMING ORGANIZATION AIR FORCE INSTITUTE OF TECHNOLOGY 6b. OFFICE SYMBOL (If applicable) AFIT/EN	7a. NAME OF MONITORING ORGANIZATION
6c. ADDRESS (City, State and ZIP Code) WRIGHT-PATTERSON AFB OH 45433	7b. ADDRESS (City, State and ZIP Code)
8a. NAME OF FUNDING/SPONSORING ORGANIZATION FLIGHT DYNAMICS LABORATORY 8b. OFFICE SYMBOL (If applicable) AFWAL/FIGX	9. PROCUREMENT INSTRUMENT IDENTIFICATION NUMBER
8c. ADDRESS (City, State and ZIP Code) WRIGHT-PATTERSON AFB OH 45433-6553	10. SOURCE OF FUNDING NOS. PROGRAM ELEMENT NO. / PROJECT NO. / TASK NO. / WORK UNIT NO.
11. TITLE (Include Security Classification) SEE BLOCK 19	
PERSONAL AUTHOR(S) BRUCE T. CLOUGH 1LT USAF	
13a. TYPE OF REPORT MS THESIS 13b. TIME COVERED FROM _____ TO _____	14. DATE OF REPORT (Yr., Mo., Day) 1984 DECEMBER 15. PAGE COUNT 210
16. SUPPLEMENTARY NOTATION APPROVED FOR PUBLIC RELEASE: IAW AFR 190-17	

17. COSATI CODES		
FIELD	GROUP	SUB. GR.
01	03	

18. SUBJECT TERMS (Continue on reverse if necessary and identify by block number)
INHERENT RECONFIGURATION; LOOP TRANSMISSION; MULTIVARIABLE CONTROL SYSTEM; FLIGHT CONTROL SYSTEMS; QUANTITATIVE FEEDBACK THEORY, CONTROL SYSTEMS

19. ABSTRACT (Continue on reverse if necessary and identify by block number)

TITLE: ~~ROBUST~~ RECONFIGURABLE FLIGHT CONTROL SYSTEM FOR A STOL AIRCRAFT DESIGN USING QUANTITATIVE FEEDBACK THEORY

THESIS CHAIRMAN: DR CONSTANTINE H. HOUPIS

Approved for public release IAW AFR 190-17.
LYNN E. WOLAVER 16 DEC 85
Dean for Research and Professional Development
Air Force Institute of Technology (AFSC)
Wright-Patterson AFB OH 45433

ABSTRACT

Quantitative Feedback Theory developed by Dr Isaac Horowitz of the University of Colorado is used to design the control laws for a Short Take Off and Landing (STOL) aircraft. Compensators are presented for two longitudinal variables, angle of attack and forward velocity, which are controlled via the use of five separate control surfaces: canard, stabilator, ailerons, upper and lower thrust reversing vanes. The final design must exhibit robust qualities over three flight conditions despite surface failures.

20. DISTRIBUTION/AVAILABILITY OF ABSTRACT UNCLASSIFIED/UNLIMITED ☒ SAME AS RPT. ☒ DTIC USERS ☐	21. ABSTRACT SECURITY CLASSIFICATION UNCLASSIFIED
22a. NAME OF RESPONSIBLE INDIVIDUAL	22b. TELEPHONE NUMBER (Include Area Code) / 22c. OFFICE SYMBOL

DD FORM 1473, 83 APR EDITION OF 1 JAN 73 IS OBSOLETE.

UNCLASSIFIED

SECURITY CLASSIFICATION OF THIS PAGE

The state-space matrix representation of the aircraft is developed from pertubation equations using linearized aerodynamic data. Transfer functions relating servo input signals to aircraft outputs are obtained from the state-space equations. The original output set included the flight path angle and velocity; however, the non-minimum phase characteristics of the flight path angle precluded its use by the type of Quantitative Feedback Theory used in this thesis since unstable plants can arise. Instead, the minimum phase variables angle of attack and velocity are controlled. The ten separate transfer functions relating the two output variables to the five input commands form a 5 X 2 plant transfer function matrix. These separate transfer functions are combined using a weighting vector into a 2 X 2 minimum phase plant matrix for each flight condition/failure combination. Quantitative Feedback Theory is applied to the resulting plants to yield robust control.

A single set of fixed compensators and prefilters are designed to handle the entire plant set, consisting of three single-surface failures and two dual-surface failures at each flight condition. For these failures neither Fault Detection/Identification, nor scheduled compensation, is required. Surfaces are assumed locked at zero degrees deflection after failure, generating no net moment after failure. Digital simulations have shown the control to be robust over the three flight conditions and surface failures. Loop bandwidths for the velocity and angle of attack loops are 35 and 12 rad/sec respectively. Control surface rates and deflections are shown to saturate only for the double failure cases.

Quantitative Feedback Theory effectively controls the aircraft despite large uncertainty due to flight condition changes and/or control surface failures without identification. Application of QFT eliminates the use of identification to achieve robustness and the associated false alarm and missed detection problems. Efforts to expand upon the base of flight control design using this method are recommended, especially direct design in the discrete domain. Research should also continue on developing a computer-aided design program to expedite the synthesis of controllers using QFT.

END

FILMED

3-86

DTIC